Electrostatic Microplastic Removal for Freshwater Environments

A Major Qualifying Project

Submitted to the Faculty of

Worcester Polytechnic Institute

in partial fulfillment of the requirements for the

Degree in Bachelor of Science

in

Mechanical Engineering

Authors

Mitchell Mudge

Kelly Perfetto

Alyssa Richardson

Aaron Rosner

Advisor

Professor Wodin-Schwartz

May 2, 2022

A Major Qualifying Project submitted to the Faculty of Worcester Polytechnic Institute in partial fulfillment of the requirements for the degree of Bachelor of Science in Engineering Sciences.

This report represents the work of one or more undergraduate students submitted to the faculty as evidence of completion of a degree requirement. WPI routinely publishes these reports on the web without editorial or peer review. For more information about the projects program at WPI, see http://www.wpi.edu/Academics/Projects.

Acknowledgments

We would like to thank the following individuals for helping with the completion of this project, without whom it would not have been possible.

First, we would like to thank Professor Wodin-Schwartz for advising our project and providing support, guidance and feedback throughout the entire year.

Additionally, we would like to thank Jacquelyn Burmeister, the senior environmental analyst of the Worcester Department of Public Works & Parks, who assisted us with resources and connections.

We would also like to extend thanks to Richard Eberheim, who we consulted for help with code writing.

Lastly, we want to thank Noel Lange, a student at the University of Kansas. She works with microplastic filtration through electrostatic separation and was very helpful in answering our many questions related to her research.

Table of Contents

Table of Figures

Table of Tables

Abstract

Microplastics are a prevalent issue in every ocean and most freshwater systems and pose health complications for all studied organisms to date. Most collection solutions are only available on a large scale and for saltwater systems. Technology for freshwater extraction does exist but is focused on potable water rather than ecosystems. This project aimed to create a small freshwater microplastic separation system utilizing existing technology that would not disrupt the ecosystem. After evaluating ten existing microplastic separation technologies, electrostatic separation was selected because it is economically viable, environmentally neutral, and easily scaled to fit our application. We iteratively designed four modular subsystems of a belt operated electrostatic separator system and performed technical analysis to optimize operations.

1. Introduction

Currently there are around 51 trillion pieces of plastic in the ocean, a large portion of which are microplastics (Geyer et al., 2017). Microplastics are plastic pieces less than 5mm in diameter. They have become ubiquitous in the environment and are harmful to all studied organisms to date. These plastics can leach toxic chemicals into the environment while also causing physical harm and damage to organisms when ingested. The amount of plastic production is accelerating, leading to millions of metric tons entering freshwater systems and eventually the ocean (Andrady, 2011; Koelmans et al., 2019). Most plastics take hundreds of years to decompose, causing extreme harm to the environment and organisms (Bose et al., 2020). For example, a disposable plastic water bottle takes around 450 years to fully decompose (NOAA Marine Debris Program et al., 2020).

In the last few years, research has gradually increased on microplastics, leading to heightened concern about the dangerous impact they have on this planet and human health. Plastic has been underestimated for decades leading to over eighty percent of marine pollution consisting of plastic (Marine Plastic Pollution, 2021). Specifically, the extraction of microplastics from organic-rich freshwater samples is challenging and limited information is available in the literature. A study about these plastics was conducted in 2011 along the shoreline of Lake Huron, Canada. This resulted in the first documented record of the breakdown of freshwater beach plastics based on surface textural and compositional analysis. The study was completed by using both scanning electron microscopy (SEM) and infrared spectroscopy (FTIR) which resulted in finding a total of 3,209 plastic pieces on an area of only 85 m^2. The predominant type of plastic in the lake was polyethylene which appears to be more resistant to chemical weathering than polypropylene (Silvia et al., 2022). This study confirmed that there is a need for more research and testing in freshwater especially after learning about the large amount of plastic in such a small area.

Most of the microplastic separation system designs on the market today have been created to remove microplastics on a large scale for saltwater systems only. Technology for freshwater extraction does exist but is focused on potable water rather than use in ecosystems. However, many of these technologies could be adapted to a small-scale system. Some system designs require introducing further chemicals into the environment to collect the plastics (Farner et al., 2020; Koistinen et al., 2017). These chemicals include polyacrylamide (PAM) and

aluminum chloralhydrate (ACH). Other systems were not easily scalable either for this project or for small ecosystems.

This project aimed to create a small freshwater microplastic separation system that would minimize natural ecosystem disruption. After evaluating ten existing microplastic separation technologies, electrostatic separation was selected because it is economically viable, environmentally neutral, and easily scaled to fit our specific application. We iteratively designed four modular subsystems of a belt operated electrostatic separator mechanism and performed technical analyses to optimize operations. This resulted in the system being able to operate continuously and independently while being capable of being used for small-scale freshwater microplastic filtering and could be scaled up for larger use in the future. In the future this system could be scaled up for larger use and run unassisted for multiple day long cycles. This device aims to assist with cleaning local ecosystems, preventing further damage to the marine and global environments, and ultimately improving human health.

2. Background

2.1 The Fundamentals of Microplastics

Microplastics are becoming a prevalent and widespread issue globally. These plastics originate from a variety of sources and impact all organisms and environments they encounter. There are multiple different ways to combat the spread of microplastics, and research on this topic has been increasing over the last decade.

2.1.1 Origins

Approximately, eight million metric tons of plastic enter the oceans every year (Andrady, 2011). Plastic pollution causes harm to the environment and to organisms, including fish, bivalves, turtles, aquatic mammals, aquatic birds, and humans that may consume any of these animals. Most aquatic plastic pollution originates from freshwater systems (Koelmans et al. 2019). Plastic will stay in aquatic environments indefinitely because there are no naturally occurring organisms that can digest plastics. Instead of being returned to the environment, as is the case with most organic compounds, plastics continue to physically degrade into smaller particles (NOAA Marine Debris Program et al., 2020).

Microplastics, or nurdles, are the terms given to these physically minuscule plastic particles shown below in Figure 1. While there is no consensus on the exact size range for microplastics, an acceptable size range is from 0.25 mm to 5 mm (Lusher et al., 2015). Regardless of the size of these particles, they enter rivers and tributaries and cause harm to freshwater ecosystems (Hermsen et al., 2019). These plastics can break down while being transported in freshwater systems, or while in the ocean. This breakdown is commonly caused by exposure to UV radiation and saltwater (The Economist, 2018). Eventually, plastics work their way through these systems and end up in the ocean where they become caught in large circular currents called gyres. Microplastics are easily spread across the globe, causing serious damage to any organism or environment (Lusher et al., 2015).

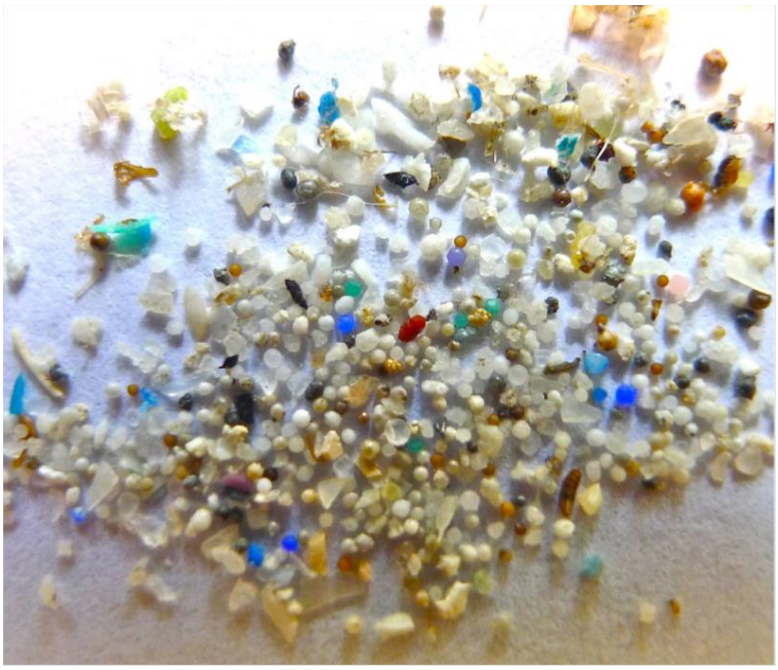

Figure 1. Approximate Size and Shape of Oceanic Nurdles. These nurdles range in size from approximately 0.25 mm to 5 mm (Oregon State University, 2015).

2.1.2 Definition of Microplastics

Microplastics are classified as plastic particles that are less than 5 mm in length which can be seen in Figure 2. These particles come in two forms, primary and secondary. Primary microplastics are manufactured plastic particles that are originally less than 5 mm in size, which are usually in the form of microbeads and used in abrasives, plastic powders for manufacturing, and personal care products. Primary microplastics usually come in the form of microbeads, or pellets. Secondary microplastics are particles that have resulted from the breakdown of larger plastic particles in smaller pieces, fragmenting from use, as well as plastics breaking down in waste stream from environmental exposure. Secondary microplastics usually come in the form of fragments, or synthetic textile fibers. The widespread use of plastics in all areas has led microplastics to be found in various water bodies including lakes, rivers, the ocean, and in ocean and river sediment. Through these avenues, microplastics have found their way into various forms that lead to human consumption, including aerosolized dust particles, in drinking water, and inside fish and other marine mammals that could find their way into being consumed by humans (Kannan, Vilmalkumar 2021; Bellas, 2016).

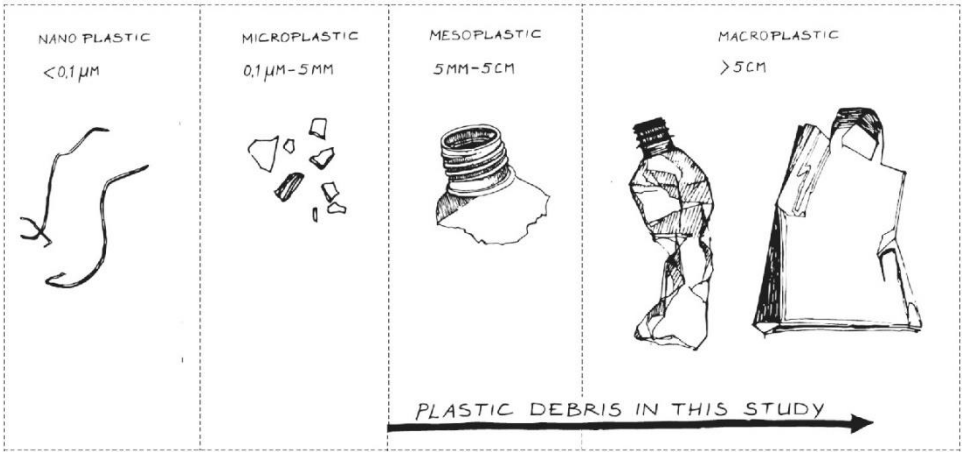

Figure 2. Commonly Accepted Size Range for Plastics. Microplastics are in the 5mm range (Van Emmerik & Schwarz, 2019).

Many plastics end up in the rivers and seas as a result of littering, sewage, and illegal dumping activity. Regardless of origin, all plastic pollution that enters the environment eventually degrades into microplastics (U.S National Library of Medicine, 2017). Due to the complexity around manufacturing plastic parts, most plastics are originally manufactured as nurdles and then molded into their final shape (Andrady, 2011). A portion of these plastics can enter environments directly at this small size through manufacturing processes or shipping accidents.

2.1.3 Sources of Microplastics

Plastic and microplastic pollution in freshwater systems has a high correlation with human activity (Koelmans et al., 2019). Pollution can occur due to high population density, urbanization, wastewater treatment, and waste management. Microplastics can also enter freshwater systems through natural processes including wind, rainfall-induced surface runoff, and artificial means such as littering and direct pollution (Van Emmerik & Schwarz, 2019). Rivers and other freshwater systems inevitably transport land-based plastic debris into the ocean. This path can be seen in Figure 3. As plastics travel downstream, they negatively impact the riverine ecosystems. When plastics or microplastics are transported through freshwater systems, they tend to accumulate in areas with heavy vegetation or other features such as dams and sluices. When this occurs, these features will act as temporary sinks for the debris.

Of the plastics that enter the ocean, the majority originate from freshwater systems, which spill out onto shorelines and get distributed throughout the ocean (Lebreton et al., 2017).

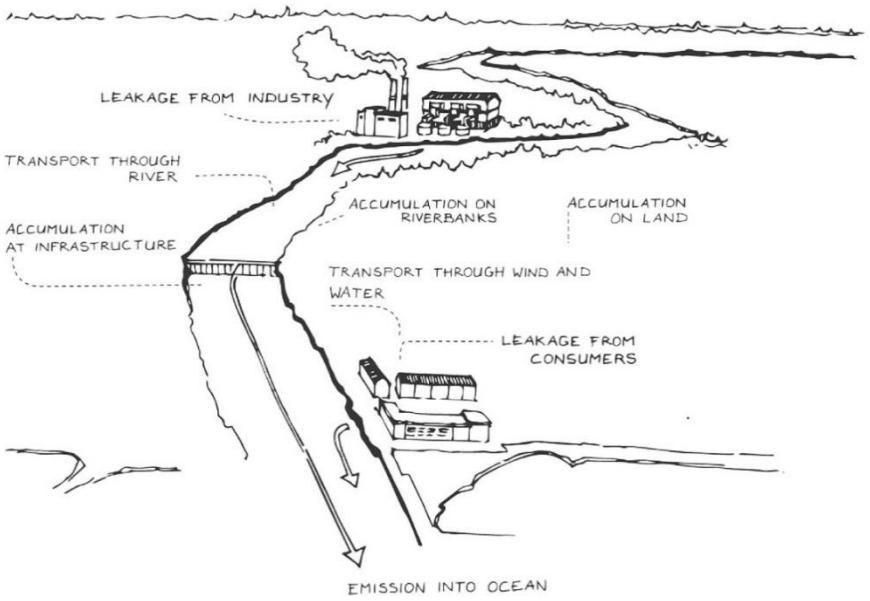

Figure 3. Plastics in Rivers. A diagram of the ways that plastics can form and accumulate in rivers (Van Emmerik & Schwarz, 2019).

The fishing industry has increasingly moved to using plastic products and equipment, some of which is improperly disposed of, contributing to the number of plastics deposited in the oceans. About 10% of plastic litter is produced by the fishing industry. According to a study conducted by the National Oceanic and Atmospheric Administration (NOAA) and the Woods Hole Oceanographic Institute (WHOI), one of the worst offenders is plastic fishing line, which can take up to 600 years to biodegrade (NOAA Marine Debris Program et al., 2020).

Despite these comprehensive studies of the origins of microplastics, the exact distributions of plastic particles throughout freshwater are not yet completely known. From the studies found (Van Emmerik & Schwarz, 2019) along with some of the team's experience collecting microplastics for study, a significant portion of microplastics within these freshwater ecosystems can be found within the top six inches of the water column. Many filtering techniques, including those for salt water, target the top of the water column for this reason, in addition to the complications that could arise from using a diving or otherwise lower device, or

one that would sift through sediment. Some of the plastics and particulate that can be found throughout riverine systems can be seen in Figure 4.

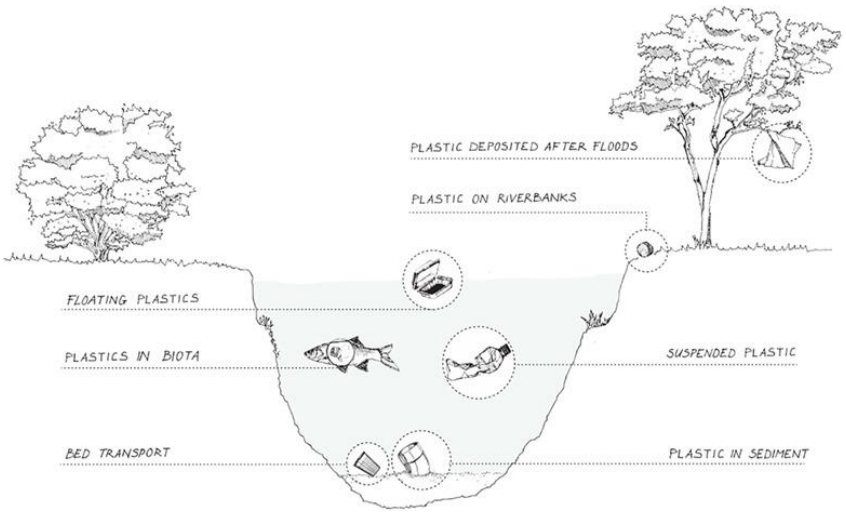

Figure 4. Plastics in Riverine Water Column. A diagram of the levels that different types of plastics float at within rivers (Van Emmerik & Schwarz, 2019).

2.1.4 Impacts and Dangers

Microplastics are causing widespread and largely unnoticed harm to humans and the environment (The Economist, 2018). Plastics were first introduced as a commodity resource in the mid 20th century and have seen an exponential increase in their usage since then. Currently, over 6.3 billion metric tons of plastic waste have been produced with only a small portion being disposed of responsibly (The Economist, 2018). Approximately only 9% of all plastic waste has been recycled and 12% has been incinerated (The Economist, 2018). A majority of the remaining 79% have made their way into aquatic systems. Our seas now contain up to 51 trillion microplastic particles, with the leading sources of plastic pollution being plastic packaging, single use plastics, and plastic fishing gear (Geyer et al., 2017; Andrady, 2011). As the popularity of single use plastics and plastic packaging have grown, so has the prevalence of microplastics.

Plastics travel through freshwater systems and accumulate in the ocean where they get caught in large circular currents called gyres. These gyres are formed by the wind and forces from the rotation of the globe (American Oceans, 2022). There are five main gyres that are spread out across the entire globe with the largest garbage patch being in the Great Pacific. These

gyres circulate microplastics which get dispersed throughout the ocean. The circular currents are helpful with keeping the ocean temperature regulated, salinity and nutrient flow but do create a negative health impact on organisms and the environment.

Plastics are often consumed by oceanic wildlife through simple water filtration, or when confused with prey (Barboza et al., 2018). Once the plastics are ingested into a single organism it can result in a ripple effect of harmful effects to all organisms in the food chain. The number of plastics consumed by a predator will be greater than that of its prey, due to a process known as biological magnification. As plastic pollution works its way up the marine food chain, it becomes increasingly likely that plastic infused seafood will make its way to the dinner table. It is estimated that if one's diet is high in shellfish, one could consume on average up to 11,000 microplastic particles every year. However, those living in countries that on average consume fewer shellfish still ingest about 1,800 microplastics every year. Humans are believed to consume at least 50,000 microplastic particles a year from food and water (Cox et al. 2019).

Over 400 species of animals have been severely affected by plastic pollution either through entanglement or ingestion (Galloway et al., 2016). Their effects have been observed in zooplankton, shellfish, seabirds, fish, turtles, and mammals (Lusher et al., 2015). In a laboratory study, the negative impacts from the plastic ingestion were shown to cause gut blockage and physical injury, oxidative stress, altered feeding behavior, and reduced energy allocation, with additional effects on growth and reproduction (U.S National Library of Medicine, 2017). Specifically with humans there has not been extensive research on the effects of microplastics in the human body but, plastics found in human lung tissue can be correlated to a higher risk of lung cancer (Koelmans et al., 2019).

Within recent years, studies have shown that some of the organisms consuming these microplastics are keystone species (Barboza et al., 2018). If these species die off due to microplastic pollution, local marine ecosystems could die off or change drastically. It takes around 450 years for one singular plastic water bottle to fully decompose. Figure 5 highlights commonly used plastics with the amount of time they each stay in the environment. Microplastics have not only been found in aquatic life, but also occasionally in some processed table salt, honey, and both bottled and tap water.

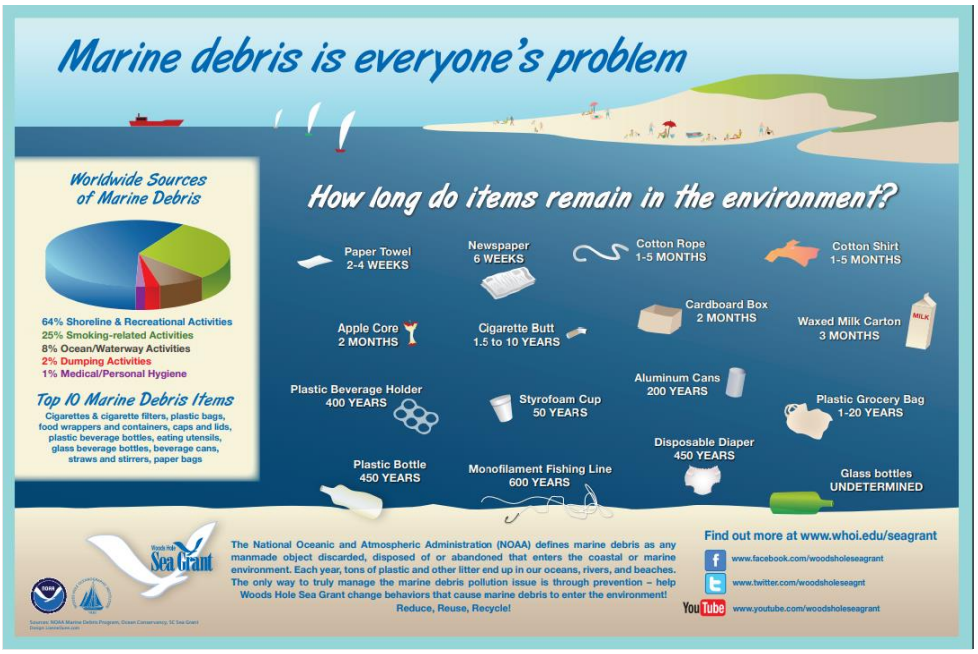

Figure 5. Marine Debris is Everyone's Problem. Poster about marine debris from NOAA and WHOI. This poster provides information about how long common beach litter takes to break down in the ocean. This can be accessed in a larger format (NOAA Marine Debris Program et al. 2020).

2.1.5 Action Against Microplastics

To date, only about fifty studies provide viable datasets for the concentration of microplastics within freshwater sources (Koelmans et al., 2019). There have been two major studies conducted that focus on quantifying microplastic emissions from rivers, both of which used a catchment-based approach (Lebreton et al., 2017; Schmidt et al. 2017). They differ in their use of calibration parameters, calibration datasets, and how they conceptually treated dams. Despite these differences both studies had reasonably similar values for the yearly global riverine emissions of plastics into the ocean, estimating 1.15–2.41 million metric tons a year (Lebreton et al., 2017; Schmidt et al., 2017). They do, however, differ with regards to their conclusions about the global distribution of riverine plastic output. In the study conducted by Lebreton et al. (2017), the top twenty polluting rivers emit 67% of the global total, while Schmidt et al. (2017) concluded that the top ten emit 88–95%. Across multiple studies regarding freshwater systems, the lack of harmonization in the sampling methods for microplastics makes it difficult to compare studies (Dris et al., 2015; Koelmans et al., 2019; Kooi & Koelmans, 2019).

Additionally, the actual environmental impacts from microplastics in freshwater systems remains unknown (Koelmans et al., 2017).

2.2 Separation Methods

The removal of microplastics and other similar particles has been a problem on the minds of many. Various methods have been devised and tested for microplastic filtering. Many of these systems are used for wastewater treatment, potable water filtration, or marine microplastic filtration.

2.2.1 Mechanical Separation

Mechanical separation encompasses the simplest methods of microplastic removal. These processes work by forcing water laden with microplastics (henceforth referred to as "slurry") through a physical filter, usually either a screen or membrane. Screen type filters typically focus on removing larger microplastic particles as they are less fragile than membrane type filters. Because of this, they require less preprocessing of the slurry to remove larger foreign bodies such as sticks, dirt, or other debris.

The Manta Trawl in Figure 6 below is one example of such a system useful for sampling microplastics in the surface layer of the water column. The natural current of the water catches a wing like structure to keep the trawl afloat, while simultaneously forcing water through the fine mesh drag net suspended by it (Hamidian et al., 2021a). The Manta Trawl exemplifies the typical use of screen type filtration systems: slurries with higher concentrations of foreign bodies, such as oceans, rivers, and other outdoor water systems.

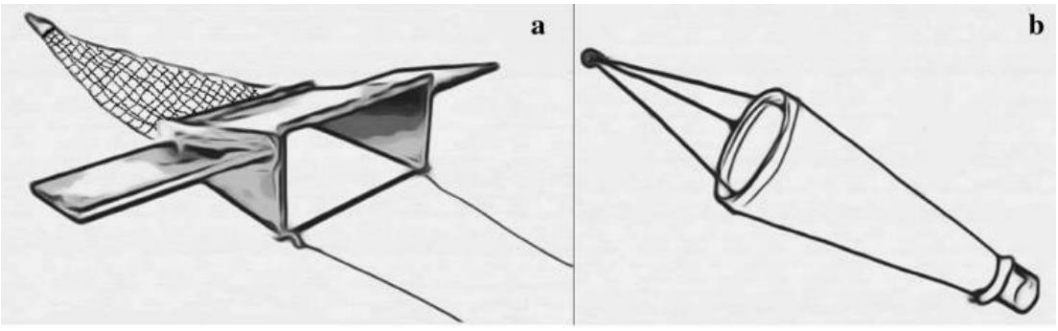

Figure 6. Manta Trawler and Plankton Net. Two microplastic filtering methods. A) Manta trawler. B) Plankton net (Hamidian et al., 2021a).

Membrane filters are more suited for indoor, industry, and research applications. The membranes are thinner and more delicate than screen or mesh filters but can be used to filter much smaller microplastics. Some of these membranes have a filtration size of 0.2 μm, which is significantly smaller than what can be created with traditional mesh (Hamidian et al, 2021b). Because of their efficiency with smaller microplastics, membrane filtration is commonly used in wastewater treatment plants as part of a membrane bioreactor system. Koistinen (2017) examined membrane bioreactors in place at the Kenkäveronniemi wastewater treatment plant in Mikkeli, Finland. These membrane bioreactors are a complex system which combines membrane filtration with suspended biological growth filtration techniques. Overall, this study found that the MBR was able to remove 99.9% of microplastics within the wastewater (Koistinen, 2017). Membrane filters have a longer reuse period and can withstand more use and wash cycles than traditional filter media. However, MBR systems are large and expensive, requiring supporting infrastructure such as pumps and prefiltration.

2.2.2 Coagulation and Agglomeration

Coagulation and Agglomeration processes concentrate the microplastic particles in each sample of water such that they can be more easily removed. This can be achieved by one of several different methods, and results in particle concentration in lumps around a foreign body, or via stratification.

Chemical coagulation focuses on concentrating microplastic particulate into “lumps” using a chemical additive (Lapoint et al., 2020). Typically, this process is used in wastewater treatment facilities. The primary benefit of chemical coagulation is that it can be used along with other processes such as froth floatation or mechanical separation methods. Froth flotation shown in Figure 7 is a process that combines chemical coagulation along with mechanical flocculation as a method of separation (Zhang et al., 2021). Plastics are generally hydrophobic and will link up with bubbles in the material. This method is like the dissolved air floatation filtration method in that air bubbles are used to bring plastics to the surface. However, froth floatation uses chemical coagulants rather than the same degree of air compression in the liquid.

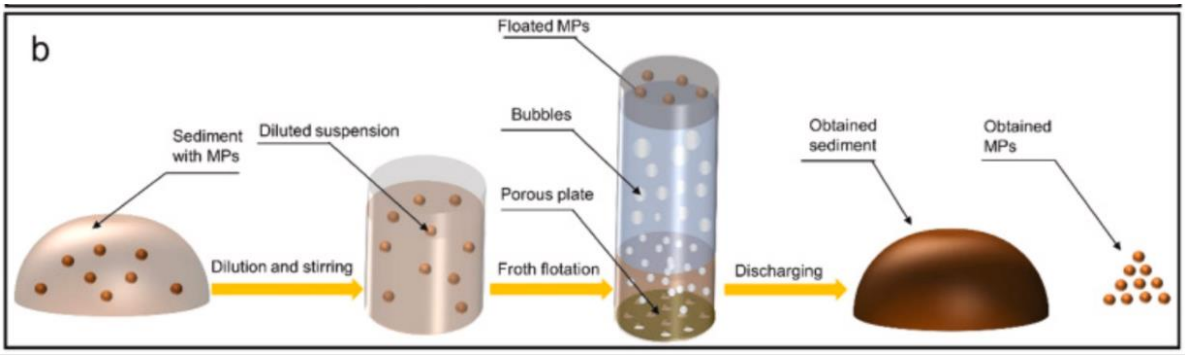

Figure 7. Froth Flotation System. Schematic illustration of the froth floatation system (Zhang et al., 2021).

Micro-submarines, originally developed for oil removal, have also been found to coagulate with microplastics and form chains (Sun et al., 2020). These micro submarines are small, approximately 30um in diameter. These “hedgehog”-like balls that each singular sunflower pollen grains that can be filled and treated with chemicals to have different properties. These particles attract and connect to microplastics and other micro-submarines, forming together in chains which can be seen in Figure 8 below. These micro submarines can also be magnetized with an additional process while being created, allowing them to be manipulated with magnets.

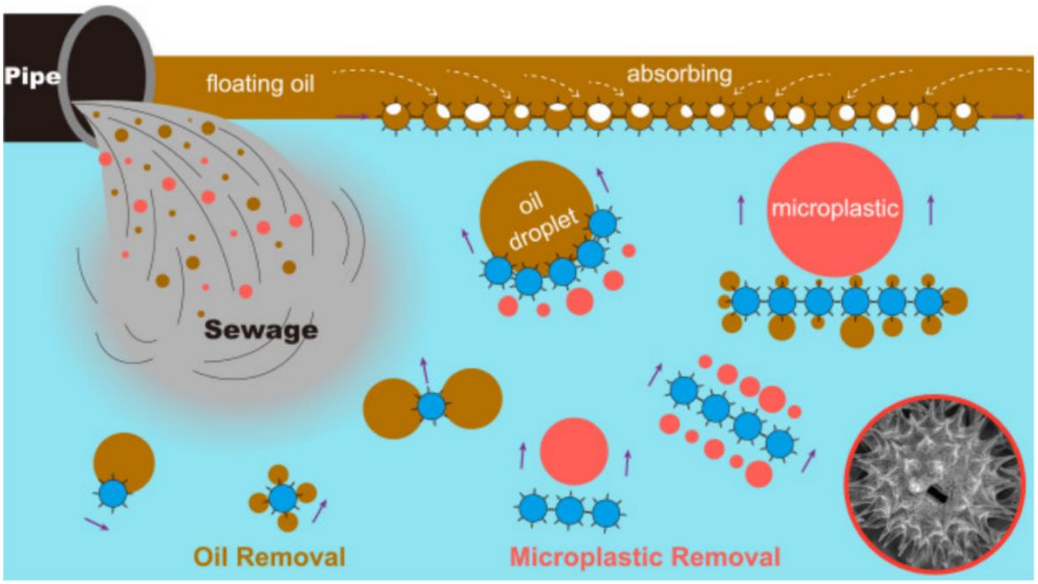

Figure 8. Microsubmarines. Diagram of microsubmarines as used for microplastic removal (Sun et al., 2020).

2.2.3 Density Separation

Density separation relies upon the physical properties of plastics. Many commercial plastics that make up microplastics are less dense than water or can be otherwise altered such that they will float to the surface of water and be collected via mechanical methods such as mesh panels.

The hydrocyclone shown in Figure 9 is a system in which a large amount of water carrying suspended microplastics enters the hydrocyclone, and produces a centrifugal flow (Ruys, 2019). The larger particles move toward the outside of this flow. The finer particles are carried out of the hydrocyclone flow into the upper tube. The lighter microplastic particles are easily separated from the flow. The commercial size of this unit has a foot diameter and requires a flow of 400 gallons per minute at 30 psi. This flow can be adjusted based on the nozzle sizes and overflow and underflow variations. This device is currently being used for wastewater treatment and is seeing increased usage and design iterations in commercial fields.

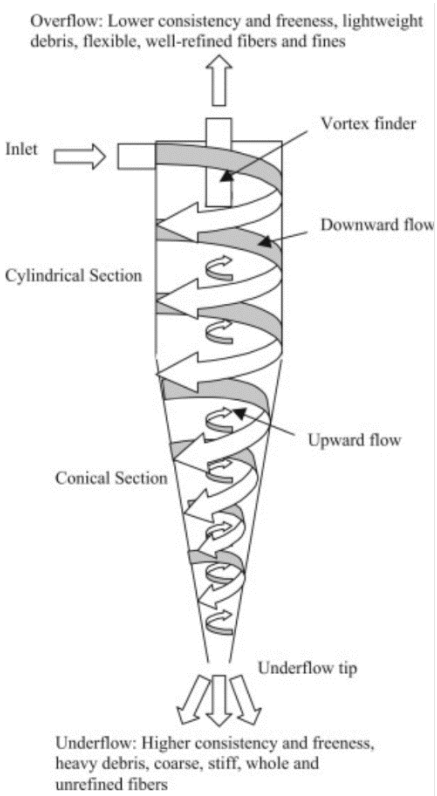

Figure 9. Hydrocyclone. Hydrocyclone diagram, displaying the main components of a working system (Ruys, 2019).

The dissolved water density floatation technique and technologies are commonly used for separating microplastics from soil as seen in Figure 10 (Li et al., 2021). The soil is mixed into a water and sodium bromide solution. Based on their density, the floatation levels will be different for the soil and different densities of microplastic particles. This device incorporates a circulation system and has plastic particle recovery rates ranging from 92% to 99.6%. The testing included biodegradable and non-biodegradable microplastics within a range of typical microplastics sizes and densities. Recovery was slightly better when the particles were denser and larger in diameter.

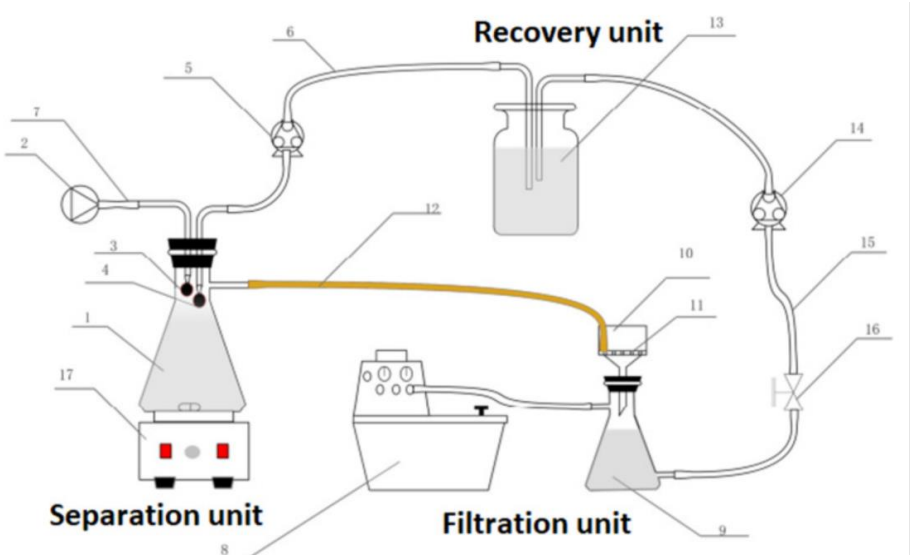

Figure 10. Microplastic Separation. Diagram of soil microplastic extraction and separation (Li et al., 2021).

Dissolved air filtration is primarily used in the final stages of wastewater treatment (Koistinen et al., 2017). For use with microplastics specifically, the chemical used would be polyaluminum chloride, which would be added to the wastewater to be treated and increase flocculation (Koistinen et al., 2017). Coagulants help particles join to form larger particulate groups, making them more able to bond to dissolved air bubbles. (Lapoint et al., 2020). Water is saturated with air at a high pressure, producing microbubbles similar to carbonation. The air bubbles stick to the solids and cause them to float to the surface, where the particles can then be removed more easily from the surface via mechanical processes. This method was found to have a ninety-eight to ninety-nine percent success rate in the wastewater tests when using this flocculation chemical (Shen et al., 2022).

2.2.4 Oil Film Separation

Oil film separation relies upon the same principles as chemical coagulation does. This separation uses mineral oil to extract microplastics from soil suspended in water which can be seen below in Figure 11. The oils adsorb to the microplastics and separate from the water and soil. Oil film, along with chemical coagulation, can be used in concert with additional and supplementary mechanical separation and collection techniques (Kim, et al., 2022).

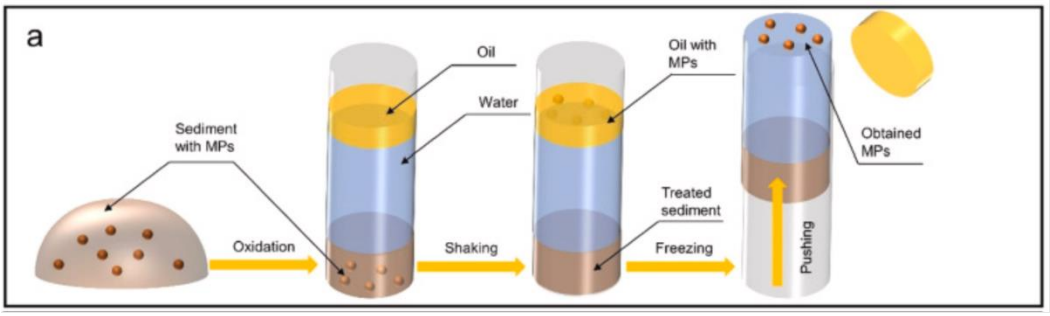

Figure 11. Oil Film Separation. Schematic illustration of the oil film separation system (Zhang et al., 2021).

2.2.5 Magnetic Separation

Magnetic separation, also known as electrocoagulation, is used in a multitude of ways to remove microplastics from water. A few types are wet electrostatic separation, ferrofluids using oil, and electrocoagulation. Ferrofluids are a nontoxic magnetic liquid that consists of oil and magnetite suspension like iron oxide powder. Ferrofluids, much like chemical coagulants, stick to the microplastic particles, and then can be fished out of the water using a magnetic system.

Wet electrostatic separation uses a conductive filter and power source. This mechanism runs current through metallic filter meshes, to increase the efficiency of physical collection methods (Quan, 2018). This method relies on the electrostatic interaction between the anode and cathode, and the latent charge that already exists within microplastics. This charge comes about from the microplastics' interaction with the environment as they meet other charged particles and as they break down, releasing energy (Shen et al., 2022). These combined factors allow the plastics to be easily attracted to electrically charged metal meshes. Figure 12 shows how an electrostatic metal separator works which is very similar to a wet electrostatic separator system.

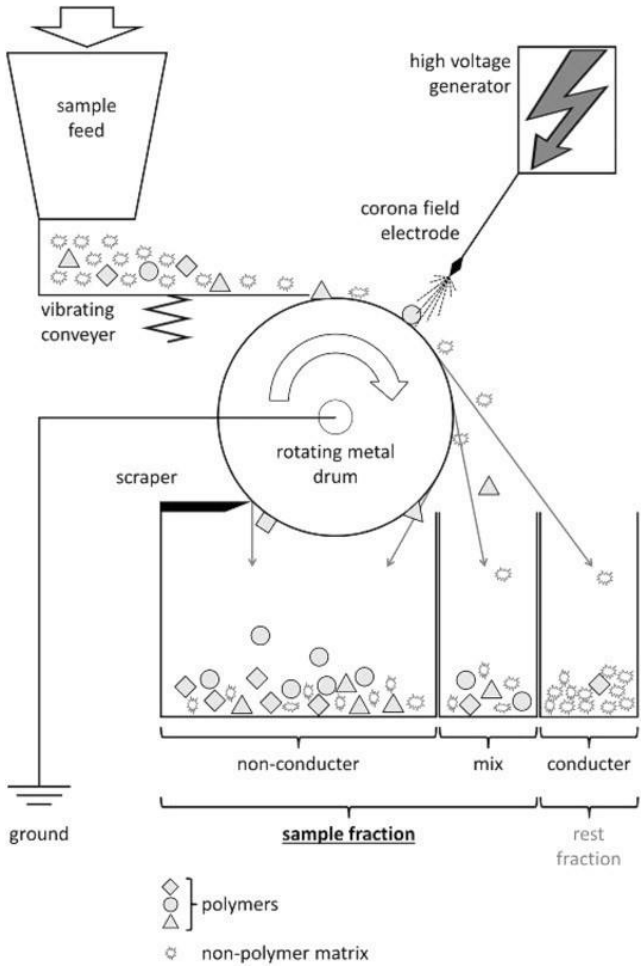

Figure 12. Electrostatic Metal Separator. Demonstrates how conductors and non-conductors can be separated via electrostatic separation (Felsing et al., 2018).

Electrocoagulation is a highly known method that focuses on using an electrical field to create coagulant electrically from metal electrodes shown in Figure 13. These coagulants are then presumed to encounter microplastics making a simple and robust method. Studies show that there is over a ninety percent removal of microplastics in wastewater streams with pH ranging from three to ten. This treatment process is known for having low capital costs, environmental compatibility, energy efficiency, sludge minimization, amenability to automation, and cost effectiveness (Perren, 2018). Unlike other methods, electrocoagulation does not use chemicals or microorganisms because they can cause significantly harmful effects to the environment.

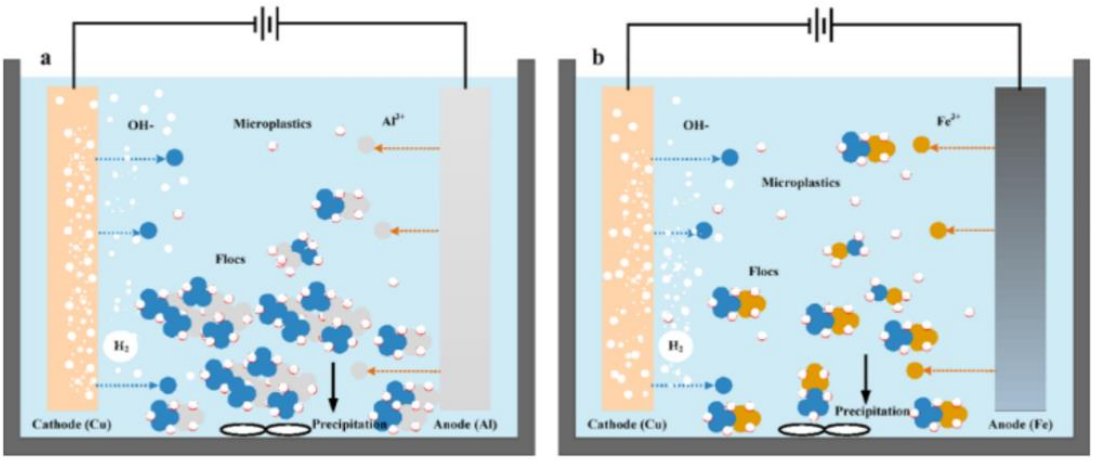

Figure 13. Electrocoagulation. Mechanism of microplastic removal from water by electrocoagulation process (Shen et al., 2022).

2.3 Conclusion

Technology is beginning to catch up to the rapidly increasing danger which microplastics present. Despite this, there is still a large gap between the pervasiveness of microplastics and our ability to remove them. One of the largest gaps is the lack of research and production in microplastic removal systems for large and small freshwater bodies. Our team has decided to focus on designing a small scale microplastic separation system which can selectively filter microplastic particulate without harming the ecosystems it is deployed within.

3. Initial Design

To begin constructing and ideating upon our initial designs, we began by breaking the entire system into subsystems that would each focus on a vital component. The main categories that were desired for the design included intake, separation, rinse, and collection. Each subsystem went through multiple iterations in order to find the most optimized designs that our team was capable of building with the time, tools and budget available to us.

Each subsystem had specific goals, which helped guide our iterations and thought process while designing them. The intake subsystem would allow the water and small particulate to flow through while preventing large objects like sticks from entering. Following this a filtration system would be needed to separate microplastic particulate from the water flow. Once the microplastics were separated there would be a subsystem to remove the microplastics and transfer them into an easily accessible collection box. The last subsystem is the collection box which needs to be able to be accessed often and conveniently.

3.1 Filtration Iterations

After researching the various methods to remove microplastics and small particles from water, we began designing a separation system that would incorporate these methods. Our plan of action first involved comparing the methods of filtration and removal as explored in the Background. Then, we planned on building and function testing the system. Current supply chain complications impacted our ability to acquire parts for mechanical and feature testing. We also had to consider the complexity of these filtration and removal systems, and the difficulty in finding the resources for these filtration methods. Many of these methods are still new, patent protected, or only found in foreign markets.

3.1.1 Pugh Matrix

In the Background, we explored a variety of methods to remove microplastics, like mechanical, density, chemical, and magnetic separation. The process of determining which separation method to iterate upon presented challenges, as the data about these methods was not readily available and decisions about our specific application had to be made based on combinations of publications on the topics and methods.

We used a Pugh matrix to rank essential properties of each possible filtering method on a scale from one to five. A five indicated a more positive outcome from that category, while a one indicated a more negative outcome. For example, a five in the "Readiness of Method" category as seen in Table 1 would indicate that this method is used in many commercial applications, and perhaps could be purchased by an average consumer. We judged these separation methods based on the use these systems had seen in the past, their efficiency at removing particulate, the readiness or off-the-shelf compatibility of the product, the physical size of the system, the ease of fabrication, the environmental impact, and the amount of maintenance needed to continually run these systems over long periods of time. All the above-mentioned categories were then given a weight to accentuate the importance of certain factors over others. These weights ranged from 0.25 to 1.

After careful consideration while ranking these systems, we eliminated all but the top three contenders: the dissolved air floatation, the hydrocyclone, and the electrostatic separation. Eliminating other methods allowed us to research and focus more specifically on the three individual methods. These top ranked methods are highlighted green in their final rankings on Table 1, and all have similar scores for the highly weighted categories. Of these top three methods, wet electrostatic separation has seen the least amount of prior use, which presented a challenge when finding data. Despite this, electrostatic separation ranked well in having a low environmental impact, which was an important factor in determining our final system.

A vital requirement for our system was to have a minimal impact on the environment. We knew that for our final prototype to have a positive impact on local ecosystems, we could not implement physically large systems, introduce new chemicals or other non-native particulate, or drastically alter the natural environment in other ways.

A large system may redirect water flow, disrupt the life cycles and habits of local species, or make the location undesirable for humans to visit. Chemical coagulants, such as the ones discussed in the Coagulation and Agglomeration section of the Background, would likely be harmful if they came into contact with animals, either through surface contact or via ingestion or inhalation. Even some normally non-reactive materials could become dangerous in outdoor environments, such as metals corroding in water, or plastics used to create the system which could get broken down in moving water. Physically large or noisy systems would be likely to cause species sensitive to these factors to move away. Similarly, altering the environment, such

as building foundations or installing large housings could disrupt the ecosystem. The environmental impact became a large component of our decision making when looking between our top three contenders, based on our Pugh Matrix results.

Table 1. The Pugh Matrix shows the weights and scores of the efficacy and viability of various microplastic filtering options we researched.

Separation Method	Readiness of Method	Environmental Impact	High Amount of Past Use	Particulate Removal Efficiency	Ease of Fabrication	Physical Size	Maintenance	Total
		5 low impact				5 smaller	5 low	Max: 22.5
Weight:	1	0.9	0.8	0.8	0.5	0.25	0.25	2.6
Dissolved Air Floatation	4	4	4	5	4	3	3	**18.3**
Wet Electrostatic Separation	4	5	3	4	3	5	3	**17.6**
Hydrocyclone	4	3	5	4	4	3	3	**17.4**
Centrifugal Separation	4	2	4	4	3	4	4	15.7
Density Separation	3	2	4	4	4	5	4	15.45
Micro-Screen Filtration w/ Disc Filters	4	2	4	4	3	4	2	15.2
Ferrofluids	3	3	2	4	4	5	4	14.75
Membrane Bioreactor	3	1	4	5	3	4	2	14.1
Filtration	3	3	2	4	3	4	2	13.5
Rapid Sand Filtration	4	1	4	5	1	1	1	13.1

Hydrocyclone technology was promising because of the amount of past usage and data that was available to us. Through further research, we decided this was not the most viable option because it would have to be a relatively large system and involve complex fluid mechanics simulations. These factors made it incompatible with our project timeline and budget. The intake would have to be dozens to hundreds of gallons per minute, as this system requires a large amount of water pressure, even at a scaled-down size (Ruys, 2019). This would not be viable in a small pond, lake, or stream such as we are intending this project to be used in. The sort of power required for this system would also be difficult to provide to remote locations that are not directly near a power source. Additionally, we discovered that this system would only

concentrate the microplastics and water into a denser slurry, rather than completely separating the plastics from the water (Borgia, 2021).

Dissolved air filtration was first appealing to us due to the reportedly high success rate in wastewater treatment plants. The mechanical components of this system also appeared easily scalable and would cause a minimal disruption to the environment. However, after we completed the Pugh Matrix and began to analyze the system in more detail it became evident that a chemical coagulant would be needed. This process would not be viable for our project, as we are mechanical engineers and have a minimal background in chemistry. Therefore, we would not be able to ensure that this chemical coagulant would not leak out into the environment in a harmful matter.

Our next highest ranked system, electrostatic filtering, is not a highly tested or researched system compared to the other two top ranked systems. Despite that challenge, electrostatic filtration does have the benefit of portability, scalability, ease of manufacturing, and a low environmental impact. Though past systems and our final design are made of materials such as plastic and copper, we determined that the long-term environmental benefits of the system will outweigh any potential breakdown of the plastics used in the intake, filter, or collection box design. This system does not require a large footprint or chemicals in the system in order to properly collect the microplastics from the surrounding water.

Electrostatic separation was the most suitable method because of its environmental neutrality and scalability, but we wanted to augment it with a method which could provide better filtration quality and easier ways to collect the particulate. By adding disc filtration after electrostatic separation, we could gain the benefits of the easy plastic collection while avoiding the negative environmental impacts that disc filters as a primary filtration method would present.

3.1.2 Electrostatic Iterations of Design

The first system we designed attempted to capitalize on the selective separation provided by electrostatic technology and the reusability and ease of collection provided by disc filters. After passing through the intake, water would flow through several electrostatic towers composed of charged copper mesh which would separate out the plastic particulate, shown in Figure 14. After a set time period, the chamber containing the mesh towers would be sealed and drained so that the system could proceed to a rinse cycle. During the rinse, cone shaped spray

nozzles would wash down the electrostatic towers with water from an onboard closed loop reservoir. This new slurry would theoretically be laden only with plastic particulate and would pass downwards through the rows of disc filters, which would periodically rotate and be cleaned by scrapers into a collection bin.

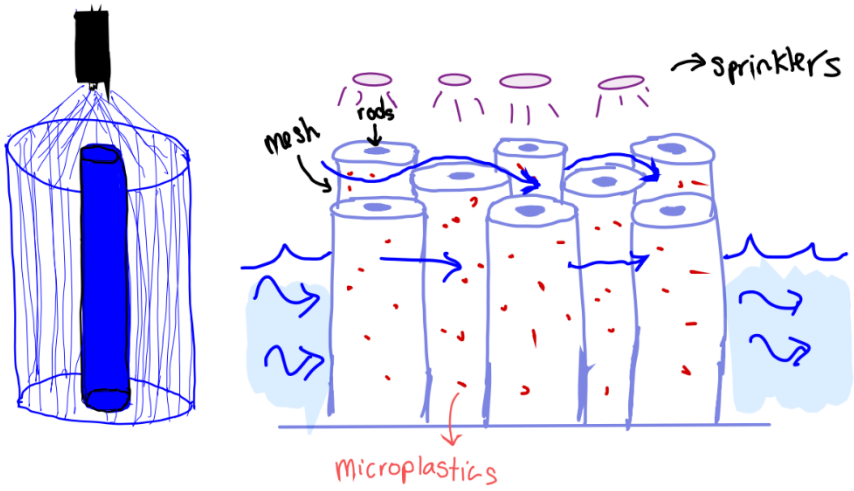

Figure 14. Electrostatic Towers

The crucial issue with this iteration of the design was its overcomplexity. Issues with unneeded complexity stemmed from the closed loop rinse process and the idea of multiple simultaneous stages. To maintain a closed loop rinse reservoir, plumbing and pumps must be installed and held within the device. Additionally, the closed loop water rinse meant that the main separation area needed to be completely sealed and entirely drained prior to the start of the rinse stage. This sealing and draining would necessitate the frequent use of several individually actuated valves, increasing onboard power consumption. Draining the chamber while the entire device was below the waterline would require a positive pressure displacement subsystem using compressed air. While we did later consider having an onboard compressor with this design, it ultimately was scrapped before this subsystem was ever designed. The necessary vertical arrangement of the disc filters presented additional challenges. The water would have to be kept from resting on top of the disc, which would cause water to flow into the plastic collection bins.

Several further design iterations were created to solve this problem. First, as seen below in Figure 15, the idea to tilt the discs was posited. Then the team supposed that a seal could be

manufactured to bisect the disc, effectively isolating the cleaning process from the rinse slurry flow. The two designs were combined, but concerns about seal degradation and accurate manufacture during the project were severe downsides to consider.

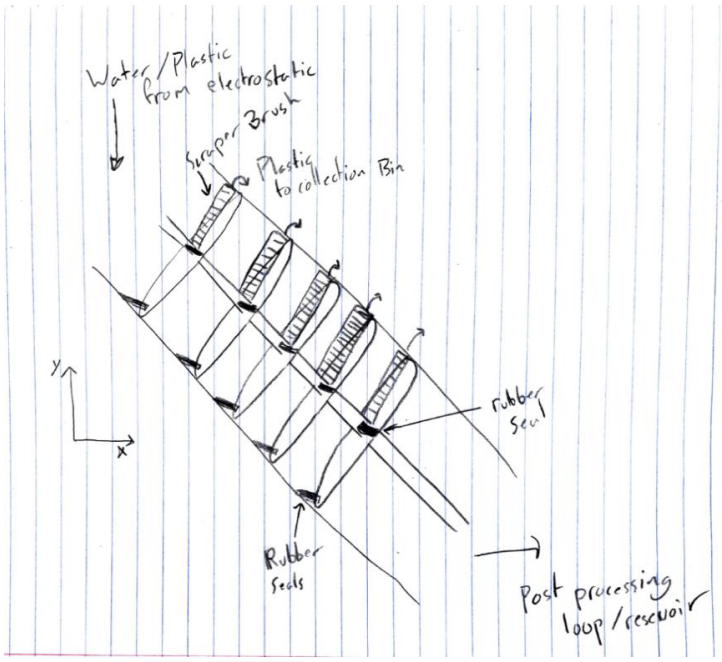

Figure 15. Disc Filter Modifications. This figure shows the intended angling of the disc filter subsystem, but also shows the first attempt at the idea of seals to prevent water from reaching the scraper brush on the opposite half of the disc.

This new assembly relied on two major assumptions. The first was that the amount of non-plastic charged particulate in any given body of water is negligible and thus will not be the cause of a significant amount of non-plastic accrual on the electrostatic towers. The second was that the weight of the water and plastic slurry from the rinse stage would provide enough pressure for the water to be pushed through the disc filters. If this design were to be built, and field testing revealed that sediment, algae, or other particulate naturally in the water column were also attracted to the electrostatic towers, the disc filters would foul much more quickly than expected. Additionally, if the weight of the rinse slurry was not enough to force the water into draining through the filter, the accumulation would make simultaneous cleaning of the filters nearly impossible, and the function of the entire system would be severely impeded. These main issues, combined with concerns about manufacturing time in the scope of this project, the

effectiveness of a simple single intake in murky or vegetated water, and the possible redundancy of a secondary filtration loop inspired the team to step back to our core concepts and revise our iterations.

When consulted about the challenges inherent in the disc filtration system, our advisor suggested that we investigate belt filters as a possible solution. As we researched belt filtration in the context of a secondary subsystem, we concluded that this method could provide certain benefits over disc filtration. The inversion of the filter media presents opportunities for particulate collection that disc filters could not, and variable length allowed for further separation of the rinse slurry flow and plastic collection. However, belt filters simply exacerbated the sealing problems which the disc filters suffered from. Without a way to seal the belt and ensure that water wasn't allowed to bypass the filter media, plastics could bypass the belt filtration and build up in the closed loop rinse system, to the detriment of the sprayer nozzles. The first iteration of sealing the belt in order to control water overflow involved creating a single downtube, with slots machined on either side to allow the belt to pass over a gasket and through the downtube. However, these slots would require custom gaskets. A fit tight enough to prevent water losses might also keep plastic particulate within the downtube. The mesh belt filter itself could also eventually abrade the gasket until it no longer functioned, creating shredded microplastic debris in the process.

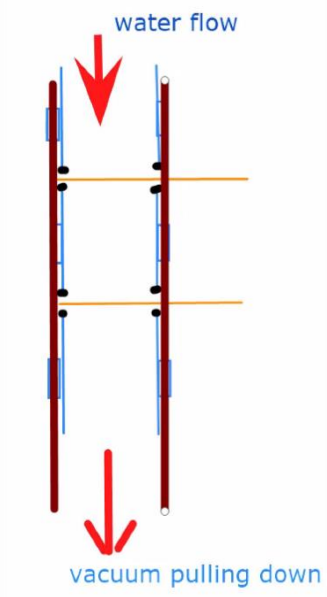

Figure 16. Down Tube for Belt Filtration. This diagram illustrates the individual pieces of tubing for the down tube, with the guide rails and sealing surfaces in place.

A complex system, shown in Figure 16 above, was designed to combat these issues. This design added a vacuum pump, vertical guide rails, and several sealing surfaces. It also amended the belt filters such that they were stationary during the filtering process rather than constantly rotating. Pieces of downtube (shown in blue, vertical), each constrained in the vertical axis by the guide rails (dark red, vertical), would be supported by weak springs such that the belt filter (gold, horizontal) could pass smoothly along the sealing surfaces (black, small dots) without abrading them. The rinse slurry would be held above the downtube by a valve until the system was ready to process it. At that time the vacuum pump would create negative pressure in the downtube, sealing the individual pieces against sections against the belt and each other. Then the rinse slurry would be released and pulled downward through the belts, filtered, and then replaced into the rinse reservoir. This system benefitted from the vacuum, ensuring that water from the rinse slurry would be compelled fully through the filtering mesh. The spring support of the downpipe sections also allowed the belt to move unimpeded once the filtering process was over, meaning that the loss of plastic particulate in this area and the abrasion of the sealing surfaces would be kept to a minimum.

The secondary filtration system poses many theoretical, mechanical, and manufacturing hurdles. Considering these challenges, we felt the secondary filtration system's benefits no longer outweighed its drawbacks. The electrostatic system would determine the percentage of plastic particulate successfully separated from the incoming water, and in effect the secondary system was an increasingly complicated way of getting that particulate off the electrostatic system and into a box. With this in mind, we refocused on the initial electrostatic separator, with an emphasis on simplicity. While an additional belt filtration system may be redundant, we realized that using belts as the vehicle of our electrostatic technology may allow us to simplify the design greatly.

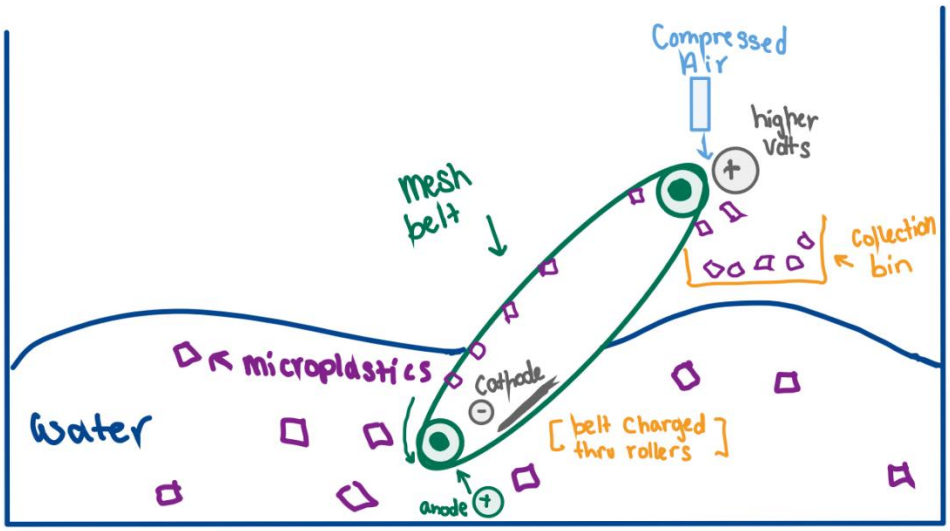

Figure 17. Rudimentary Electrostatic Belt

Figure 17 above shows the rudimentary sketch combining belt filtration and electrostatic separation. Manufacturing the belt out of copper mesh for good conductivity and passing water through the angled belt allowed for separation of the plastics and deposit in the collection bin within one range of motion. The belt would capture the particulate and carry it upwards out of the water, where a compressed air nozzle would clean the particulate into the collection bin. We considered briefly the need for a more strongly charged anode at the apex of the belt to allow for easier cleaning. After some consultation with Noel Lange, the author of our foremost research on electrostatic separation (Lange, 2018), and our own testing we determined that this anode would not be necessary.

Progressing with this design in mind, we had some concerns about the continued ductility of fine copper mesh when tensioned as a belt and cycled continuously. If the belt work hardened from repeated strain and then catastrophically failed, the entire system would be halted. As such, we decided that the copper mesh should not be in any way structural to the belt. In lieu of a simple piece of wide copper mesh two timing belts would be used, with pieces of copper mesh bridging between them. The use of multiple thin strips with gaps between them would limit the strain put on the belt during use. This presented a new challenge, however, in that the mesh strips would need to be secured to the belts while retaining their flexibility. Thus, the next step of our design iterations was conceived.

The next iteration of the belt system sought to solve these challenges by creating paddles perpendicular to the belt upon which the copper mesh could be attached. The paddles provided a greater surface area for electrostatic interaction, while also minimizing the area of the belt which would be made inflexible by the adhesive. The paddles themselves would be attached to the rubber belt by means of a 3D printed L-bracket. The cathode needed to be redesigned, as it would no longer provide a negatively charged surface area close enough to the anodes. In its place, the paddles were given an additional piece of mesh on the opposite side, allowing the cathode and anode to remain a fixed distance apart throughout the belt's rotation. A preliminary drawing of the electrostatic paddles is shown in Figure 18 below.

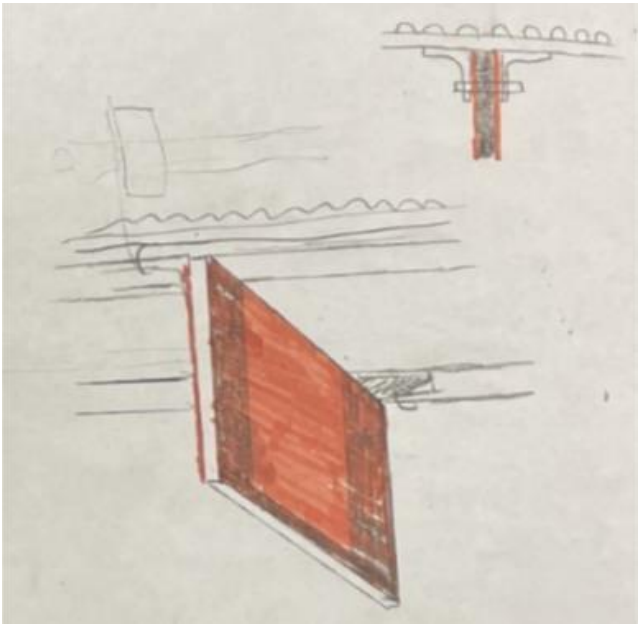

Figure 18. Drawing of Electrostatic Paddles. This drawing illustrates the interior rubber structure with the bridging piece away from the belt. In the final design this orientation has been reversed.

This iteration became the working foundation for the remainder of the project. The electrostatic chamber was simplified to a rectangular box by the omission of the secondary filtration systems. To streamline manufacturing we designed a frame, which could be assembled outside of the electrostatic chamber and then placed into it.

3.1.2.1 Power Rail Iterations

When the electrostatic system was redesigned from towers to paddles the design of the power supply had to be redesigned as well. The electrostatic mesh would now require either a stationary power source in the form of rails which would be contacted while the paddles were submerged, or a mobile power source which could accommodate the paddles' full range of motion. Initially, we decided to design a stationary set of power rails. The rails would be fixed to the sides of the electrostatic chamber and would stretch the entire length of the paddles' submerged travel. This design would also require a brush attached to each side of each paddle, such that connection could be made to both cathode and anode. This design did require that the paddles be stiff enough to maintain strong electrical connection with each rail.

To avoid these issues, we designed moving rails which could follow the path of the paddles exactly. These rails are a secondary set of belts, made from woven copper solder wicks. The belts are carried along smooth pulleys at the same rate as the electrostatic paddles, and a loop of wire soldered to the mesh paddle transfers power from the rail to the paddle mesh. Each belt has two nonconductive 3D printed pulleys and one stainless steel conductive pulley. The conductive pulley for the cathode rail is located on the bottom rear axle, and the conductive pulley for the anode rail on the top rear axle. Both axles have a spring-loaded carbon brush to maintain the electrical connection between them and the rotating axles.

3.1.3 Conclusion

After comparing each of our researched filtration and separation methods in a Pugh Analysis, we selected electrostatic separation as our main microplastic removal because of its environmental neutrality and scalability. We also wanted to take advantage of another method's easy collection, so we designed an initial system augmenting electrostatic towers with disc filtration. Due to overcomplication, system fragility, and several other factors, we eliminated the secondary filtration system and redesigned the electrostatic towers as electrostatic paddles supported by a timing belt. The subsystem is powered by an independent set of custom power rail belts.

3.2 Intake

The intake system's purpose is to ensure that foreign bodies or biological matter large enough to hamper the operation of the filtration system are prevented from entering the electrostatic chamber. However, the exact criteria that the intake system sought to meet evolved with the changes made to the main filtration system, as these changes impacted the necessary flow and preprocessing requirements. The system began simply as a conceptual representation shown in Figure 19.

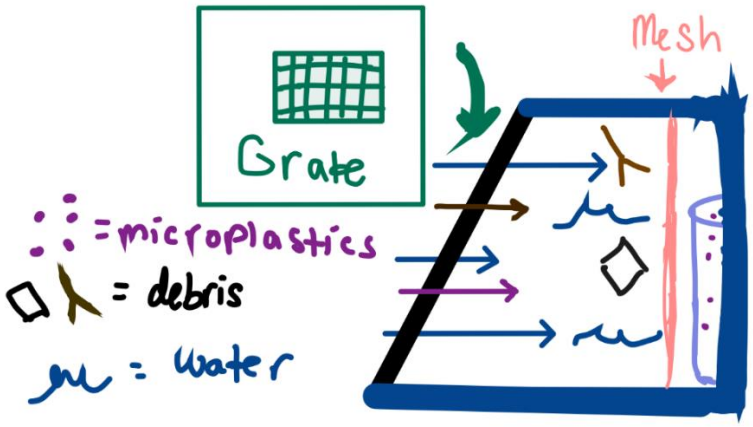

Figure 19. Initial Intake System Sketch.

3.2.1 Intake Iterations

The first intake iteration consisted of a simple stainless steel grate which would only allow small objects of about 6mm or less through, followed by a finer mesh. As we narrowed our research and decided to focus on electrostatic separation, we realized that we could focus on particulate in the 10-500 micron range and modified the intake systems accordingly. In place of an initial grate and following finer mesh, we decided to use two fine stainless mesh screens, each with a pore size of 600 micron. This way, we could eliminate the possibility of relatively larger debris which could potentially damage the much softer copper mesh used in the electrostatic system. We also wanted to ensure that the system could clean itself of debris blocking the initial screens. The system shown in Figure 20 is an early attempt at designing such a system, which had a simple single intake composed of large metal grating and a much finer mesh screen which could be removed to be cleaned.

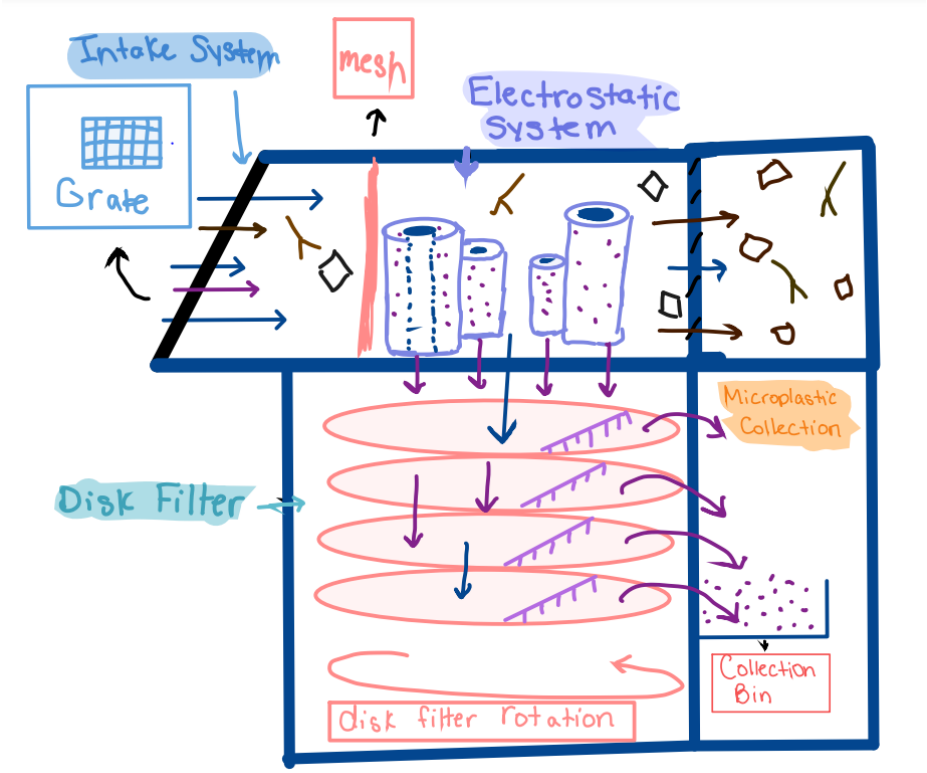

Figure 20. Initial Full System Design

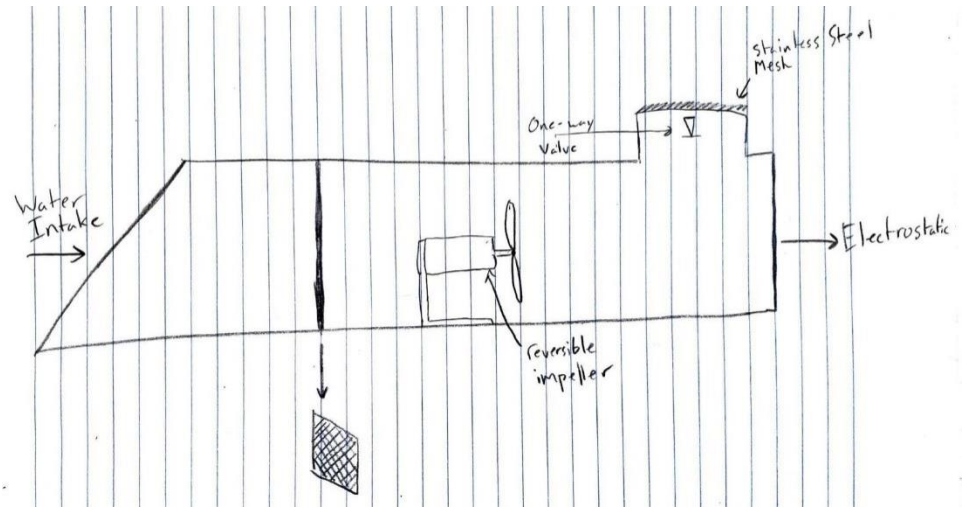

Figure 21. Initial Self-Cleaning Design. This picture shows the initial concept for a single intake with the impeller, single-directional valve, and rear intake port.

The single intake system shown in Figure 21 would be capable of backflushing the intake screen by closing the valve leading to the electrostatic chamber, reversing impeller direction, and drawing water through the secondary screen and single-directional valve located downstream of the impeller during normal flow. In this way water without debris could be used to flush the system without allowing any debris to be trapped behind the initial screens. While this design could have been effective, we thought that the inefficiency of running the impeller backwards combined with reliance on a single-directional valve for long periods of submersion merited a redesign.

Our next iteration of the intake system, shown in Figure 22, replaced the single-directional valve and accompanying mesh screen with an additional intake tube, an additional impeller, and a three-directional ball valve. In total, this system had four stages.

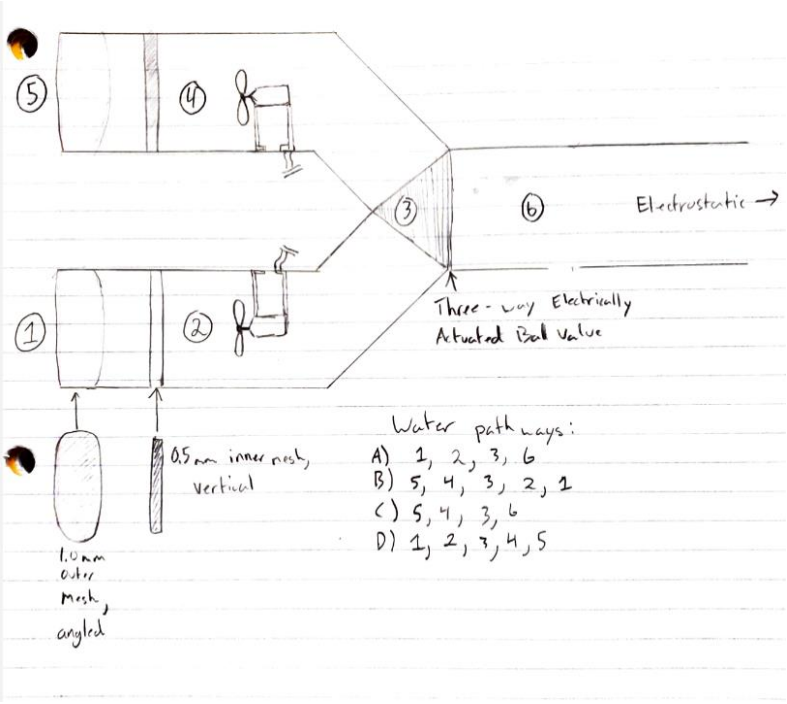

Figure 22. Dual Intake System. This iteration of the dual intake system includes the three-way ball valve. The flow of water in each of the four stages is indicated below the drawing.

In this version of the system, only one of the intake tubes would be operated during normal use. The three-directional ball valve would allow flow motivated by impeller (2) from the first tube into the electrostatic chamber at this stage. After a set time interval which could be

determined based on the properties of the water the system was implemented in, the valve would isolate the electrostatic chamber, and water would be drawn by the impeller (4) through the second intake tube, effectively back flushing the first. The system would then operate as it originally had, simply using the other intake tube. After another cycle, the backflush stage would run in reverse. The only change made to this design before prototyping was the replacement of the three-directional ball valve with three traditional "on-off" ball valves, shown in Figure 23, in order to comply with budget constraints.

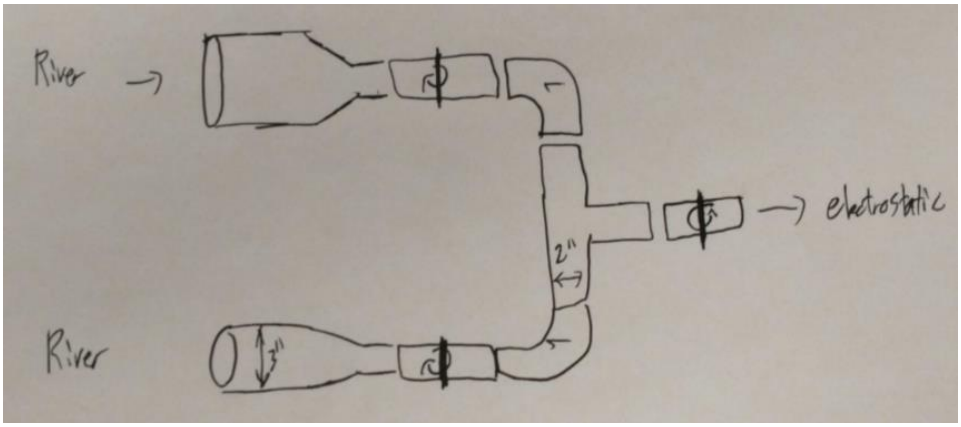

Figure 23. Pre-CAD Modeling Intake Sketch. This sketch omits the impellers and mesh screens and illustrates the intended rough design with ball valves and off-the-shelf PVC parts.

3.3 Pneumatics

The onboard pneumatic systems were introduced during the redesign of the filtration system. Originally the plastic particulate would have been scraped from the disc filters into collection bins or dropped from the belt filters, but for electrostatic paddles a new subsystem was necessary. We decided that compressed air would be the best way to remove plastic particulate from the electrostatic paddles. The air would need to be delivered over the entirety of the paddles' width and be focused enough to direct the particulate without spreading it throughout the electrostatic chamber.

3.3.1 Pneumatic Iterations

To best satisfy the requirements of our pneumatic subsystem, we decided to use an air knife with compressed air to blow the particles off the mesh paddles into the collection box. We

chose to purchase a COTS (commercial off the shelf) air knife for our application. The mounting for this air knife was chosen to be within the electrostatic belt assembly, primarily so that the airflow could be properly directed.

3.4 Collection Box

The collection bin had the least stringent requirements of any subsystem. In the initial designs, the collection subsystem was a simple rectangular bin with a collection box. However, when the pneumatic system was added to remove the plastics from the electrostatic paddles a more complex assembly was needed to accommodate the design. Therefore, the bin was altered to have an exit for the air, this helped with the air flow and pressure creating no room for the air or microplastics to transfer into the electrostatic system.

3.4.1 Collection Box Iterations

Once we had established compressed air as the mode for moving the plastic particulate off the electrostatic belt, we knew that a simple collection bin would not suffice. The current of high-pressure air would agitate the light plastic particulate, possibly re-distributing them into the electrostatic separation chamber past the separation device, and thus beyond the reach of the paddles. To combat this, we developed a bin with a series of removable mesh panels, made with decreasing pore sizes. Initially, this was a simple box, with no air outlet, and a series of curved mesh panels that could be slid into and out of the box from the side. The curve in the mesh panels was intended to guide the flow of air, directing the particulate downward and encouraging the air flow to spiral in a way that would keep particulate in the collection bin, rather than pushing it out. We realized, however, that the slots used to slide the mesh into and out of the bin would allow air and plastic to escape. We also realized that without a pressure relief system in the collection bin, there would be almost no way to ensure that the flow went in the direction we intended. As such, the collection bin was redesigned. The finalized version incorporates the flow and path of the plastics which is shown in more detail in Chapter 4.

3.5 Mechanical Linkage

With the addition of the pneumatic subsystem, a method of timing the application of compressed air to the passage of the paddle in front of the air knife was necessary. We knew that

we wanted to only have one drive motor for these systems, so the goal became finding a method of linking the rotation of the drive axle to the opening and closing of the pneumatic subsystem.

3.5.1 Mechanical Linkage Iterations

The main purpose of the mechanical valve assembly is to power the belt system, while at the same time actuating a valve that supplies compressed air to the air knife for spraying microplastic particulate off the paddles. Since the belt contains multiple separate paddles, and travels at low speed, it was clear that we needed a method for turning the supply of air to the air knife on and off each time a paddle moved across the collection box. Without such a shut off, the onboard compressor air reservoir would need to be much larger, and the compressor would require more power. For the movement of the belt, we wanted to have a way to change the speed of the belt subsystem so we could find the ideal speed for the system to move. Since the timing of the air blasts would need to be timed with the speed of the belt, we chose to create a mechanical linkage that could actuate a valve that was according to the speed of the motor. Our team looked into different designs for mechanisms that would allow us to mechanically actuate an air valve. Figure 24 below shows our first prototype. This design consists of a combination gear with teeth on the outside, and a partial set of teeth on the inside. The outside of the gear connects to a drive motor that would be attached to the drive axle of the filtration assembly. The inside teeth turn a gear mounted to the stem of an air valve (with the valve being in front of the gear shown in Figure 24) actuating it only once during one rotation of the ring gear. The valve would then be closed using a spring. This system would allow the opening speed of the valve to be controlled based on how large the valve gear was.

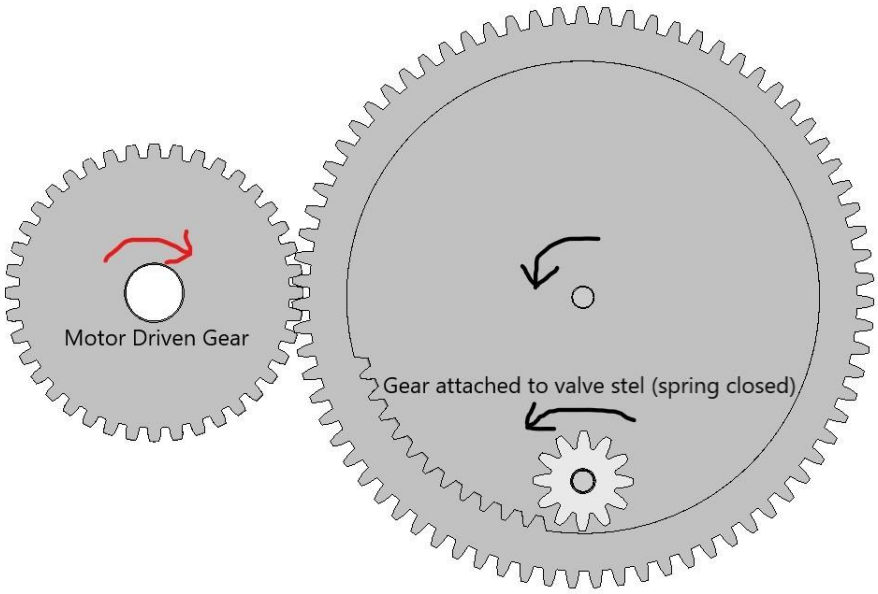

Figure 24. Prototype Valve Gear Mechanism

The second design we investigated was a linkage design, inspired by a non-collinear valve actuation mechanism shown below in Figure 25. This mechanism is actuated with a pneumatic piston (Figure 25, reference 43), and uses a Belleville return spring (Figure 25, reference 57) as the closing actuation for the valve.

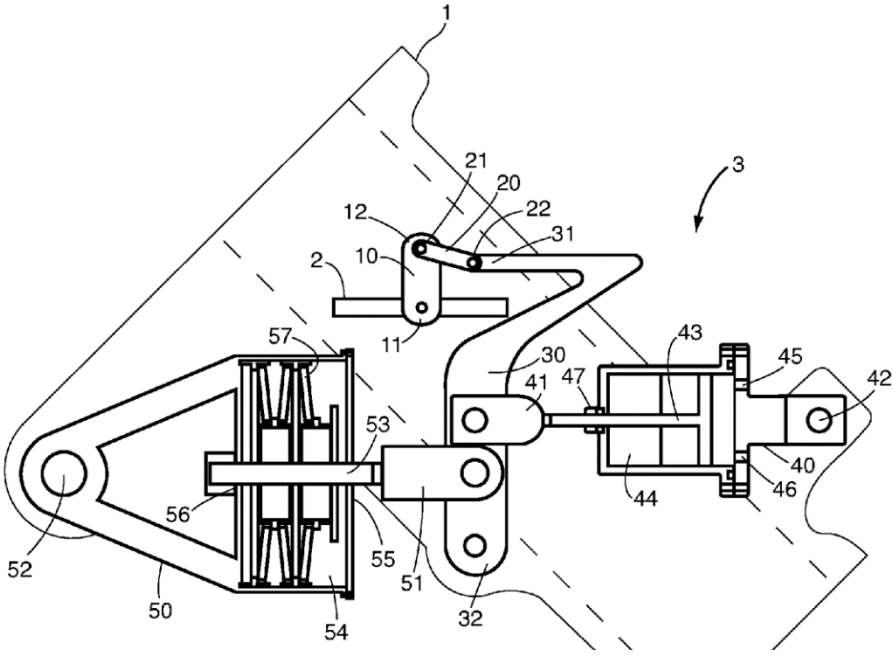

Figure 25. Non-collinear valve actuator (Richard, 2012)

We chose to create a modified 4-bar linkage for this task, inspired by the mechanism shown in Figure 25. Our final design is based on a standard 4-bar crank-rocker style linkage, with a pin-slider joint and an extension spring to close the valve. The mechanism has two major sections which are explained in more detail in Chapter 4 Final Design.

3.6 Conclusion

After finalizing each of the subsystem designs in this chapter, all parts were incorporated into a singular CAD model. Each subsystem mentioned earlier in the chapter went through several iterations, culminating with our final design. The intake system has three actuated ball valves. Inside the electrostatic chamber is the filtration system, with mesh panels that attract microplastics as they travel along a conductive copper rail. The air knife at the top of the belt system blows the particulate off the mesh into the collection box system. This is the design that was assembled and feature tested as detailed in following sections.

4. Final Design

This design section shows detailed explanations and calculations for what was needed in order to successfully complete our subassemblies and why the components were chosen to prepare an accurate and functional microplastic removal mechanism. The calculations shown in the analysis sections of this chapter influenced our design criteria when determining the qualities sizing of components. Section 4.3 Mechanical Linkage & Air Nozzle System details the design and layout of the mechanical linkages used to move the belt assembly, along with powering and correctly timing the air knife system.

4.1 Filtration System

Figure 26. Frame with Belts CAD Model

Our final CAD model is rendering in Figure 26 above, and shows the welded aluminum frame, electrostatic paddles, timing belts, and the pulleys which would support the power rail

belts. The belt is tensioned into a rounded triangular shape, with the base parallel to the bottom of the electrostatic chamber. The main assemblies inside of the filtration system are the mesh paddles connected to the drive belts, the pulleys mounted on axles, and the frame. The front-most axle, seen in the foreground of Figure 26, is mounted with slots to allow the axle to slide forwards and backwards. This movement allows for all belts to be tensioned correctly and run smoothly without the teeth skipping. The tensioner slide is set by pulling the slide out and tightening the two countersunk bolts on each side. Each axle is made of ¼ inch stainless steel D-shaft, and the pulleys are held in their alignment by set screws. The axles are mounted onto the frame using flanged bearings to allow for smooth rotation. Since we are using the axles to carry our electrical connections to both power rails, the top and bottom rear axles both use nonconductive bearings.

The two sides of the welded aluminum frame are connected at the bottom with a U-shaped bracket with holes to bolt the frame to the electrostatic chamber. Since these bolts will be under the water line, gromets were mounted in each hole to prevent water from leaking.

4.1.1 Analysis of Separation System

Paddles

Figure 27. CAD Render of the Mesh Paddles and Electrostatic Rail

The first step of finalizing the electrostatic paddles involved understanding the amount of surface area a singular paddle has. This calculation is necessary to determine the total area of all the paddles the system can clean in an hour, and thereby the amount of water the machine can process per hour. The rubber bracket as seen in Figure 27 is used to hold both mesh pieces together which needed to be excluded from the surface area being calculated. Throughout these calculations the interior surface area of the wire mesh is assumed to be negligible.

Dimensions of Outside Mesh

$$length\,[l] = 5.5\,in$$
$$height\,[h] = 1.5\,in$$
$$width\,[w] = 0.012\,in$$

Dimensions of Inside Mesh (Need to exclude rubber U-Bracket)

$$length\,[l2] = 4.75\,in$$
$$height\,[h2] = 1.25\,in$$
$$width\,[w2] = 0.012\,in$$

*Surface Area of Rubber U-Bracket **[U]***

$$Small\ Length\ Rubber\ Bracket\,[W] = 0.125\,in$$
$$Larger\ Length\ Rubber\ Bracket\,[W2] = 4.75\,in$$
$$Smaller\ Height\ Rubber\ Bracket\,[H] = 0.125\,in$$
$$Larger\ Height\ Rubber\ Bracket\,[H2] = 1.5\,in$$
$$U = 2(W \cdot H2) + (W2 \cdot H)$$
$$U = 2(0.125 \cdot 1.5) + (4.75 \cdot 0.125)$$
$$U = 0.969 \cdot 2 = 1.938\,in^2\ [Multiplied\ by\ 2\ to\ account\ for\ both\ sides\ of\ the\ mesh]$$

*Surface Area of a singular mesh panel **[SA]*** (See Figure 27)

$$SA = (5.5 \cdot 0.012) + (5.5 \cdot 1.5) + (0.012 \cdot 1.5) + (4.75 \cdot 0.012) + (4.75 \cdot 1.25) + (0.012 \cdot 1.25) \qquad SA = 8.334 + 6.0095 = 14.344\,in^2$$
$$SA = 14.344 - 1.938 = 12.406\,in^2$$

Total Surface Area of singular paddle = 2 mesh panels ***[TA]*** (See Figure 27)

$$TA = SA \cdot 2\,(two\ mesh\ on\ \sin g\ ular\ paddle)$$

$$TA = 12.406\,in^2 \cdot 2 = 24.812\,in^2$$

Number of Paddles Total ***[n]***

$$n = 18\,paddles$$

Total exposed surface area of entire mesh/paddle system ***[EA]***

$$EA = 14.5\,in^2 \cdot 18 = 261\,in^2$$

Belt System

This section details the speed at which the belt can move with the motors and mechanical linkage system currently in use. Calculations to determine the belt speed were also needed in order to time the system properly, such that the air knife was synchronized with each mesh paddle that passed it.

Rotational Speed (revolutions per min) ***[RPM]***

$$RPM = 27\,rpm$$

Diameter of Pulley ***[D]*** (Length)

$$D = 17.8\,mm = 0.0178\,m$$

Belt Speed ***[V]***

$$V = \frac{Dis\tan c\,e}{Time} = \left(\frac{\pi}{2}\right)(D)\left(\frac{RPM}{60}\right)$$

$$V = 1.57 \cdot 0.0178\,m \cdot 0.45 = 0.0126\,\frac{m}{s}$$

$$V = 0.0126\,\frac{meters}{sec} = 0.4951\,\frac{in}{sec} = 1774.08\,\frac{in}{hour}$$

Length of entire Belt ***[E]***

$$E = 42\,in$$

Separation Cycle

These calculations detail the amount of time the paddles are traveling through the water collecting microplastic particulate, the number of paddles that can be cleaned per hour and the total surface area that is cleaned per hour.

*Submerged Travel **[l]***

$$L = 14.47\ in$$

*Time paddles spend in water **[t]***

$$Time = \frac{Dis\tan ce}{Speed} = t = \frac{l}{v}$$

$$t = \frac{14.47}{0.4951} = 29.23\ \sec onds$$

*Number of Cycles per hour **[C]***

$$C = \frac{V}{E} = \frac{1774.08}{42} = 42.24\ \frac{cycles}{hour}$$

*Number of Paddles Cleaned per hour **[PC]***

$$PC = C \cdot n = 42.24 \cdot 18 = 760\ \frac{paddles}{hour}$$

*Amount of Total Surface Area Cleaned per hour **[AC]***

$$AC = PC \cdot TA = 760 \cdot 24.812 = 18857.12\ \frac{in^2}{hour}\ or\ 12.166\ \frac{m^2}{hour}$$

4.2 Intake System

The material used to design our intake system was PVC schedule 40 pipe which consisted of 3-inch diameter sized pipes with three ball valves. The diameter was chosen to allow for a high-water flow rate without excess pressure. This subsystem is designed to be able to self-clean to prevent screen fouling and clogs. The model, shown below in Figure 26, displays the initial

intakes and the three ball valves, which will be actuated by servo motors to cycle through the four phases of the cleaning and operation cycle.

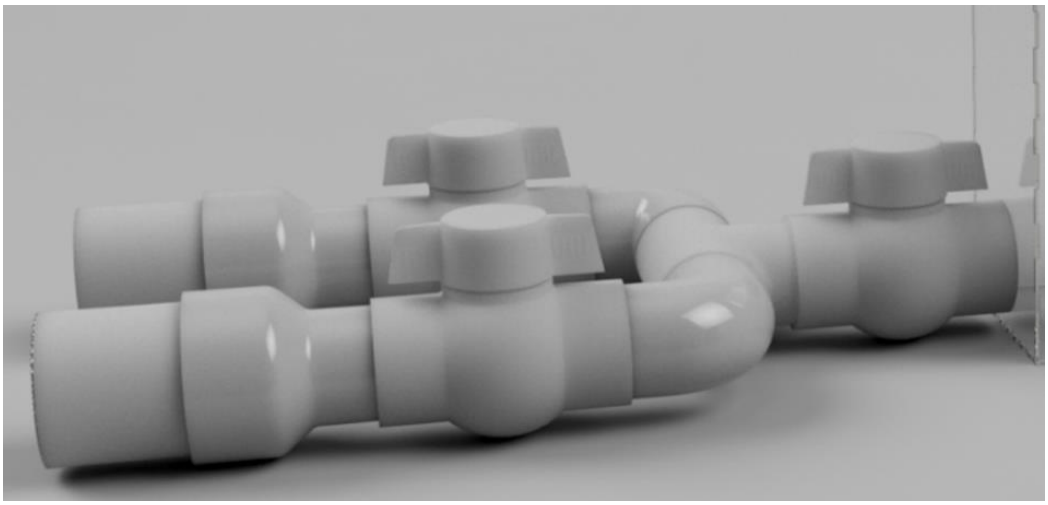

Figure 28. PVC Intake Tube Model

4.2.1 Analysis of Intake System

This section details the calculations for mass flow rate and total velocity of water such that the water speed is twice the speed of the paddles. The intake system can be seen in Figure 28.

Desired Water Velocity in Electrostatic Chamber

$$V_w = 2 \cdot V_{paddle}$$

Conservation of Mass

$$\dot{m} = r \cdot A \cdot V$$

$$\dot{m}_{eb} = \dot{m}_{in}$$

$$V_{in} = \frac{r \cdot A_{eb} \cdot V_{eb}}{r \cdot A_{in}}$$

Required Water Velocity in Intake

$$V_{in} = \frac{997\ \frac{kg}{m^3} \cdot 0.0058\ m^2 \cdot 0.0252\ \frac{m}{s}}{997\ \frac{kg}{m^3} \cdot 0.00268\ m^2} = 0.0545\ \frac{m}{s}$$

4.2.2 Servo Actuated Valves

The main design of the intake system allows for a self-cleaning cycle using three servo actuated ball valves and two brushless impellers. The servo actuated ball valves needed to be built from a few different COTS parts due to budget constraints. We first purchased the 3” PVC ball valves, and after deconstructing the handle assembly on one of them designed and 3D printed an adaptor, such that the handle stem of the ball valve could be connected to the servo motors.

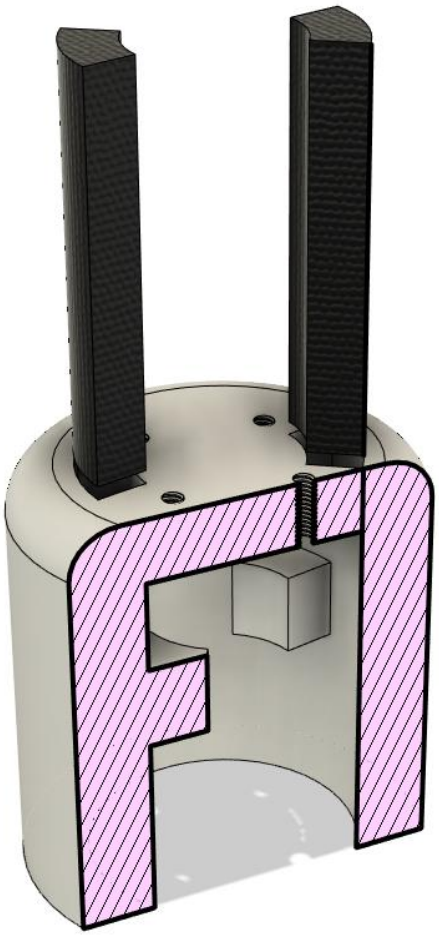

Figure 29. Cutaway View of the Ball Valve Adaptor and Pins

The adaptor shown in Figure 29 has two teeth to fit the channel-lock type handle stem of the ball valve, as well as two pins to secure the teeth in place and lock the adaptor onto the handle core. The top plate of the adaptor has holes threaded in 2-56, although when the adaptor is manufactured the part will be printed with holes sized for heat inserts. The 2-56 thread allows for the adaptor to have most standard spline servo horns bolted onto it to create a strong mechanical connection between the servo unit and the ball valve handle stem.

We also designed a simple flat sheet bracket, to be laser cut out of either acrylic or treated plywood, to hold the servo in place above the ball valve. Seen below in Figure 30, the bracket loops are placed over either side of the ball valve, and the servo motor attached to the cross bar which is attached to both bracket plates.

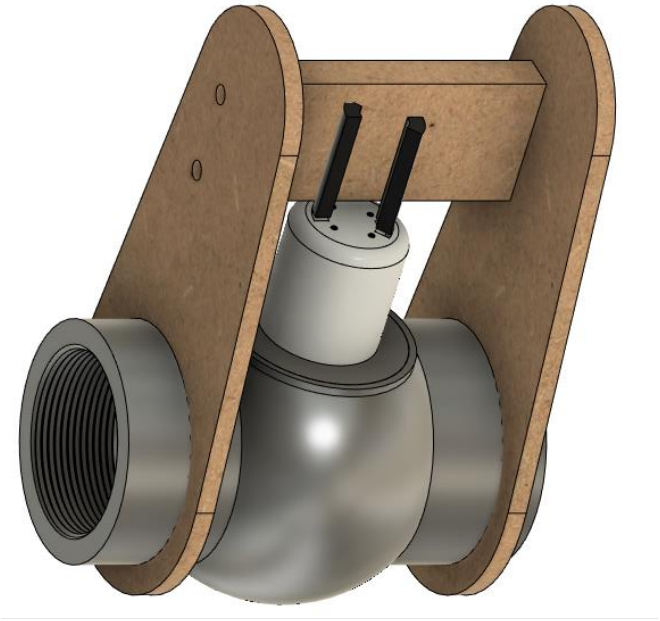

Figure 30. Servo Bracket with Modified Ball Valve and Adaptor

4.2.3 Impellers and Filter Screens

The impellers and filter screens are both affixed to the first pieces of tubing on the intake subsystem. The three-inch pipe has a piece of 0.5mm stainless steel mesh on either side, cut to match the open faces of the pipe. The primary piece of mesh will be fixed to the pipe with a waterproof epoxy resin, such that it will not be dislodged from the intake subsystem by any jostling which may occur in inclement weather. The secondary piece of mesh is sandwiched

between the pipe and the ball valve fitting, such that it can be removed for access to the impeller.

The impellers will be located in the middle of this segment of pipe. We are using COTS impellers intended for use in RC watercraft, so not much needs to be done to adapt these impellers to our application. The housing will be slid entirely into the 3” initial intake pipe, and then bolted into place with a rubber gasket to ensure that no water is allowed in past the primary screen. The wiring will be ported through the side of this pipe, and the hole around the wires sealed.

4.2.4 Self-Cleaning Cycle Code

To operate the self-cleaning cycle, each of the three servo motors and both brushless impellers will be wired to an Arduino Uno. This Arduino unit will be responsible for actuating the valves and controlling the flow supplied by the impellers. In order to accomplish this, we built a simple state machine, which can be found in Appendix A. The state machine switches between 4 preset cases, each of which dictates a position to the servo motors, and powers or deactivates the impellers according to the desired direction of flow. The switch between each case is dictated by a set time interval. Figure 31 below shows in detail the four stages with the change in servo and impeller function for each.

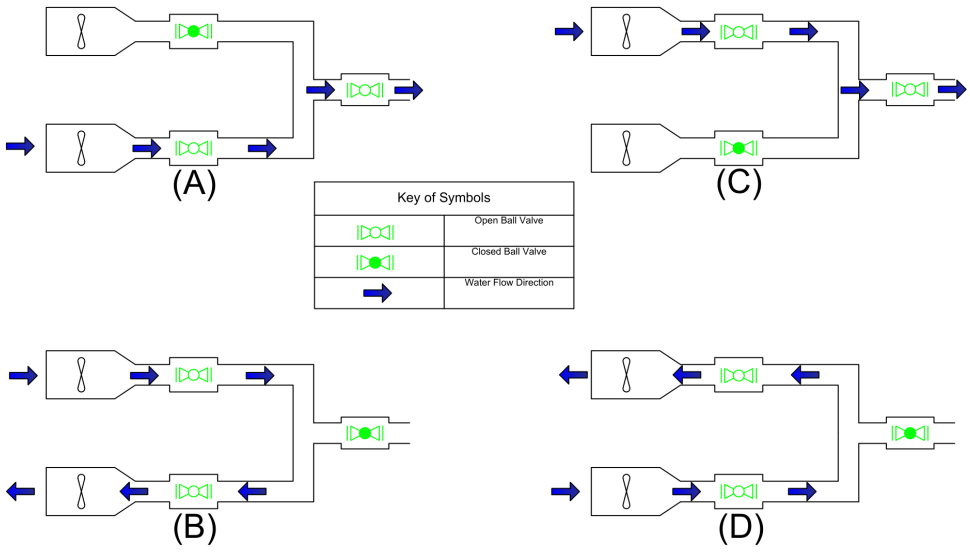

Figure 31. Valve Positions and Flow. This graphic depicts the water flow and valve positions for each of the four stages of the self-cleaning cycle.

4.2.5 Conclusion

The full intake system incorporates COTS parts and manufactured assemblies. The main structure is assembled out of 3” and 2” PVC pipe, with modified 2” PVC ball valves. The prescreening mesh is cut to the size of the pipe and either adhered to the pipe opening or pressed between segments. The self-cleaning system uses COTS impellers, servo motors, and a custom built bracket to hold the entire assembly together. An Arduino Uno runs a state machine code to ensure that the self-cleaning cycle runs properly. In the correct application, the intake subsystem should be able to run indefinitely so long as it is supplied with power.

4.3 Mechanical Linkage & Air Nozzle System

The air knife, shown in Figure 32 below, consists of 58 0.02-inch openings in a line creating a flat fan shaped spray pattern.

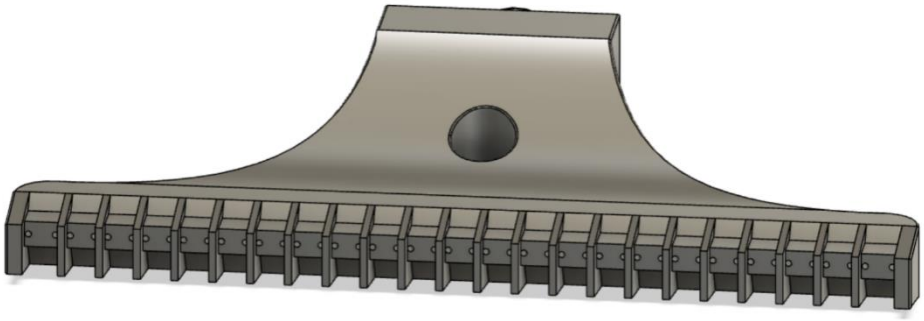

Figure 32. Air Knife CAD

The spray pattern of this air knife has a spray angle of 14°, and we found through testing that a pressure of ~40 psi through our valve system is sufficient pressure to supply the air knife. The air knife was mounted onto the belt assembly using a horizontal bar attached to either side of the metal frame. The end of the nozzle is positioned at an upwards angle into the collection box, shown in Figure 33 below, such that it makes a 130° incident angle with the mesh panels in the collection box, reducing the likelihood any microplastic particles will make their way out of the collection box. This system continually pushes particles that are stuck to the mesh further into the collection chamber. The air knife design satisfies each of our requirements for this system.

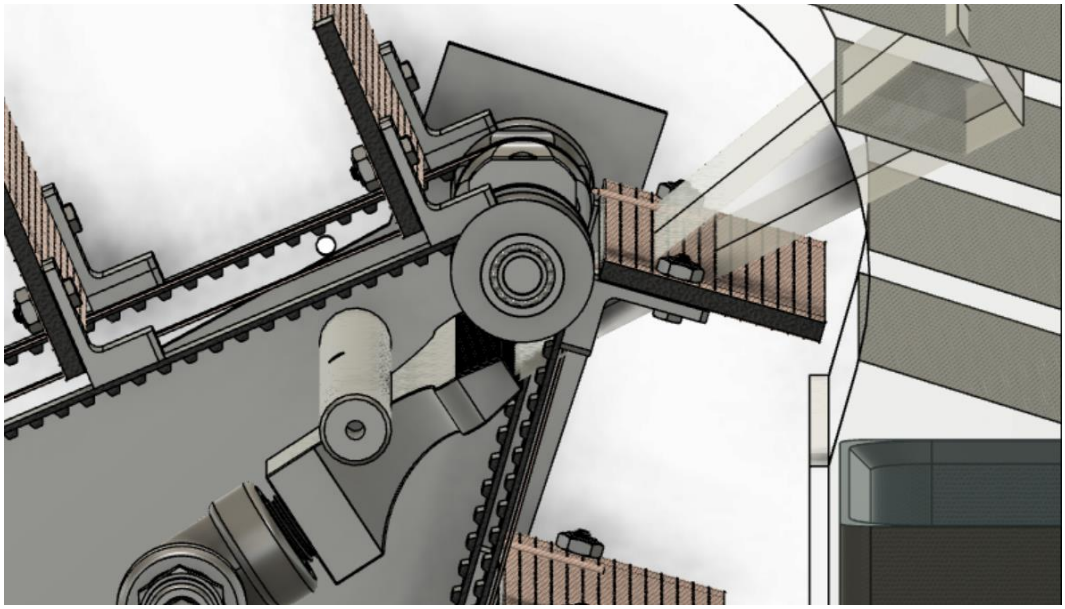

Figure 33. Air Knife Particulate Angle into Collection Box

4.3.1 Analysis and Determination of Linkage System

For the operation of the valve assembly, a 90° ball valve was chosen because of its quick actuation and smooth operation. With a ball valve in mind, and the need for “blasts” of air for every revolution, we then identified the measurements for the four-bar linkage. The design requirements for the four-bar linkage are as follows. First, the linkage must be able to move in a 90° arc for actuation of the ball valve. Second, the arc motion must be a quick motion so the valve will be open for no more than 50% of one revolution of the crank. Third, the linkage must be able to operate smoothly, and not get stuck in a toggle position. With these design requirements in mind, we consulted the Hrones and Nelson Atlas to identify a four-bar linkage that would suit our application. We chose to use a standard crank-rocker four bar linkage, with a parallel ground link, and a crescent shape coupler curve.

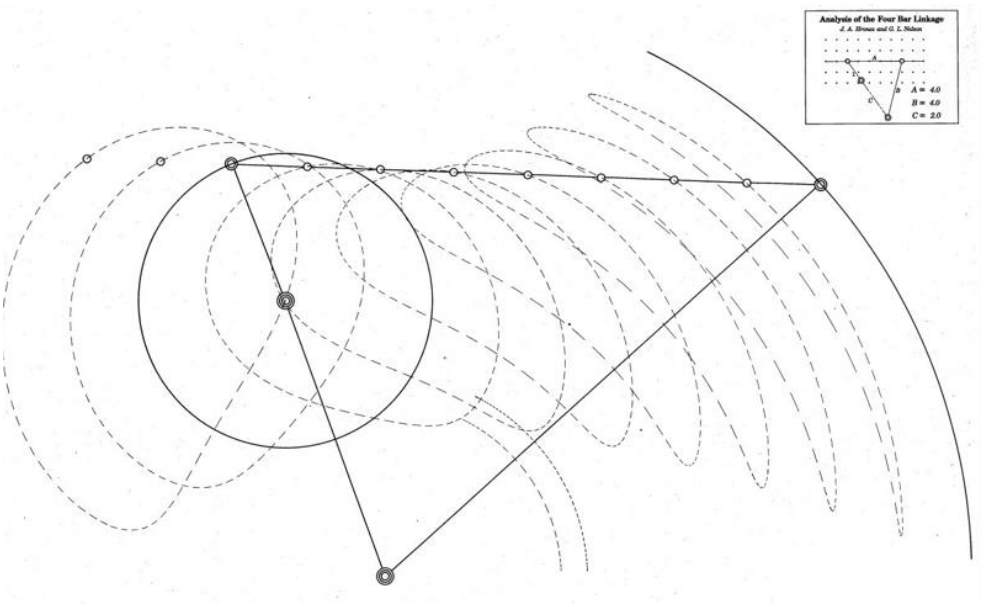

Figure 34. Hrones and Nelson Atlas Page 683 (Hrones, 1951)

Using the measurements specified in the Hrones and Nelson Atlas, as seen in Figure 34, we performed the initial setup of the coupler curve using Desmos. This allowed us to better visualize the movement of the linkage, as well as analyze the velocity and acceleration of the output linkage. The linkage itself as taken from the Hrones and Nelson atlas (Hrones, 1951) had the correct coupler curve profile we were looking for, but the movement of the output linkage would be too slow to quickly actuate the ball valve and prevent excess air pressure from being wasted. We then tweaked the dimensions of each link to maximize the angular acceleration of the output link. Our final four bar linkage can be seen in Figure 35 below. Ground Link (orange): 3.7”, Crank Link (black): 1.43”, Coupler Link (red): 3.77”, Rocker/Output Link (blue): 1.5”.

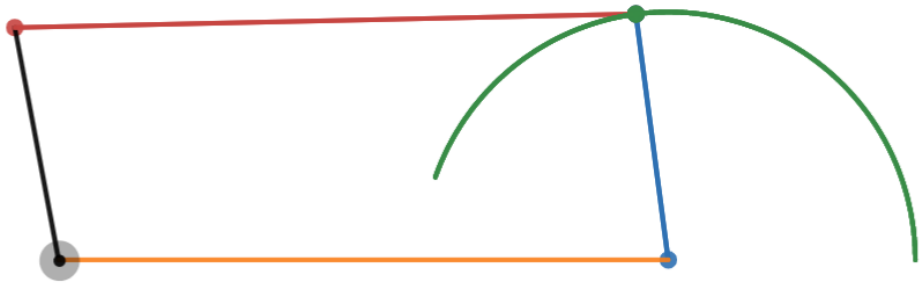

Figure 35. Four Bar Linkage Coupler Curve

We performed a motion analysis of the linkage using SOLIDWORKS to analyze the motion profile of the mechanism. All measurements were taken at the joint between the rocker/output link, and the coupler link. As seen in Figure 36 the linear displacement of the linkage has a peak displacement of 65 mm that quickly returns to 0. Figures 37 and 38 detail the peaks of the angular acceleration and velocity over time for this system.

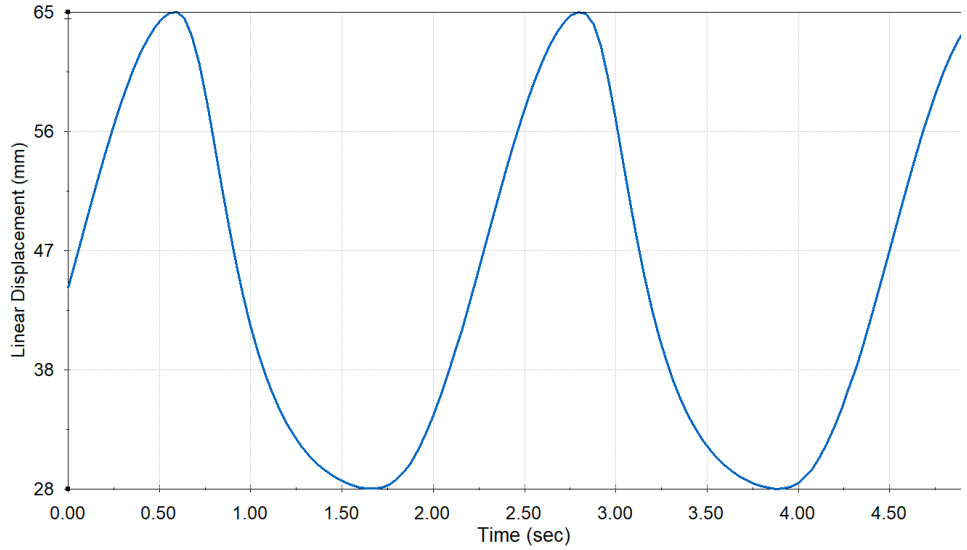

Figure 36. Linear Displacement (X-Direction) at the End of the Valve Link

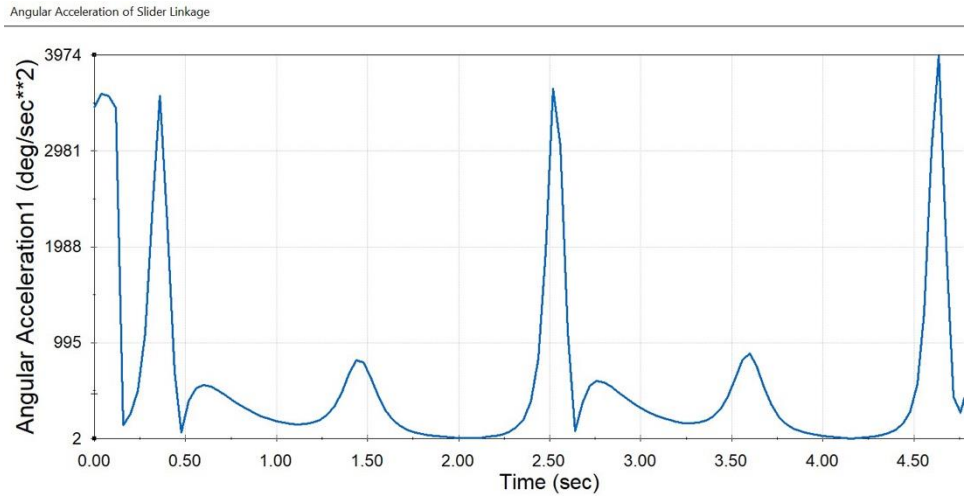

Figure 37. Angular Acceleration of the Valve Link

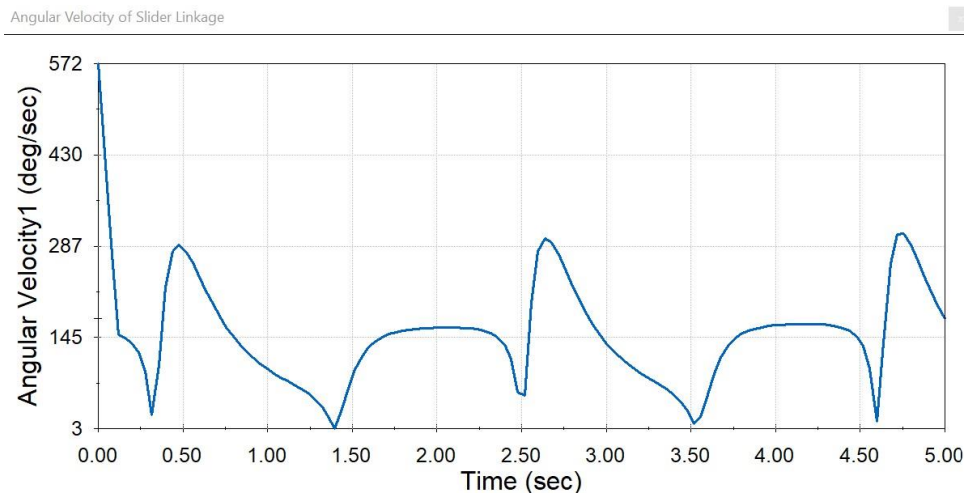

Figure 38. Angular Velocity of the Valve Link

Next, because of the nature of our four-bar linkage, we needed a method to prevent the coupler linkage from pulling the ball valve past its closed position and essentially re-opening the ball valve in the other direction. To solve this issue, we devised a slider-spring mechanism to prevent the rocker linkage from moving past it's 0° starting position. A spring mounted to the top of the valve pulls the valve closed when the coupler link moves past the 0° position. The force required to close the valve was estimated to be ~1.5lb/in, so we chose a 1.5" long steel music wire extension spring rated at 0.29lb/in.

The CAD rendering of the valve mechanism can be seen in Figure 39 below. The system is located on the outside of the acrylic box near the air knife system. On the left side there is the drive motor mounted on a bracket, and the drive gear. The drive gear doubles as a coupling, with the main drive axle for the belt on the bottom, while attaching to the motor at the top. There is also a mount for a carbon brush on the back side of the plate, creating an electrical contact through the brush to the axle, further connecting to the conductive pully for the positive power rail.

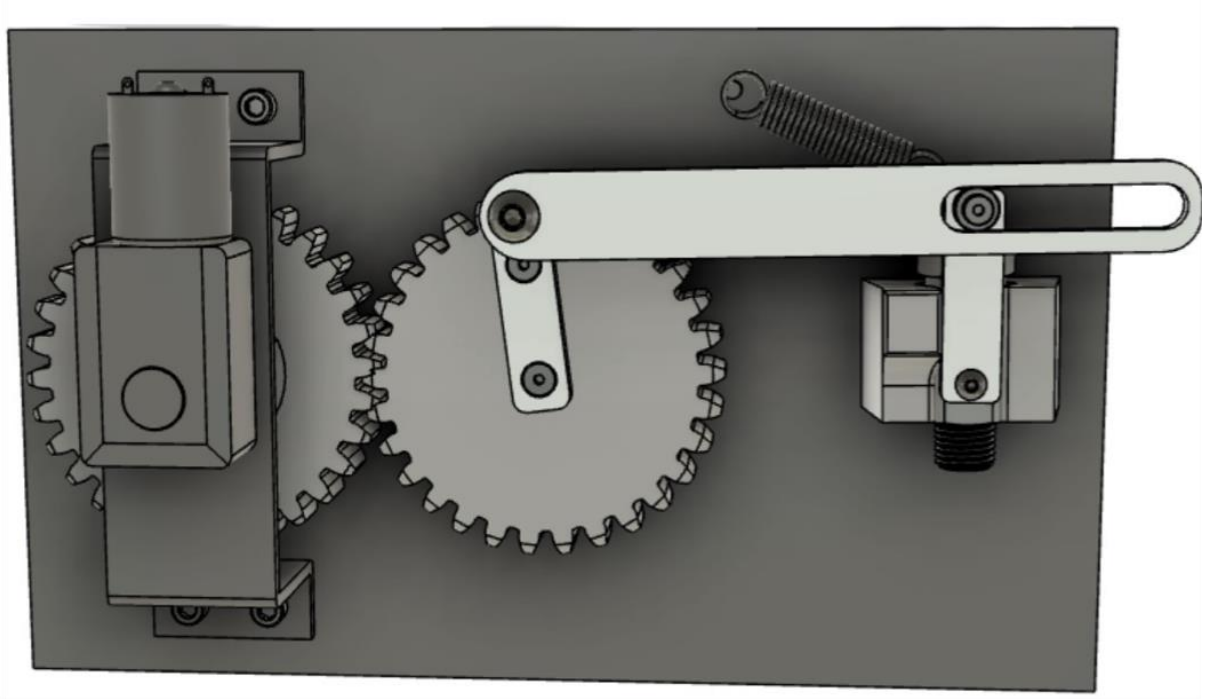

Figure 39. CAD Rendering of the Mechanical Valve Assembly

On the right side of this mechanism as shown in Figure 39 is the crank gear for the four-bar linkage. This slider serves to allow the output link, which is attached to the stem of the valve, to be quickly opened and quickly closed to create a short “blast” of air as a paddle moves across the air knife. Because of the relative lengths of the crank and output links, the movement of the output link is an arc from 0° when directed straight upwards to fully open at a 90° angle in 41% of the time it takes for the crank link and gear to make one full rotation. The coupler gear, shown on the right side of the mechanism under the drive motor, is connected to the top-most shaft in the filtration system. The coupler gear has holes where heat inserts are installed such that bolts can tighten onto the flat in the D shaft. The pulleys used are sized so that one rotation of the drive pulley moves the belt from one paddle to the next.

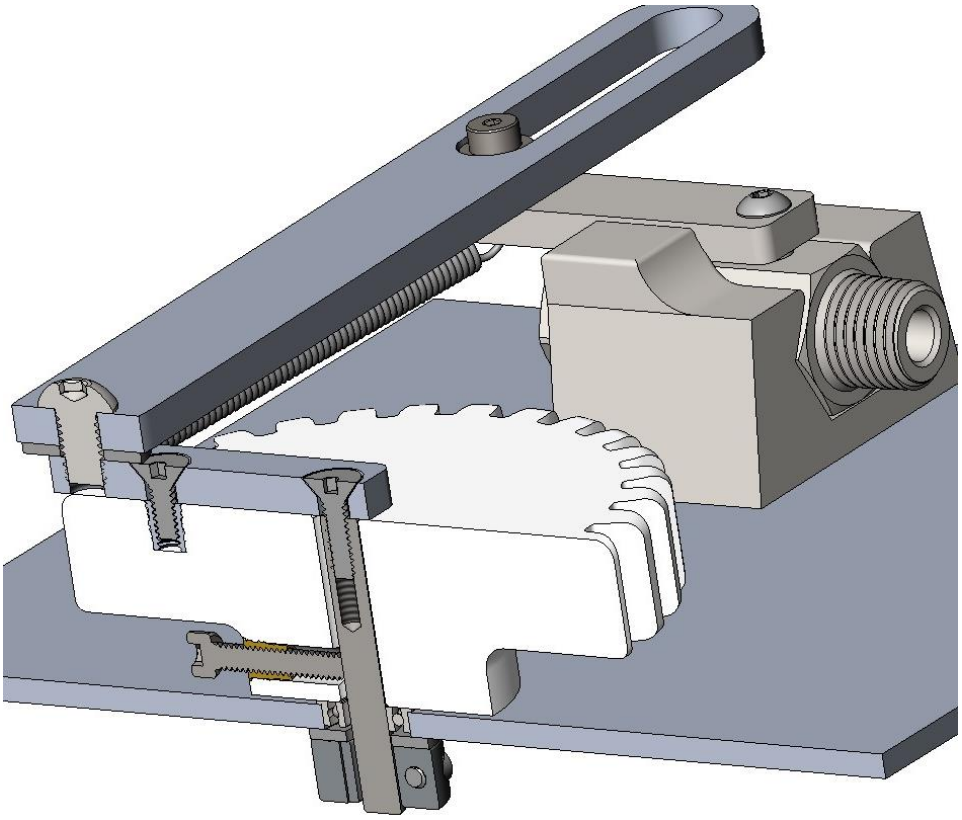

Figure 40. Crank Gear Section View

The crank link is attached to the top of the crank gear, shown in Figure 40 above, with two countersunk screws. The crank gear is mounted onto the main plate with a ¼" stainless steel D shaft that goes through a ball bearing press fit into the mounting plate. The shaft is secured at the bottom end with a ¼" clamping shaft collar, with a nylon slip washer in-between the shaft collar and the mounting plate to prevent friction. The crank gear is connected to the shaft with a set screw, threaded into a brass hear insert installed into the plastic gear.

Looking at the angular acceleration, and angular velocity of the joint between the valve link and the coupler link, we knew that the slide joint there would need to operate smoothly at high speeds. Because of the high acceleration and deceleration of this linkage, we also wanted the joint to be as light weight as possible. We chose to have the rotating pin inside the slider be a steel ball bearing, held in place with an alloy steel shoulder bolt. The two parts can be seen below in Figure 41 and 42. The shoulder of the shoulder bolt is 1/8” matching the inner diameter of the ball bearing. The shoulder bolt has a 4-40 thread that is threaded into a tapped hole in the end of the valve link.

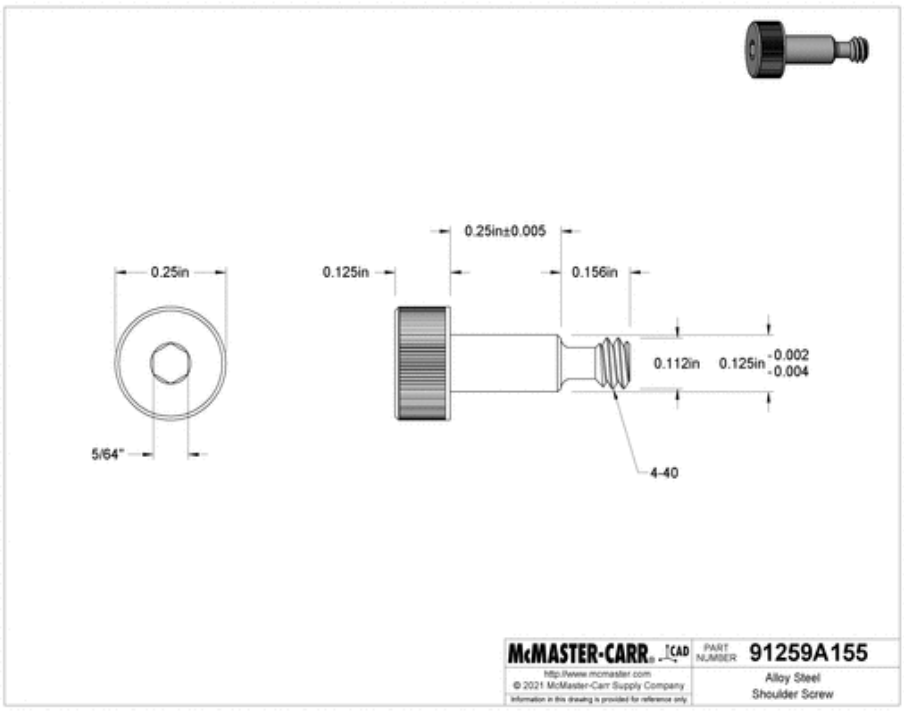

Figure 41. McMaster 91259A115 Shoulder Screw

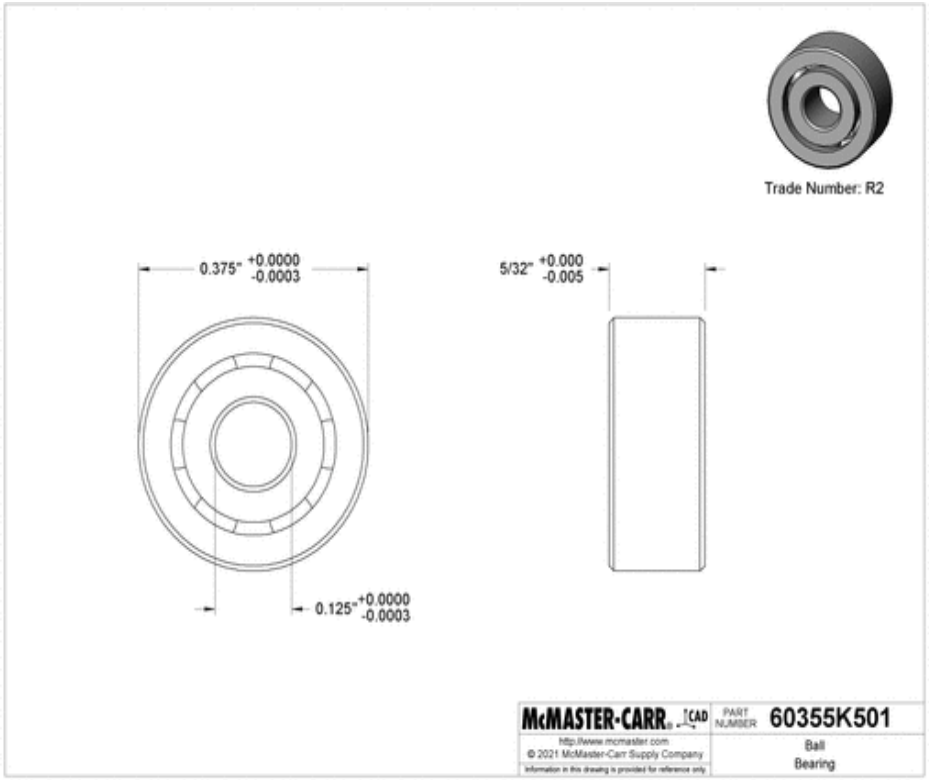

Figure 42. Mcmaster 60355K501 Ball Bearing

Since the size of the shoulder bolt was only 1/8”, we wanted to verify that the shoulder bolt could hold up to the force placed on it by the slide linkage while the valve is opening. We simulated the situation in SOLIDWORKS using a static FEA study. The simulation setup can be seen in Figure 43 below. To simplify the mechanism, the simulation only includes the valve link, the coupler link, the bearing, and the shoulder bolt.

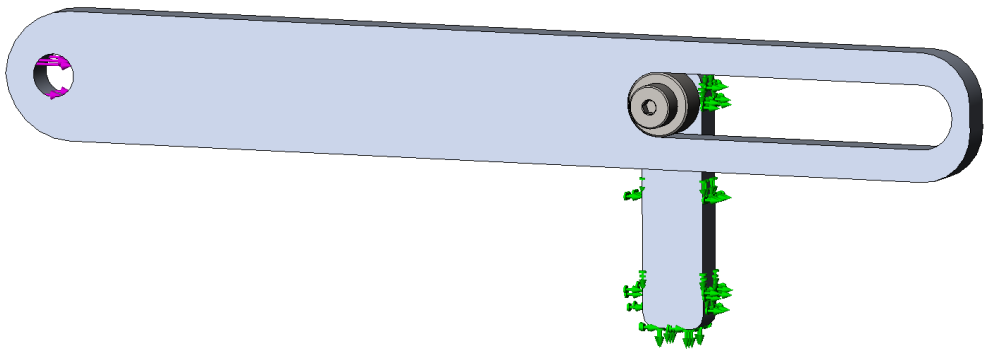

Figure 43. FEA Simulation Setup for Slider & Bearing Connection

We chose to look at the point where the crank link first contacts the valve like while it is in the closed position. The angle between the coupler and the valve links is assumed to be 90°. To calculate the force on the coupler link, we needed to account for the force of the motor, and the force of the spring keeping the coupler link in place. The calculations are shown below.

$$Force\ on\ coupler\ =\ Fmotor\ -\ Fspring$$

$$Fmotor\ =\ force\ from\ motor$$

$$Fspring\ =\ force\ from\ spring$$

$$Lspring\ =\ 1.5\ in\ =\ length\ of\ spring\ extension$$

$$T\ =\ 60\ \frac{kg}{cm} = Motor\ Torque\ 24\ volts$$

$$r\ =\ 3.81\ cm\ =\ radius\ of\ crank\ link$$

$$k\ =\ 2.9\ \frac{lb}{in}\ =\ spring\ cons\tan t$$

$$Fmotor\ =\ \frac{T}{r}$$

$$Fmotor = \frac{60\ Kg \cdot cm}{3.81cm} \cdot \left(9.81\ \frac{m}{s^2}\right) = 154.49N$$

$$Fspring = k \cdot Lspring = 2.9\ \frac{lb}{in} \cdot 1.5in = 4.35lb$$

$$1N = 0.2248lb$$

$$\frac{4.35\ lb}{0.2248} = 19.35N$$

$$Force\ on\ coupler = 154.49N - 19.35N = 135.14N$$

The force of 135.14N applied to the joint, shown above, was placed inside the ¼" hole at the end of the coupler link in line with the motion of travel. The valve link was fixtured in place, and the threaded section of the shoulder bolt was bonded to the top of the valve link to simulate it being threaded into the piece. The resulting stress and deformation can be seen below in Figure 44. The maximum on the shoulder bolt was 44,208 PSI, with the two highest stress concentrations being on the front and back side of the shoulder bolt from the bending moment induced by the coupler link pressing against the bearing. The maximum allowable shear stress on the shoulder bolt is 84,000 PSI, so a maximum stress of 44,208 PSI means that this bolt can safely handle the stress during operation, with a safety factor of 1.9. Figure 43 shows the true deformation of the shoulder bolt, while Figure 46 below shows the maximum deformation of the shoulder bolt, with the image showing the displacement at 50x true scale to better visualize how the shoulder bolt is deformed.

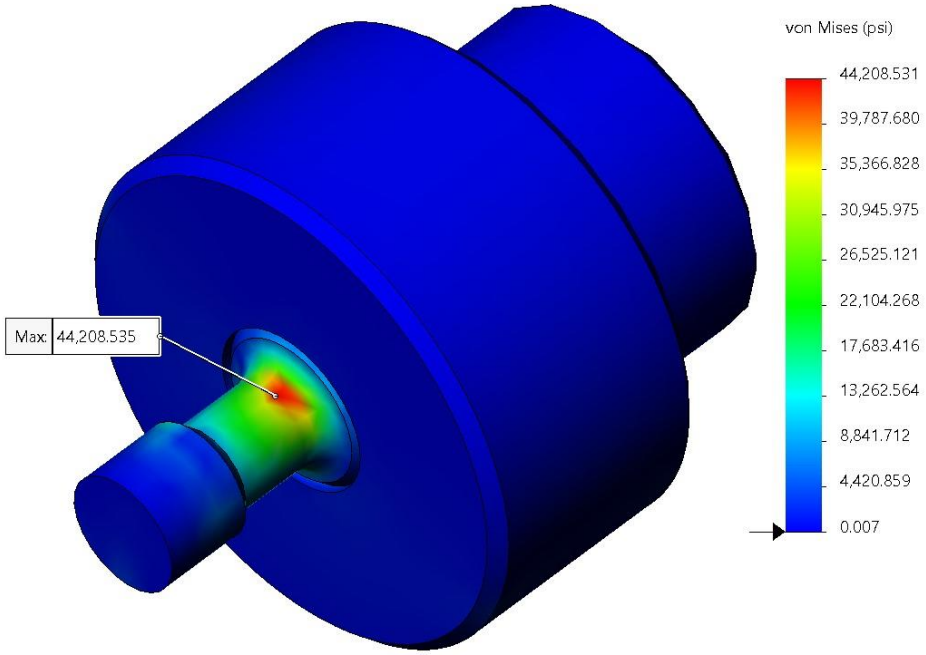

Figure 44. Stress on Shoulder Bolt from Slide Linkage, True Deformation

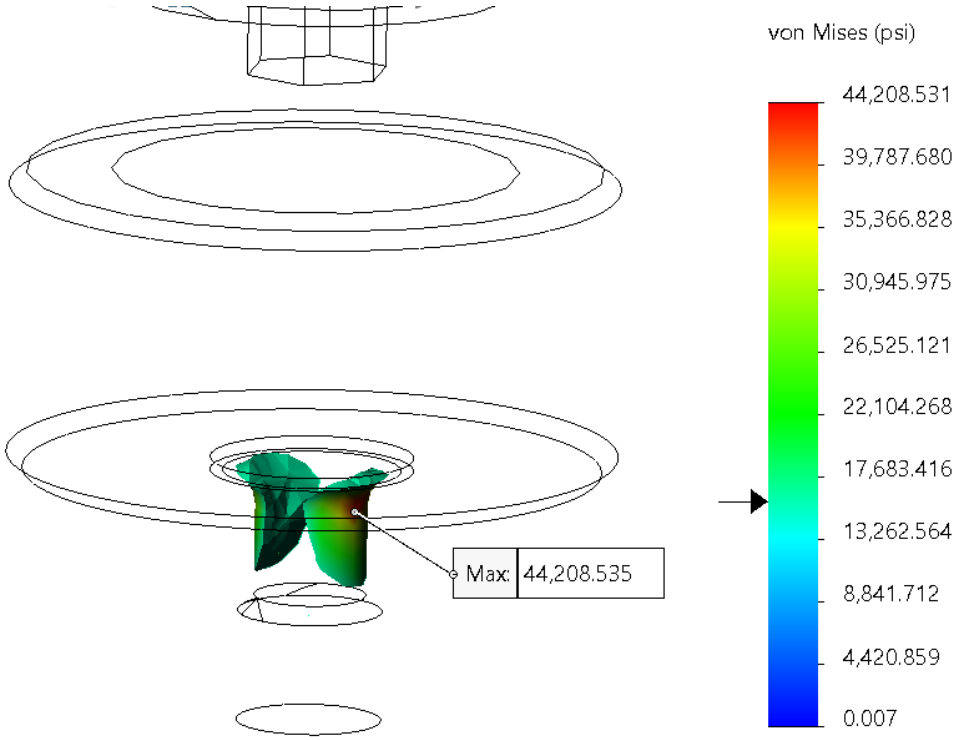

Figure 45. ISO Clipping View Showing Areas of >16000PSI, True Scale Deformation

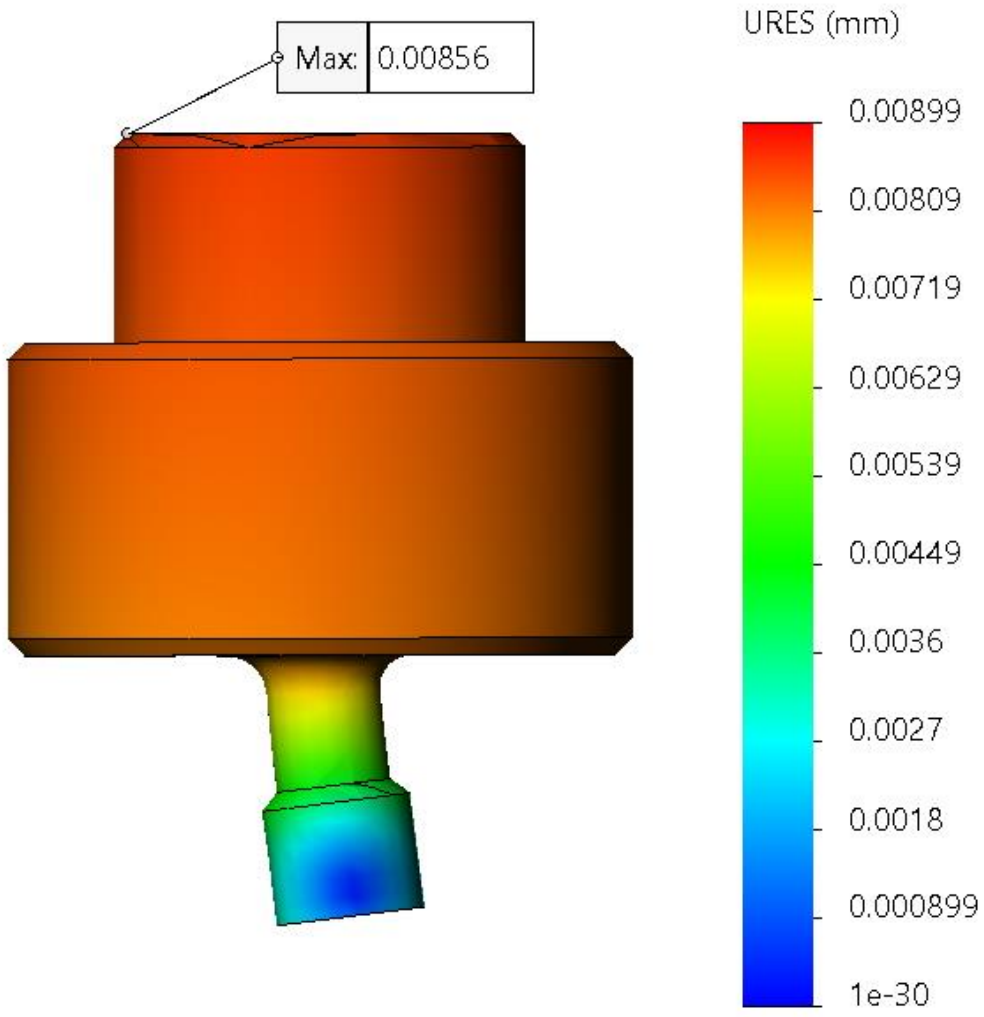

Figure 46. Shoulder Bolt Displacement, Shown at 50x True Scale

The valve holder/hard stop is shown below in Figure 47. This part securely holds the ball valve in place, while also preventing the valve link from rotating past the closed position. This part was made using FDM 3D printed PLA. The hard stop will be hit consecutively by the valve linkage each time the spring pulls the valve closed. To determine if the current design could hold up to the force of the valve closing without deforming over time, we simulated the situation using a FEA study in SOLIDWORKS.

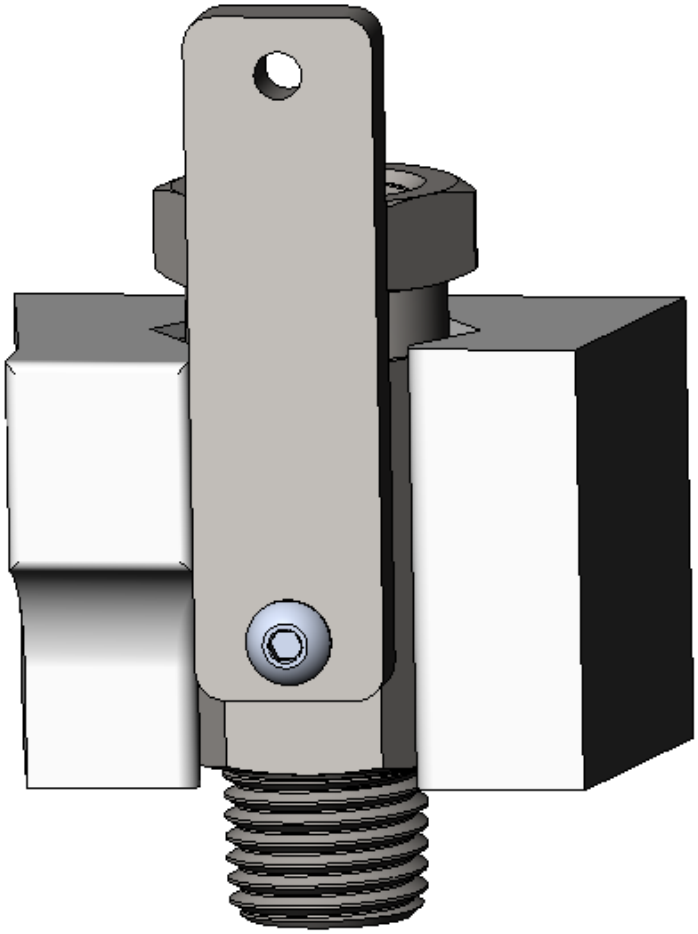

Figure 47. Simulation Setup for Valve Linkage Hard Stop

To simplify the simulation, only the valve holder and the ball valve were used in the simulation. The bottom face of the valve holder was fixtured in place, and a force was applied to the face of the hard stop. The force applied by the valve link onto the hard stop was found using the calculations below.

$$Fspring \ = \ Force\ applied\ by\ spring$$

$$Flink \ = \ Force\ applied\ by\ link$$

$$Lspring \ = \ 1.5\ in \ = \ length\ of\ spring\ extension$$

$$m \ = \ 21g\ (Mass\ of\ Alu\min u\, m) \ + \ 7g\ (Mass\ of\ bearing) \ +$$

$$5g\ (Mass\ of\ bolt) \ = \ 33g \ \ r \ = \ 20mm \ = \ radius\ of\ link\ at\ point\ of\ contact$$

$$k = 2.9\,\frac{lb}{in} = spring\ cons\tan t$$

$$\omega = angular\ velocity = 293\,\frac{deg}{sec}(from\ figure\ 36)$$

$$293\,\frac{deg}{sec}\cdot\frac{\pi}{180} = 5.114\,\frac{rad}{sec}$$

$$Fspring = k \cdot Lspring$$

$$Flink = m \cdot r \cdot \omega^2$$

$$Flink = (33g \cdot 0.001)\cdot(20mm \cdot 0.001)\cdot\left(5.114\,\frac{rad}{s}\right)^2 = 0.01726N$$

$$Fspring = k \cdot Lspring = 2.9\,\frac{lb}{in}\cdot 1.5in = 4.35lb$$

$$1N = 0.2248lb$$

$$\frac{4.35\,lb}{0.2248} = 19.35N$$

$$Total\ Force = 0.01726N + 19.35N = 19.36726N$$

Figure 48 below shows the maximum force on the valve holder from the valve link. The stress concentration is in the thinnest section of the valve holder along the inner surface. The maximum stress was 45.8psi, and the maximum displacement, shown in Figure 49, was 0.007mm, since the stress is within the elastic region of PLA, the current design is stiff enough to prevent bending over time.

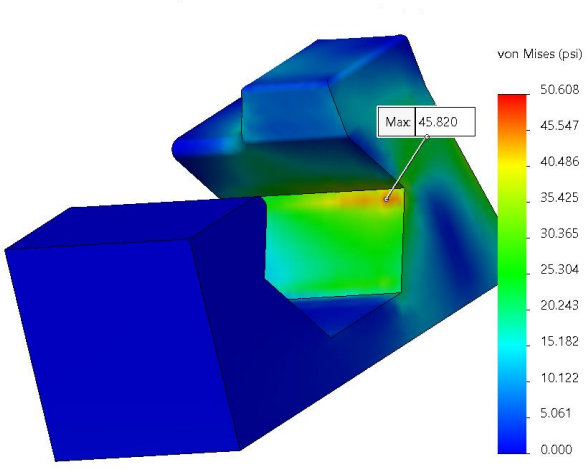

Figure 48. Stress on Valve Holder Hard Stop

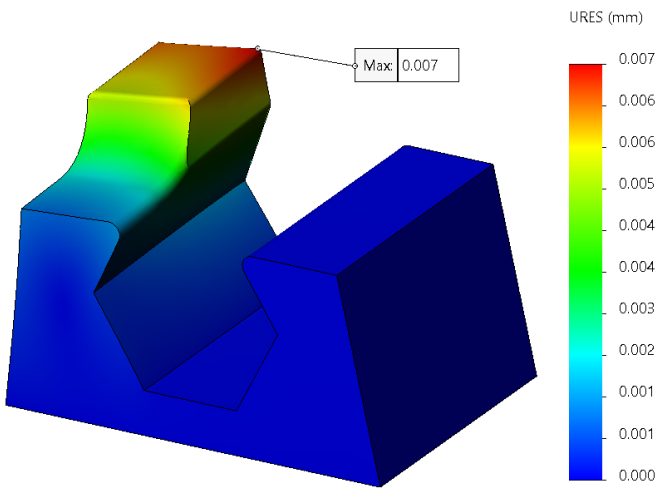

Figure 49. Displacement of Valve Holder, Shown at 400x True Scale

4.4 Collection Box

In the design of the collection bin shown in Figure 50, the mesh panels were designed such that they could be removed from the bin for cleaning. We added a pressure relief vent in the rear of the top panel, with a piece of 10-micron mesh to cover it. We also have a removable drawer at the bottom of the bin. With the changed mesh panel geometry, a wind barrier was included which extends downwards at an oblique angle from the top panel.

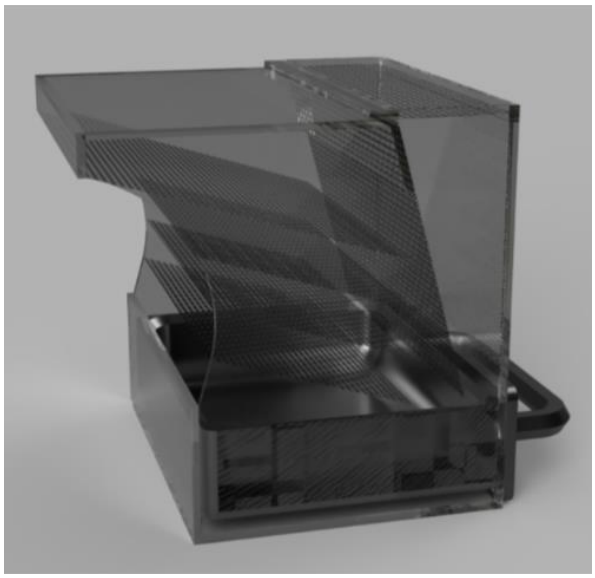

Figure 50. Final Collection Box Design. This collection box features decreasing mesh sizes as the particles would travel downward, and a flow vent panel on top of the box.

In the final configuration the mesh panels no longer direct air flow, instead separating the particulate from the flow and pushing it downwards towards the drawer. The air and particle flow can be seen in Figure 51. The airflow can be seen in blue, and the particulate path is shown in orange. The air from the air knife forces the particulate upward (1). The particulate and air travel over the mesh panels (2) and are directed downwards along the rear mesh panel by the wind barrier. The air is then spiraled back into the initial mesh by the shape of the bin (3). In this way, the pressure relief should allow air to escape in a less agitative manner as soon as the air knife adds pressure to the main chamber (4), instead of air escaping through the side slots while still laden with particulate. This design of the collection bin should fully capture the plastic particulate from the paddles. Figure 52 shows this render in more detail, with the initial angle of the air knife against the mesh paddles shown as a metallic render.

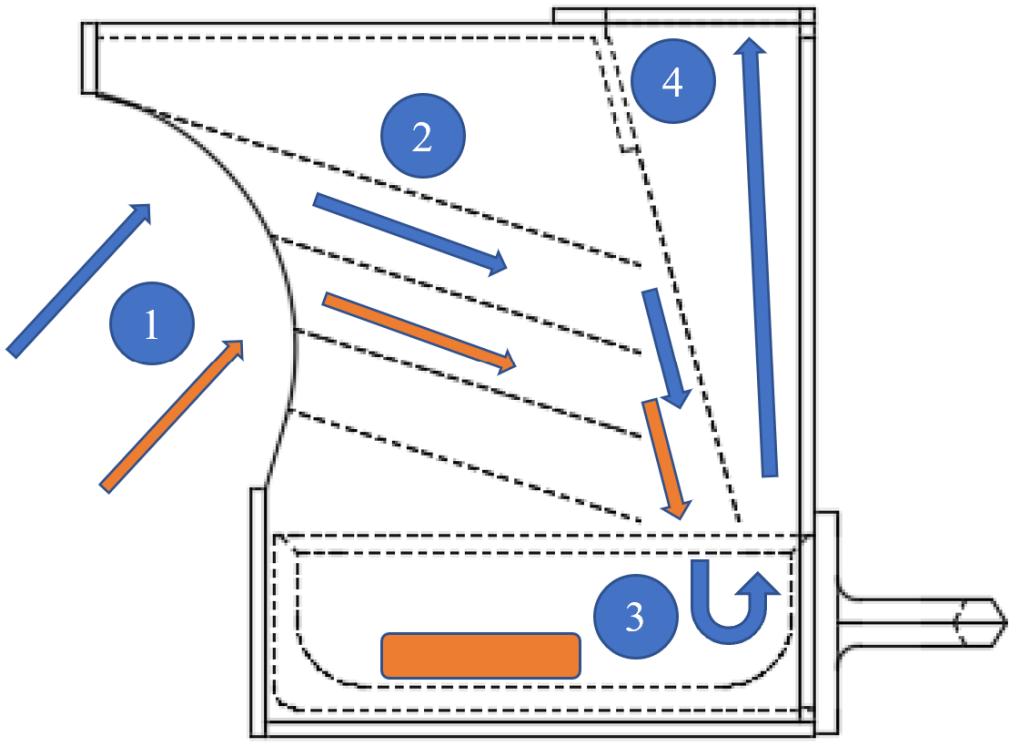

Figure 51. Path of Particles in Collection Box

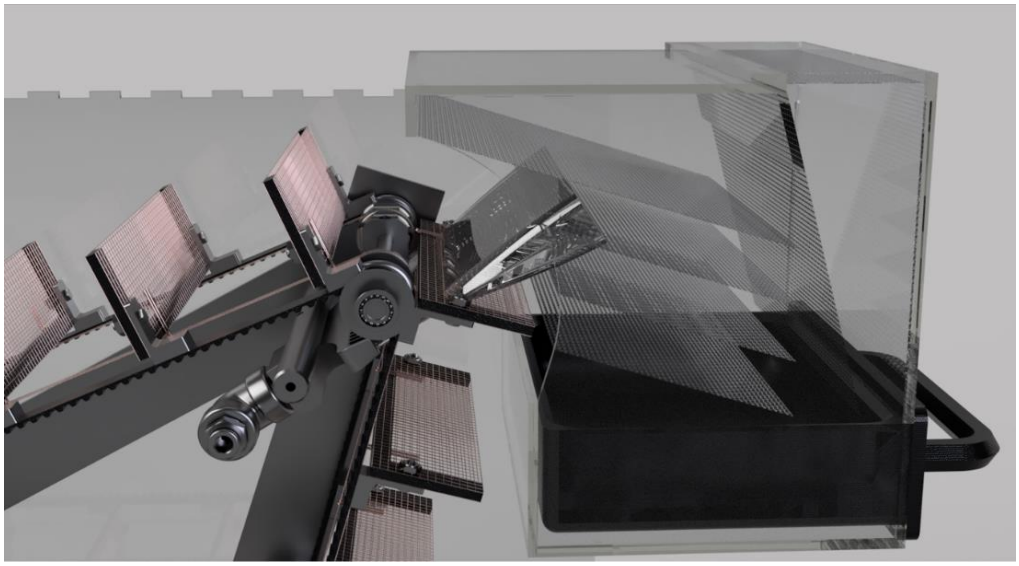

Figure 52. CAD Render of the Air Knife and Collection Box

4.5 Conclusion

The complete mechanism which includes all subassemblies detailed above can be seen below in Figure 53. The entire 3D CAD design for this mechanism assisted greatly with the ease of transiting to prototyping and manufacturing which is discussed in the following section. This model made it easy for placement and precision of all the different subsystems.

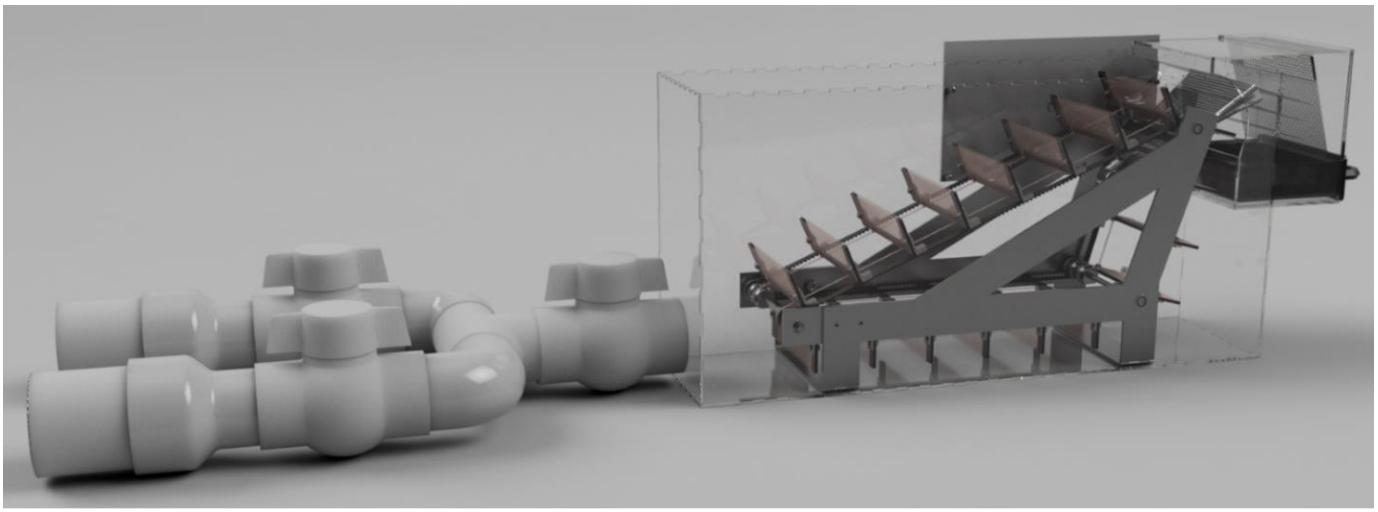

Figure 53 . CAD Render of the Entire Final Iteration Design of the Electrostatic Separation System. This figure shows all mechanical components of this design, including the intake system, electrostatic box, mesh paddles and electrostatic rails, air knife, and collection box.

5. Prototyping and Final Assembly

In the prototyping and manufacturing phase the team realized the CAD model designs. One of the initial stages of prototyping involved creating preliminary physical models out of cardboard and other basic materials, to physically conceptualize the details and size of the full assembly. Images of this preliminary model can be seen in Figures 54 and 55. We assembled stand-ins for each subassembly, but this model predated the collection box and mechanical subsystem. Each subsection using the final components was then assembled and tested separately before they were combined for the final product.

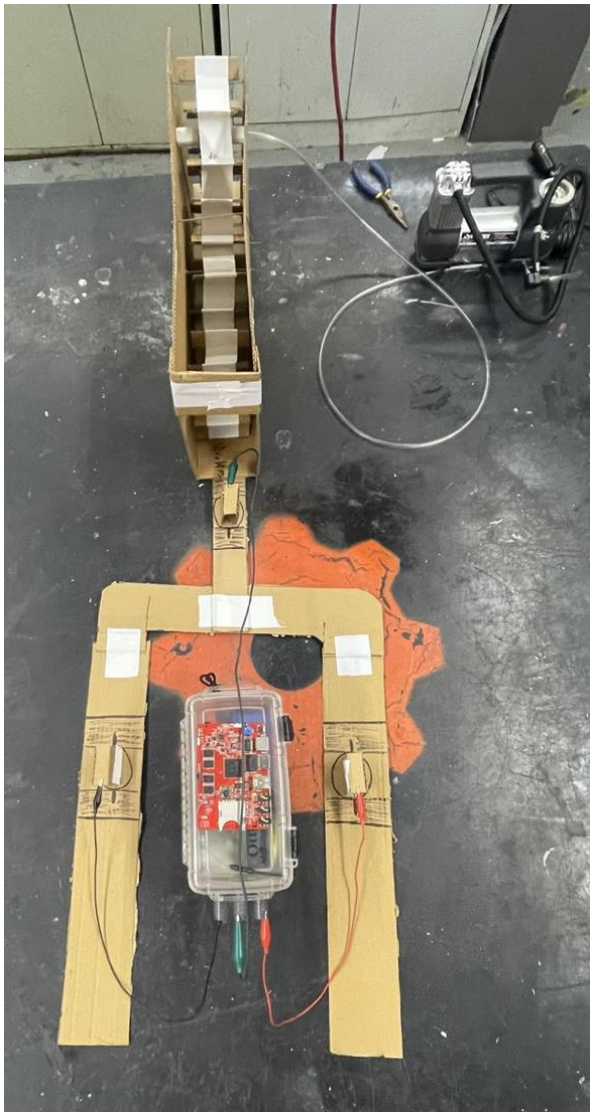

Figure 54. Overhead View of Preliminary Model

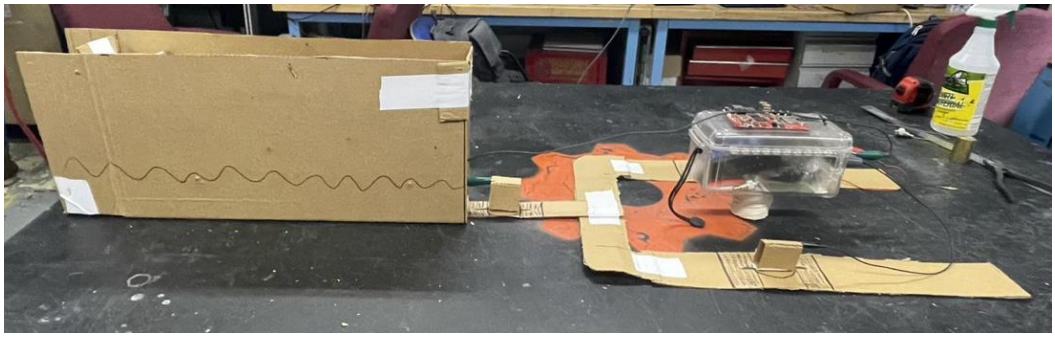

Figure 55. Side View of Preliminary Model

5.1 Filtration Assembly

The filtration assembly consists of four main components: the electrostatic paddles and rubber belts, the frame, axles, and pulleys, the power rails, and the electrostatic chamber. The first three sub-assemblies listed fit within the electrostatic chamber. This chamber is constructed of laser cut 0.09-inch-thick clear acrylic and is sealed with a combination of caulk along the vertical seams and Flex Seal™ along the interior base. There are circular holes cut near the base for the coupling to the intake system and an outlet port. This outlet port was sealed with 0.5 mm mesh.

5.1.1 Electrostatic Paddles and Rubber Belts

The final filtration assembly consists of the mesh paddles on belts and connected to the power rails. The mesh paddles are made of 0.5mm copper mesh, attached to both sides of a rubber bracket. These in turn are attached to L brackets which have been adhered to the rubber belts. Construction of these paddles began with finding the correct sized rubber belts. This influenced our final design multiple times, as we ran into both supply challenges, and seeing the belts in person. We occasionally had to change the belt width we were using based on the availability of other components and changes to the final design made after the purchase. The rest of the filtration assembly was manufactured by the team.

The rubber brackets were cut using a bandsaw, based on a form using CAD measurements. These measurements considered the finalized spacing of the purchased rubber belts. The mesh panels were measured against the rubber brackets and cut using tin shears. The two sides of mesh were then adhered to the brackets using epoxy. Getting these meshes to adhere using only epoxy was a challenge, so the brackets were first adhered using small amounts of hot

glue. The epoxy was used to properly seal the remainder of the mesh and allow the paddles to remain flexible. After sealing these, we realized that there was still the possibility of the opposing mesh sides touching and causing shorting issues while in use, so we inserted small spacers made of the same rubber as the rubber brackets to insure this didn't happen.

The belts were measured parallel to each other, and eighteen marks were made for the spacing of each paddle. The L brackets were adhered to the rubber belts with super glue, as we believed this would provide a large amount of adhesion for the small space. We were not concerned about flexibility here, since the 3D printed brackets were already rigid, and had a small adhesion area relative to the belt.

5.1.2 Frame, Axels, Pulleys

The frame of the filtration assembly is made of welded 6061 0.125" by 1.5" aluminum bar. This frame was built to hold the entirety of the subassembly, and then fit within the electrostatic chamber. This frame, freshly welded, can be seen in Figure 56 below, without the axles and pulleys present. The holes in the bottom of this assembly screw into the base of the electrostatic chamber, and there are two holes on each side of the back of the frame to hold two of the axles. The final axle is held by a bracket that attaches at the front of this frame. This setup is to allow for tensioning and de-tensioning of the belts while assembled.

Figure 56. Welded Frame Assembly

The pulleys for this subassembly that are not made of metal to conduct along the power rails are 3D printed and were designed with holes such that heat inserts could be installed to house set screws. The axles were manufactured from ¼ inch D-shaft, with was measured to length according to the CAD, and checked against the physical frame. The set screws of each pulley were aligned with the flat of the D-shaft.

5.1.3 Power Rails

After these three components were assembled, we ran into an issue. The paddle assembly and L bracket were too thick for us to properly use the bolts we had chosen for this purpose. The bolts were too short to allow for the nut to properly attach the paddles on the other side. At this point, we decided to similarly attach the paddles to the L brackets with superglue. We moved in this direction rather than finding other bolts because we wanted to be able to move into testing the assembly as soon as possible. A detailed image of this sub-assembly can be found in Figure 57, featuring the two-sided mesh paddle, rubber brackets, spacers, and L bracket attached to the rubber belt.

Figure 57. Final Paddle Attachment Method

The final major stage of the filtration assembly manufacturing was creating the power rails. These rails were made of woven copper belts, which had to be cut and tensioned while the filtration assembly was mostly put together, as shown in Figure 58. This was done in order to ensure that the rails would not fall off the pulleys they were meant to be attached to. These rails becoming detached could result in electrical shorts, or a lack of power to one or both sides of the paddles. After finding the appropriate length for these rail wires, they were sewn together using thread, and secured with small knots, as shown in Figure 59.

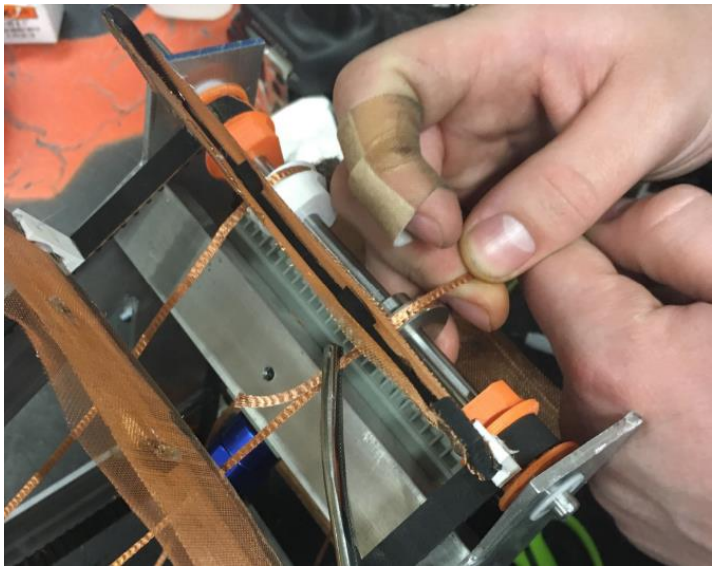

Figure 58. Tensioning Copper Power Rail

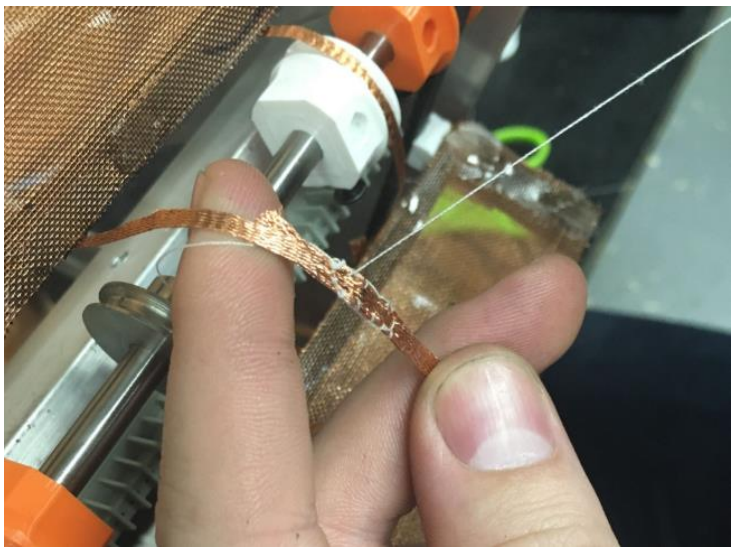

Figure 59. Securing Copper Power Rail

For the final stage of the filtration assembly, we had to ensure that the rails connected to the paddles consistently and in the correct locations. Due to the proximity of the underside of the paddles to the rails that was not evident in our final CAD, we decided to insulate the areas of the paddles that were most likely to inadvertently touch the rails. This insulation can be seen on the paddle in Figure 58, most prominently visible on the right side of the paddle. After this, we needed to find a way to properly connect the rails to the paddles, such that the correct sides would be charged. Our original plan had been to weave a wire through the power rail near the appropriate side of the paddle, solder it into place, and solder the other end of the wire to the mesh of the paddle.

However, we found this would not work the way we had envisioned for multiple reasons. The first issue was that the wire we intended to use was thick enough to significantly alter the weave and tension of the power rail, leaving a large gap. We felt that this could disrupt the travel over the power rail's pulleys, and lead to the power rail falling off. The second issue was that while we attempted to properly time the power rail to the timing of the pulleys, we were not completely successful. The power rails slide slightly differently, and even a 0.04-inch difference between the power rail pulley and the rubber belt pulley resulted in the test paddle and connecting wire becoming distant from each other after only a quarter turn around the system. Due to these foreseen issues, we decided to follow a different approach. Some of the same material that the power rail was made of was looped around the power rail and attached on both ends via solder to the meshes. This can be seen in detail on the left in Figure 58, and part of the process can be seen in Figure 59, where two teammates are soldering the wire into place.

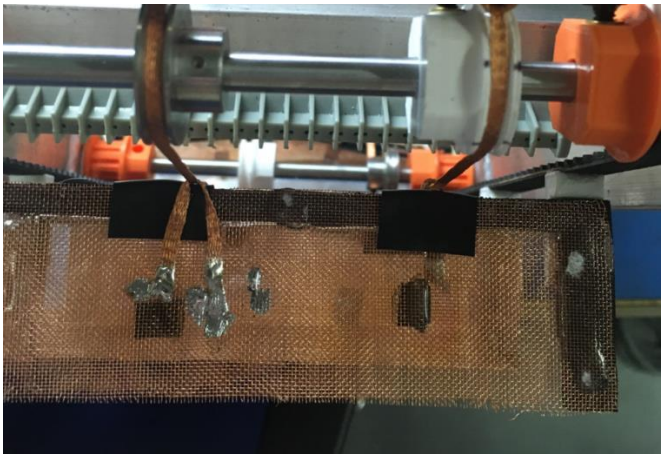

Figure 60. Power Rail to Paddle Final Connection

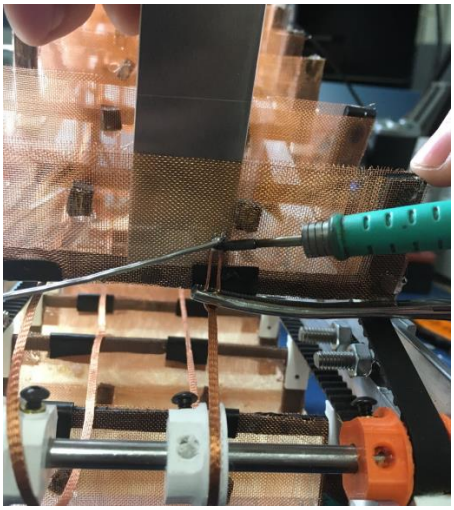

Figure 61. Power Rail to Paddle Connecting Process

5.2 Intake Assembly

Prototyping of the intake subsystem began with the lo-fi prototype early in the design process. We cut placeholder pieces for each of the PVC fittings and pipe lengths from cardboard as shown in Figure 60 and then laid them out with the other subsystems as seen above in Figures 54 and 55. This created a visual representation of the final prototype, which allowed us to determine whether this was the right size and scale we wanted before purchasing any materials. Without proper servos, most of the assembly work was basic cutting to length of the PVC pipe and fitting it together in the correct form. Once the individual pieces of PVC pipe had been cut, we began the process of modifying the pieces which would house the impellers and to which the stainless-steel mesh would be secured on the front of the pipe.

Figure 62. Accurate Layout of the Intake System with Cardboard

To secure the impellers within the 3” diameter PVC pipe sections, the existing impeller housing needed to be modified. Specifically, the standoff running lengthwise along the outside of the housing needed to be shortened by about a quarter of an inch. This was accomplished using a belt sander. Once the standoff was shortened, the holes which it came with were enlarged with a #35 drill bit and then tapped for UNC 6-32 thread, resulting in the finished impeller in Figure 63. The hole pattern was drilled to the outside of the pipe in which the impellers were to be housed using masking tape before being bolted into the pipe. We made a custom rubber gasket to seal the pipe such that no water would exit or enter the intake screens. An additional hole was drilled to route the impeller wires, which were then sealed in place with silicone caulking.

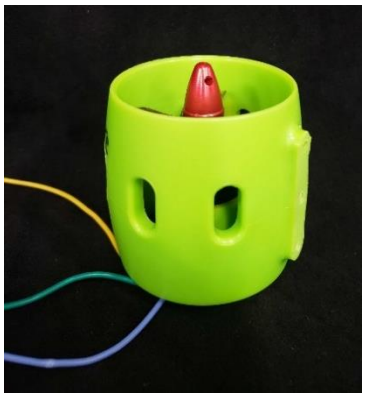

Figure 63. Finished Impeller

The stainless-steel mesh was placed on both sides of the initial 3” PVC section which houses the impellers. The primary mesh screen was cut into a circle such that it matched the open face of the pipe and held in place with a marine grade epoxy. The secondary mesh was intended to be removable, and as such was simply cut to size and placed such that it would be pressed between the face of the pipe section and the flange in the ball valve. This way, the impellers could still be accessed if something was broken or needed to be adjusted. With the screens and impellers in place, the ball valve adapters on, and the plumbing fitted the intake subsystem was fully assembled.

5.3 Mechanical Linkage & Air Nozzle Assembly

The air nozzle attachment assembly, shown below in Figure 64, was fabricated out of a 1” x 0.5” piece of aluminum bar stock. Both ends of the aluminum bar are drilled and tapped for 8-32 screws, and there are countersunk 8-32 holes on either side of the welded frame for securely holding the air nozzle assembly in place. The air nozzle itself, seen in Figure 32, is attached upside down to the center of the bar, mounted to be parallel with the mesh paddles. The ideal mounting angle for the air knife would be 33° from horizontal, such that the air pattern makes an approximately 130° incident angle with the mesh panels in the collection box. Due to the nature of mounting the bar inside the frame, it was difficult to get the alignment correct so it is likely that the actual angle is slightly off.

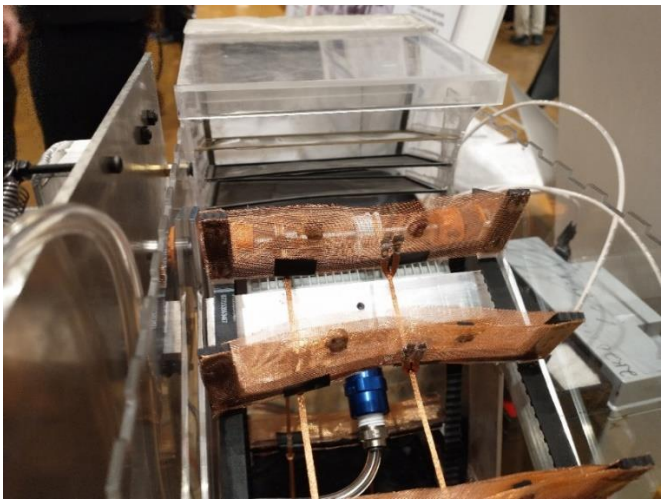

Figure 64. Air Nozzle Assembly

The air knife is connected to a length of ¼" clear flexible PVC tubing with a male-to-male ¼" NPT adapter, and a push-to-connect tube fitting. That flexible tube was fed through a hole in the side of the electrostatic chamber and connected to the valve of the valve assembly using another ¼" push-to-connect fitting shown below in Figure 65.

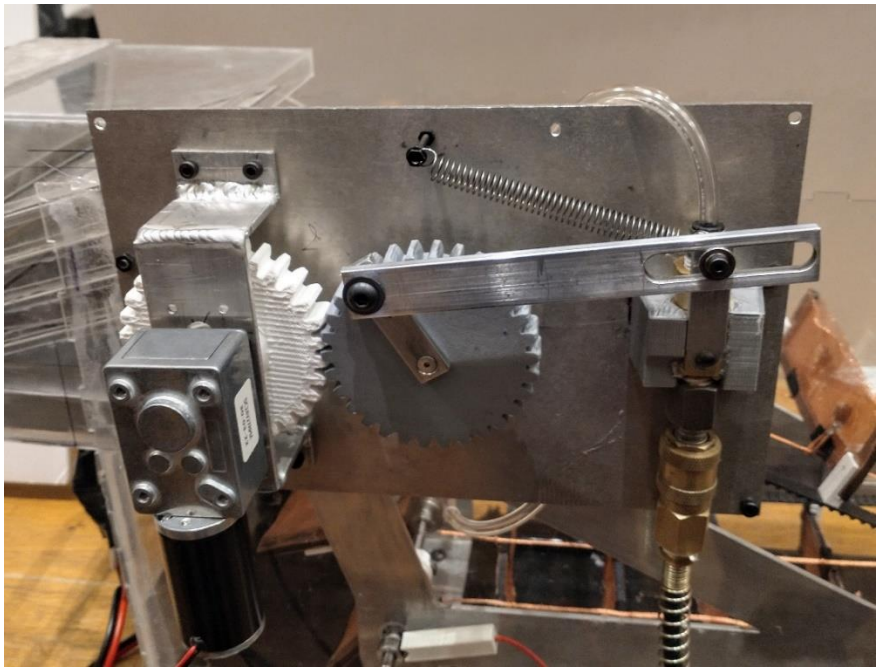

Figure 65. Finished Mechanical Linkage Assembly, Closed Position

Figure 65 above shows the assembled mechanical linkage assembly. The base plate was fabricated out of 1/8” 6061 aluminum plate, with holes for mounting both gears, the motor bracket, as well was 4 machined standoffs connecting it to the electrostatic chamber. The motor is mounted onto the mail plate with a welded bracket. The bracket is attached to the motor with countersunk screws and bolted onto the mail plate of the assembly. Two ¼" ID bearings are press fit into the main plate, as seen in Figure 66, for the drive hear and the crank gear. On the back side of the mounting plate, there is a shaft collar mounted onto the main drive shaft.

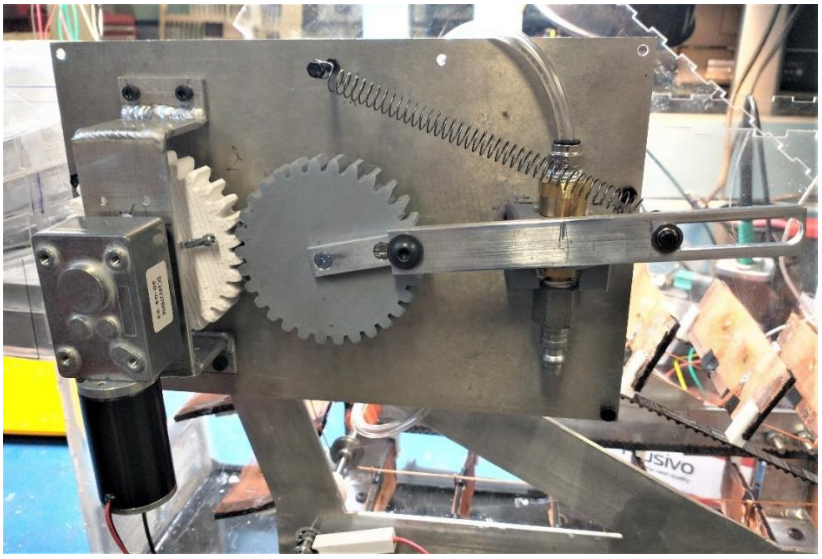

Figure 66. Finished Linkage Assembly, Opened Position

A housing is attached to the back of the plate with adhesive, holding a carbon brush with a spring against the collar such that the brush is in constant contact with the shaft collar. The spring keeping the valve link closed is attached to the main plate using a bolt, as seen in Figure 66, and hooked around the shoulder bolt holding the bearing in place. Both the drive gear and the coupler gear were 3D printed out of ABS plastic and have threaded brass 6-32 heat inserts installed with bolts to attach them to the steel D-shafts. The linkage mechanism, along with the filtration system are powered with a 90° worm gear motor, rotating at 27 RPM at 24v with a peak torque of 60 kg*cm. The motor can be seen on the left side of Figure 66.

5.4 Collection Box Assembly

The collection box is made of the same 1/8-inch laser cut acrylic as the electrostatic chamber. The main box and guides for the mesh panels were assembled using epoxy, as shown in Figure 67. The mesh frames which sit inside the box are similarly made of laser cut plastic, with 74-micron mesh stretched over the frames and super glued in place. These mesh panels were then slid into place within the box, along with the 3D printed collection drawer. This full assembly can be seen in Figure 68, attached to the assembled electrostatic chamber, with the collection drawer in the lower left of the image, and the mesh panels inside the box. This subassembly was the simplest in terms of assembly, as this section did not involve any moving components.

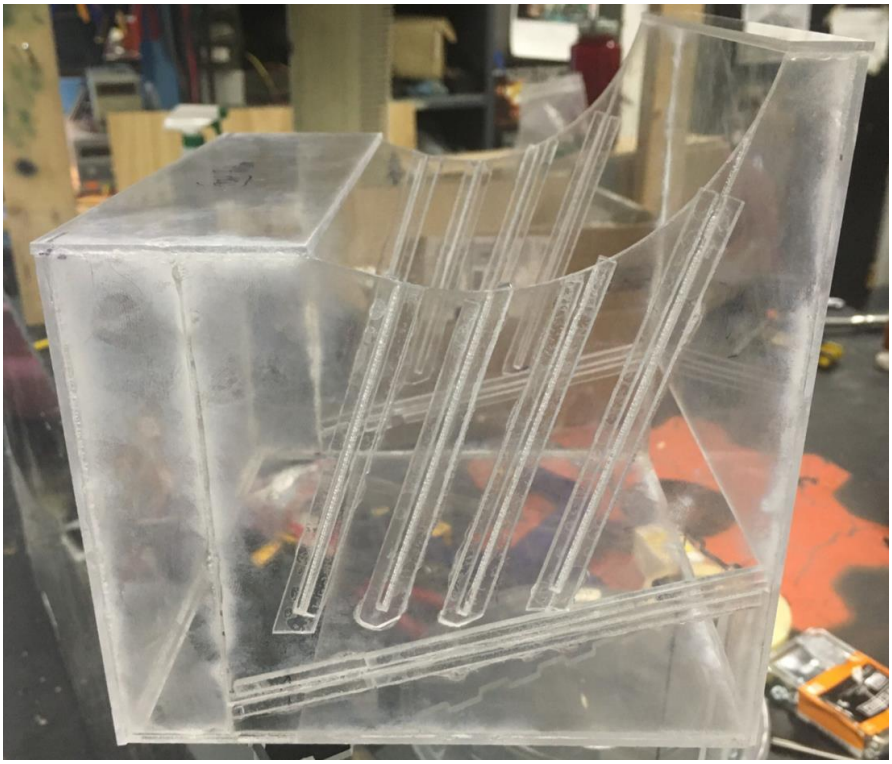

Figure 67. Assembled Collection Box

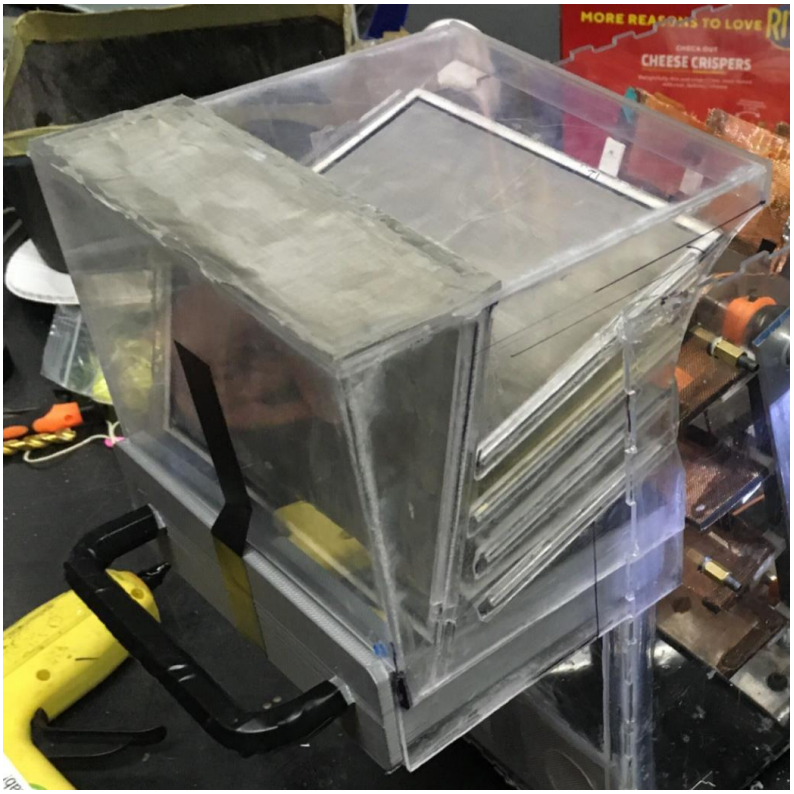

Figure 68. Fully Assembled Collection Box System

5.5 Conclusion & Lessons Learned

After the individual sub-assemblies were constructed, we assembled the final prototype, as shown in Figure 69. The intake system simply inserted into the constructed hole located on the front of the electrostatic chamber. The air knife assembly was properly aligned within the frame, and the mechanical linkage subsystem was attached via four manufactured standoffs to the outside of the electrostatic chamber. The drive axle was attached, along with the pneumatic tubing for the air knife, to the linkage system. Finally, the collection box was glued to the top edge of the collection box. To be properly put in place, part of the collection box siding was removed.

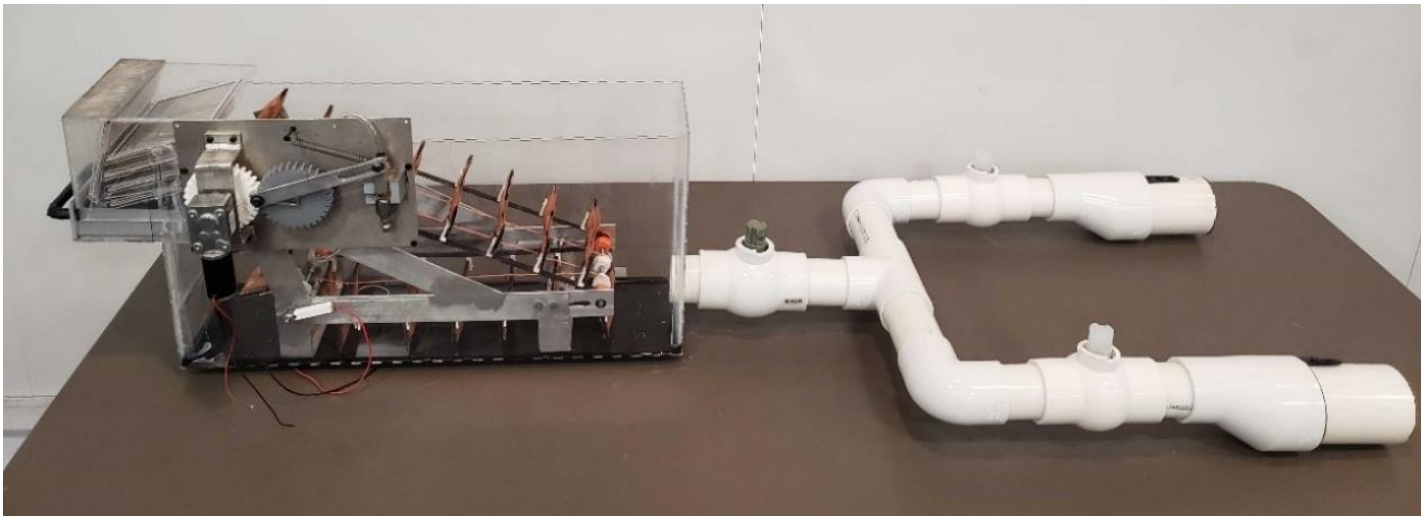

Figure 69. Full Assembly

The assembly of this prototype went well, and we only had to make minor adjustments over the course of this prototype assembly. These small changes, however, began to add up, and we discussed multiple times how we would have designed the system differently overall. One of our biggest challenges came from the assembly and manufacturing of the filtration and mechanical subsystems.

Due to the addition of the mechanical linkage subsystem after the design of the electrostatic chamber, the system could no longer be entirely assembled outside of the chamber and then slotted into place as intended. The drive axle had to extend out of the box, meaning that it had to be inserted from the side. This added a step to our assembly process, but after some

deliberation the team decided that a box redesign was not necessary for this project. The frame and belts would be assembled outside of the box with the top rear axle removed, then slotted in. Once the top rear axle was added, the belts could be tensioned and the mechanical linkage subsystem attached.

6. Testing

Due to the time constraints of this project, the team was unable to conduct field tests of the complete system. However, throughout the course of assembly we designed and ran feature tests specific to the function of each subsystem. These tests were run to provide proof of concept for each subsystem and ensure they were manufactured according to the specifications of our design. By the end of feature testing on each individual subsystem they were able to simultaneously run together with proper timing. The electrostatic and air knife systems were connected to the mechanical linkage system. This led to the belt and paddles moving around the pulleys while the air knife was spraying each paddle. This full feature test was viable when figuring out any last-minute tweaks that needed to be altered. The key parts to focus on during the test were that the air knife was correctly spraying the paddles, and there was consistent air flow that traveled through the collection box without air circling back to the electrostatic system.

6.1 Filtration Tests

When testing the filtration system, we used two separate types of plastic particles, and two mesh systems. Our preliminary electrostatic test involved microplastic particles we ground ourselves and charged mesh panels a few inches apart. The second test used purchased microplastic particles and a replica of the mesh paddles used in the electrostatic belt assembly.

6.1.1 Preliminary Electrostatic Tests

Before testing and examining these systems, we demonstrated the efficacy of the electrostatic effect on microplastic particles. We cut squares of copper mesh and created a small batch of microplastic particles by grinding orange PET pellets down and sifting them through a 500 micron sieve. The particles were mixed into a water reservoir through which the mesh was run while connected to a power supply to act as an anode. The plastic particulate exhibited strong adhesion to the copper mesh even when the cathode was far from it. This basic test provided confirmation that these particles will stick to the paddles even when a strong charge is not detected between them. In Figure 70 below, the plastic particles are stuck to electrostatic copper mesh.

Figure 70. Testing Microplastic Electrostatic Charge. The orange plastic particles collected on electrically charged 0.5mm copper mesh.

6.1.2 Belt System Tests

During preliminary testing of the electrostatic belt system, we mounted a drill to the drive axle, shown in Figure 71, to slowly move the belt in both directions to locate any issues found. This allowed us to gage if there were any movement, clearance, tolerance, or tension issues with the system. This method enabled us to catch flaws in the belt and paddles during assembly, which were then amended.

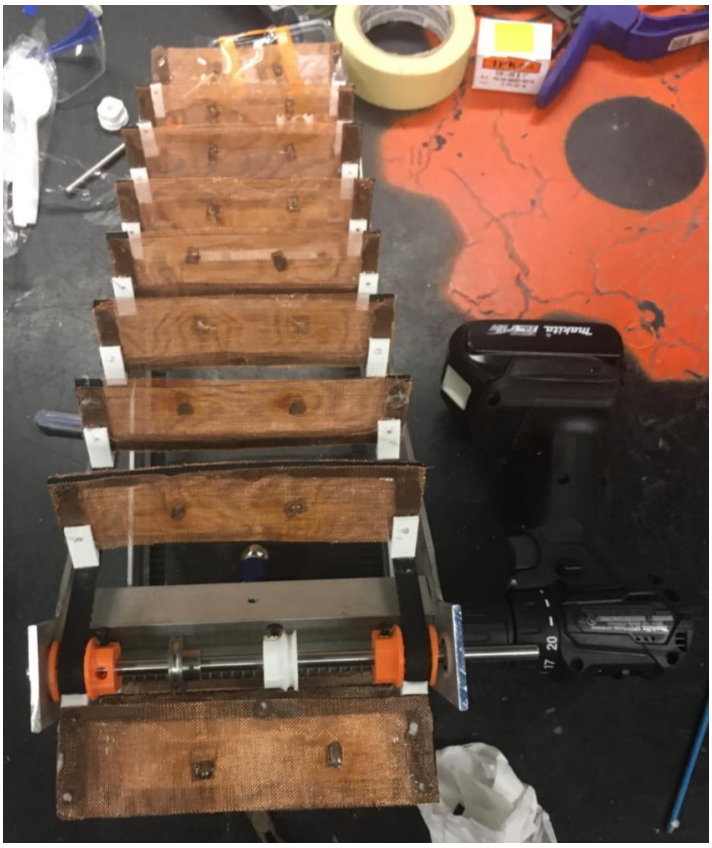

Figure 71. Testing Belt System Out of Box. The drill, on the right, was used to easily turn the axle, with a low torque rate and low speed, in order to simulate the motors being used in the final assembly.

While setting up our testing we were able to adjust the front idle axile to control tension. Since there were two belts, one on each side, this precision on the tension needed to be as accurate as possible. During tests we learned that if the belts are not tensioned equally one belt could skip a tooth and end up causing the belts to be out of sync, causing the paddles to detach and impact the entire system. Once the belts were equally tensioned the system ran steady, consistent, and smoothly without having any clearance problems.

6.1.3 Electrostatic Attraction Test in Water

To obtain proof of concept for electrostatic separation we created a test paddle and ran a few quick separation tests. Each side of the paddle was connected directly to our project power source, which was two motorcycle batteries providing 24V. The test was set up in an isolated water reservoir. To the reservoir was added and thoroughly mixed 2L of water, 0.5g of 500-

micron microplastic particulate, and 0.5g of iodized salt. The salt was added to mimic the salinity of freshwater according to the United States Office of Naval Research, which classifies freshwater as having salinity less than 0.5g/L (*Freshwater - New World Encyclopedia*, para. 5, n.d.). Though this is an exceedingly high concentration of microplastics, we lacked equipment to accurately measure plastic separation on the scale that would be realistic in a field setting. Despite this, the test provided a proof of concept for the electrostatic separation method.

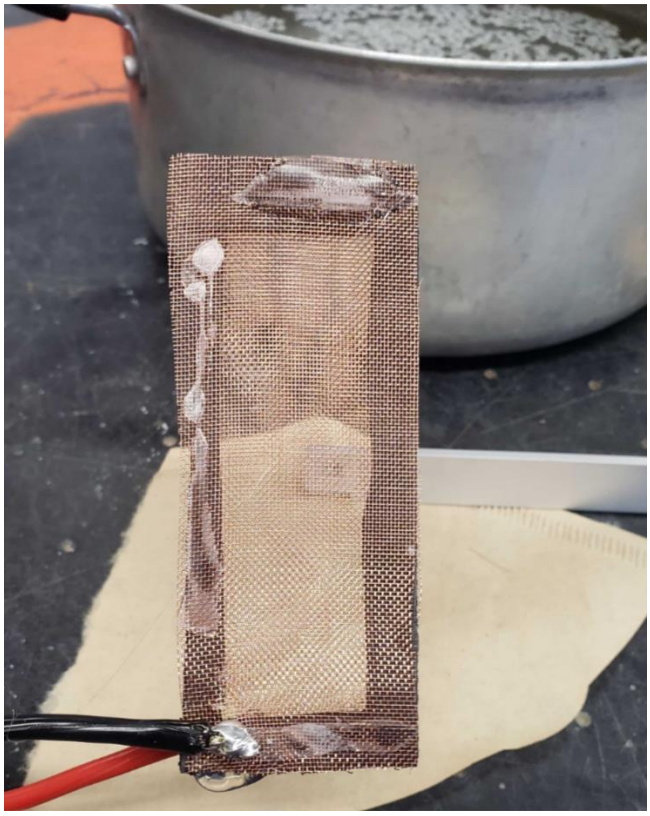

Figure 72. Test Paddle. This test paddle has slightly less interior surface area than the actual paddles on the assembly, as additional interior spacers were required to account for the heavier jumper wires used in this test.

We tested with 500-micron particulate, as this was the largest particle size we aimed to collect and would be the least likely to be electrostatically influenced due to its size. The power to the test paddle, shown in Figure 72, was switched on and the paddle was submerged and gently propelled through the water for 29 seconds, the amount of time that each paddle on our system will spend submerged and travelling through the water. The paddle was then rinsed

through a 20-micron filter, which was weighed. This weight was compared to the wet, empty weight of the filter to determine the mass of plastic particulate collected by the paddle. The paddle averaged a collection of 0.01g of microplastic collection in 29 seconds. One of these test run results is shown in Figure 71. As compared with the results of testing in Figure 69 even visually, the paddle has a significant layer of microplastic particles attached to its surface. Further testing with real world plastic concentrations will be required to ascertain the efficacy of the electrostatic paddles.

Figure 73. Test Paddle with Particulate

6.1.4 Power Rail Tests

As the power rails are not as elastic as the rubber belts, we constructed them with the rubber belt already tensioned. The copper weave was looped over the pulleys, tensioned by hand, and clamped in place while the connection was sewn together. Images of this tensioning process can be seen in Figures 58 and 59. The paddles attached to the power rail consistently stayed in

the correct position and tracked along the pulleys with the electrostatic belt. Each rail was tested for electrical shorts to the frame, and to the side of the paddle with the opposite polarity. The rails were also tested for continuity to ensure that a strong electrical connection was maintained from the power source to each paddle throughout the full range of motion. Once the electrical systems checks were completed, we moved on to the next set of feature tests.

6.2 Intake Tests

For the intake system we tested the actuation of the three ball valves and the two impellers, such that the intake system could cycle through each of its four stages. Unfortunately, we were unable to secure servo motors strong enough to actuate the 2-inch PVC ball valves due to budget constraints. We designed a bracket and adapter such that these servos could be implemented if purchased and wrote a basic program (see Appendix A: Arduino Intake Code) that would run both the impellers and servos according to the rinse stages and a set interval. The code that we wrote will run each stage of the full rinse cycle on a set interval of 5 hours. This interval can be modified according to the clarity and density of debris of the water. The intake system without servos can be seen in Figures 74 and 75 below, displaying the areas where the ball valves would be actuated and the mesh on the entrance to the intake.

Figure 74. Intake System

Figure 75. Intake System Entrance with Mesh

6.3 Mechanical Linkage and Air Knife Tests

For testing of the mechanical linkage, seen in Figure 76 below, we first confirmed that the movement of the mechanism was smooth with no mechanical interference or excess friction in any of the links. We ran the linkage for several hours and then inspected its components for signs of unnatural wear or stress. We found no signs of physical weakness or wear, though we did discover that one shaft collar was misaligned and corrected it. In addition, we inspected the linkage as it was running to ensure that it was not putting undue strain on the motor, and that the belt and valve timing operated consistently. We also confirmed that our motor was sized correctly by measuring the current pull throughout the cycle. We measured the base current for when the motor was moving the belt with the valve assembly in the non-actuated state as 0.48 amps. The peak current for the motor while actuating the valve assembly was 0.62 amps or 14.9W, and since the motor reaches its peak power at 16.8W the motor was within its operational range.

For the timing of the valve assembly our theoretical timing was at a ratio of 1:0.4, meaning that for 1 full rotation of the crank link the opening and closing of the valve/output link would take 0.4 of a revolution. We measured the actual timing to be 1:0.5. This is a large difference because the movement of the belt and the valve is mechanically connected. Therefore, the overall timing will not be affected, but the belt system's overall speed will be slower. This discrepancy is most likely caused by the accuracy of manufacturing and the motor slowing down slightly while under load. This in turn pushes against the return spring and the friction in the valve assembly. It is also possible that the manufacturing of the linkages was not exact. All the links were machined using a manual mill by our team, and due to manufacturing errors with the positioning of features the links may not be as precise as physically able. From a combination of both issues, the valve mechanism as assembled does not perfectly match our modeled design.

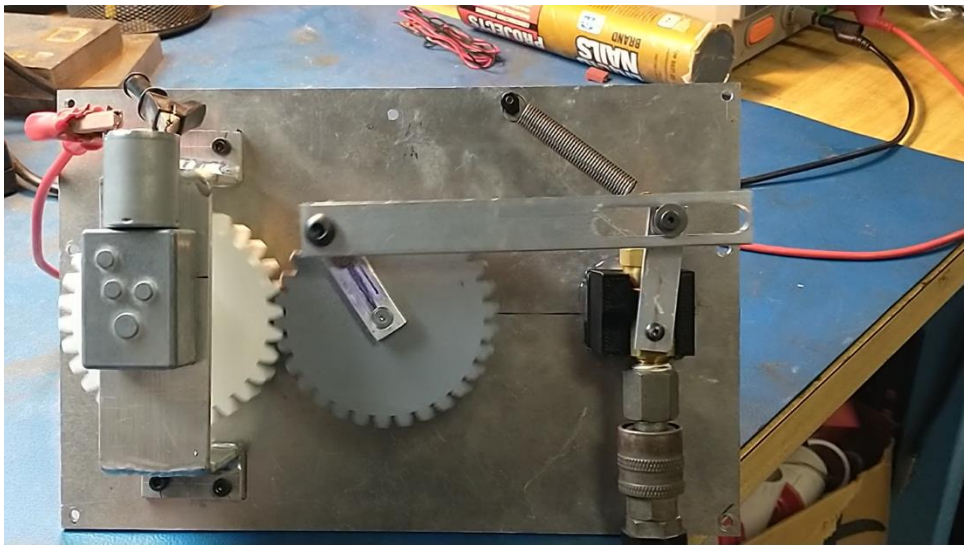

Figure 76. Testing Mechanical Linkage. After this function test was performed, the motor in this figure broke and was replaced with a similar motor that has a different RPM. The bracket holding the valve in this picture is a temporary print and was replaced with a new bracket which was epoxied in place. After these replacements, the motor and bracket performed well.

6.4 Collection Box Tests

The criteria determining success for the collection bin were secure connection and proper alignment. For these function tests we simply verified that the bin was securely fixed to the electrostatic chamber, and that it was properly aligned such that it sealed with the top panel and did not interfere with the paddles as they rotated about the top axle. We also tested that each of the mesh panels could be slid freely into and out of its place. The collection bin can be seen securely in place in Figure 77. We also confirmed that the air knife was properly working in conjunction with the box, such that we did not feel any air coming back out the entrance to the box and was exiting from the expected mesh panel area.

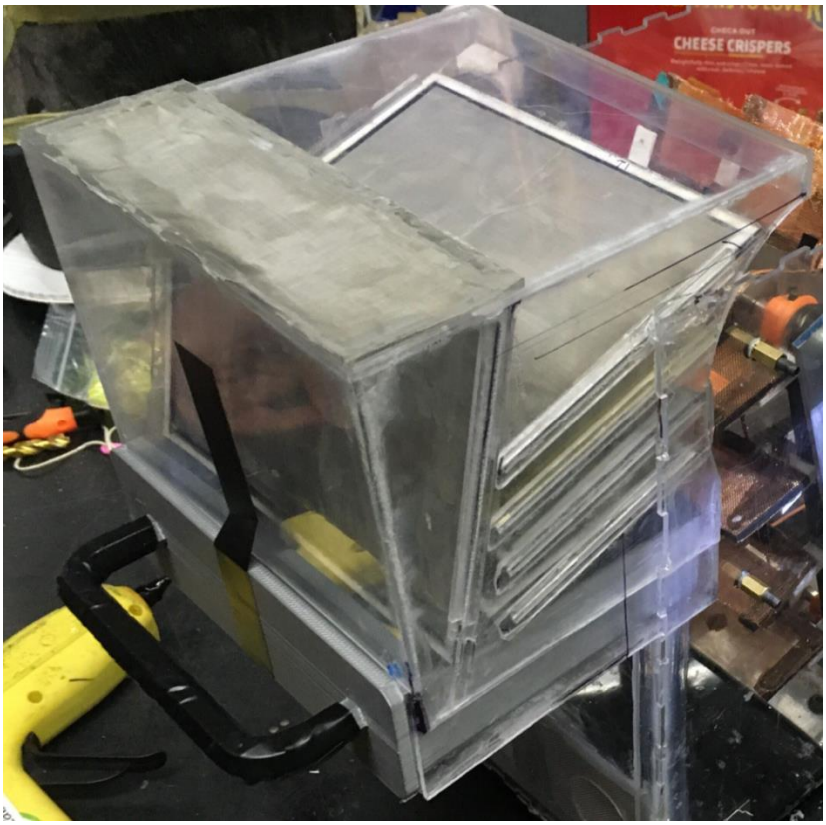

Figure 77. Collection Bin as Part of Full Assembly

6.5 Conclusion

Based on the subassembly tests, we were able demonstrate the full functionality of many of the sections of this microplastic separation prototype. During testing we made small adjustments to our system in order to ensure smooth movement. Some of these adjustments included tensioning the belts and power rails, adjusting bearing seating, and fine-tuning the air pressure.

The code written to run the self-cleaning intake subsystem runs properly and could actuate all four stages if the correct servos are sourced. The belt filtration system has a full range of smooth movement, and the electrical rails deliver a strong connection from the power brushes to each paddle without shorts, while staying in line with the electrostatic paddles. The mechanical system actuates the air knife correctly and smoothly, and pressure is properly regulated. The collection box allows for pressure release only through the designated exhaust mesh, and there were no pressure leaks along the seams of the box.

7. Conclusion

During this project, our team designed, prototyped, manufactured, and feature tested a novel electrostatic based microplastic filtration device for application in oft-overlooked freshwater environments. We accomplished our goal of proving the conceptual validity of a heretofore untested filtration method for this medium.

The feature tests of our final separation system proved that our mechanism was able to function as expected. These tests were able to be done with minimal errors thanks to the creation of a precision 3D CAD model, especially for the subassembly sections. Our final design, while not fully optimized for field tests, is a large step towards filling the previously empty niche of freshwater microplastic separation.

This project presents a novel system for selective filtration in an application where traditional filtration and separation methods would have unintended negative effects on the surrounding environment. A healthy freshwater ecosystem requires the water to be densely populated with particulate and microorganisms larger than the microplastics to be removed. Not only would these quickly foul a filter with a small enough pore size to remove microplastic particulate, but their removal could also have catastrophic effects for the ecosystem the filtering device is attempting to help. Our application of electrostatic technology seeks to fill this gap, allowing for selective filtration of microplastics while remaining neutral in its effect on all other aspects of the environment.

8. Broader Impacts

Throughout the course of our project, the impacts of our device and microplastic removal method on the environment were at the forefront of our considerations, design iterations, and testing. When first conceptualizing our project, we decided that the best use of the engineering knowledge that we have gained in our time at WPI is to have a positive effect on the environment. While we did not follow strict written guidelines, our project was guided by this sense of stewardship of our local ecosystems, especially after some of our team members spent time exploring the impacts of microplastics on the Worcester watershed.

8.1 Environmental Impact

Our project was originally inspired by the large negative environmental impact microplastics have on all studied components of the environment that they come into contact with. As discussed in section 3.2.1 Environmental Interaction, after eliminating some methods, our primary mode of choosing which method of separation we would use was based on the overall environmental impact the system or device would have. In our final design iteration, we avoided harmful chemical coagulants, large or loud systems, and harmful metals or other materials. In future designs meant to be deployed in the field for extended periods of time, the materials would be more robust and less environmentally interactive, unlike the materials we used for prototyping, such as plastics. While we did use plastics for our prototype, this was deemed acceptable by our group, as these plastics are meant to be durable and reusable and will not be discarded after a single use.

The State of California has been at the forefront of implementing wide scale microplastic regulation, and openly accepts the danger microplastics present to the health of the public. The State of California publishing a risk report in 2021 outlining the hazardous potential of microplastics, and the sources of microplastic pollution (Brander et al., 2022). There were also provisions made in California Health and Safety Code section 116376 requiring the State Water Board to establish regulations on the proliferation of microplastic particulates in drinking water (*SB-1263 Ocean Protection Council: Statewide Microplastics Strategy.*, 2018).

The Microbead-Free Waters Act of 2015, made as an amendment to the Federal Food, Drug, and Cosmetics Act, states “The Microbead-Free Waters Act of 2015 prohibits the manufacturing, packaging, and distribution of rinse-off cosmetics containing plastic

microbeads." (Pallone, 2015). The act prohibits the interstate commerce and manufacture of plastic microbeads, defined as "any solid plastic particle that is less than five millimeters in size and is intended to be used to exfoliate or cleanse the human body or any part thereof" (Pallone, 2015).

8.2 Societal Impact

While we were unable to do market research for our end prototype within our project's time frame, it is our hope that providing a template and demonstration of a small-scale and economically viable system for filtering microplastics will show that eliminating microplastics from the environment is a goal that can begin as a local effort. At the beginning of the ideation stage, the team considered the merits of creating a larger system, to be implemented in appropriately sized areas. However, we determined that a smaller scale project would be more feasible for small environmental volunteer groups, municipalities, and individuals to implement.

9. Future Work

Future work on this project should begin with field testing, as this fell outside the scope and time constraints of the project. Our hope is that one day this system could be scaled for municipality and volunteer use in rivers and lakes. We also believe it would be beneficial to run more detailed testing, which would include finding the range of sizes of microplastics that could best work with this system. Tests to establish effective intake cycle intervals for water with differing levels of floating debris could be run to determine how long and intensive rinse stages must be to adequately backwash the intake screens. In this way benchmarks for interval settings could be established based on water clarity. Air flow testing with colored smoke or airborne particulate would help to ensure that the air stream flows through the intended pathing within the collection bin. Increasing the autonomous run time and conducting long-term field tests with organic and manufactured debris would also be an important next step. The entire system should be made more robust such that it can survive extended periods exposed to the elements, especially through inclement weather. Determining the amount of time that the system can run autonomously would be helpful when being scaled for larger areas. Further research and testing about the scalability and manufacturability of a variety of sizes based on our final iteration would also help to indicate the viability of this electrostatic separation system. Finally, we would like to conduct an analysis of the system's power requirements, so that we can create further iterations with an even greater positive environmental impact. Long-term field tests would help determine if power sources such as solar panels would be viable as a major component of future designs.

References

Andrady, A. L. (2011). Microplastics in the marine environment. *ScienceDirect, 62*(8), 1596-1605. https://doi.org/10.1016/j.marpolbul.2011.05.030

Anonymous. (2018). Too much of a good thing. *The Economist, 426*(9081), 55-57. https://search-proquest-com.ezpxy-web-p-u01.wpi.edu/docview/2014511819?OpenUrlRefId=info:xri/sid:primo&accountid=29120

Barboza, L. G. A., Vethaak, A. D., Lavorante, B. R. B. O., Lundebye, A.-K., & Guilhermino, L. (2018). Marine microplastic debris; an emerging issues for food security, food safety and human health. *Marine Pollution Bulletin, 133*, 336-348. https://www.sciencedirect.com/science/article/pii/S0025326X1830376X#bb00

Bellas, J., Martínez-Armental, J., Martínez-Cámara, A., Besada, V., & Martínez-Gómez, C. (2016). Ingestion of microplastics by demersal fish from the Spanish Atlantic and Mediterranean coasts. *National Library of Medicine,* 109(1), 55-60. https://doi.org/10.1016/j.marpolbul.2016.06.026

Borgia, F. (2021). Chapter: Performance Analysis and Modeling of microplastic separation through Hydro Cyclones. *IntechOpen*. https://www.intechopen.com/chapters/78027

Bose, A., Andreu, I., de Oliveira, T. T. S., Machado, M. C., Tripathi, A., & Vimbela, G. (2020). Interaction of cyanobacteria with nanometer and micron sized polystyrene particles in marine and fresh water. *Langmuir, 36*(14), 3963–3969. https://doi.org/10.1021/acs.langmuir.9b03644

Brander, S.M., Hoh, E., Unice, K.M., Bibby, K.R., Cook, A.M., Holleman, R.C., Kone, D.V., Rochman, C.M., Thayer, J.A., Monteiro, S. S., Rocha-Santos, T., Prata, J. C., Duarte, A. C., Girão, A. V., Lopes, P., Cristovão, T., & da Costa, J. P. (2022). A straightforward method for microplastic extraction from organic-rich freshwater samples. *Science of The Total Environment, 815.* https://doi.org/10.1016/j.scitotenv.2022.152941. Retrieved April 30, 2022 from https://www.opc.ca.gov/webmaster/_media_library/2021/05/Microplastics-Risk-final-report.pdf

Bui, X.-T., Vo, T.-D.-H., Nguyen, P.-T., Nguyen, V.-T., Dao, V.-T., & Nguyen, P.-D. (2022). Microplastics pollution in wastewater: Characteristics, occurrence and removal

technologies. *Environmental Technology & Innovation, 19.* https://doi.org/10.1016/j.eti.2020.101013.

Corcoran, P. L., & Zbyszewski, M. (2011). Distribution and degradation of fresh water plastic particles along the beaches of Lake Huron, Canada. *Water, Air and Soil Pollution, Dordrecht, 220*(1), 365-372. https://doi.org/10.1007/s11270-011-0760-6

Cox, K. D., Covernton, G. A., Davies, H. L., Dower, J. F., Juanes, F., & Dudas, S. E. (2019). Human consumption of microplastics. *Environmental Science and Technology, 53*(12), 7068-7074. https://doi.org/10.1021/acs.est.9b01517

Dris, R., Imhof, H., Sanchez, W., Gasperi, J., Galgani, F., Tassin, B., & Laforsch, C. (2015). Beyond the ocean: Contamination of freshwater ecosystems with (micro-) plastic particles. *Environmental Chemistry, 12*(5), 539–550. https://www.publish.csiro.au/EN/EN14172

Farner, J. M., Hernandez, L. M., Lapointe, M., & Tufenkji, N. (2020). Understanding and improving microplastic removal during water treatment: Impact of coagulation and flocculation. *National Library of Medicine, 54*(14), 8719-8727. https://pubmed.ncbi.nlm.nih.gov/32543204/

Felsing, S., Kochleus, C., Buchinger, S., Brennholt, N., Stock, F., & Reifferscheid, G. (2018). A new approach in separating microplastics from environmental samples based on their electrostatic behavior. *Environmental Pollution, 234,* 20-28. https://doi.org/10.1016/j.envpol.2017.11.013

Freshwater - New World Encyclopedia. (n.d.). Retrieved April 25, 2022, from https://www.newworldencyclopedia.org/entry/Freshwater#References

Galloway, T. S., & Lewis, C. N. (2016). Marine microplastics spell big problems for future generations. *National Library of Medicine, 113*(9), 2331-2333. https://pubmed.ncbi.nlm.nih.gov/26903632/

Geyer, R., Jambeck, J. R., & Law, K. L. (2017). Production, use, and fate of all plastics ever made. *Science Advances, 3*(7). https://www.science.org/doi/10.1126/sciadv.1700782

Hamidian, A., H., Razeghi, N., Wu, C., Yang, M., & Zhang, Y. (2021a). Microplastic sampling techniques in freshwaters and sediments: a review. *Environmental Chemistry Letters, 19*(6), 4225-4252. https://doi.org/10.1007/s10311-021-01227-6

Hamidian, A. H.m Ozumchelouei. E. J., Feizi, F., Wu, C., Zhang, Y., & Yang, M. (2021b). A review on the characteristics of microplastics in wastewater treatment plants: A source for toxic chemicals. *Journal of Cleaner Production, 295.* https://doi.org/10.1016/j.jclepro.2021.126480

Hrones, J. A., & Nelson, G. L. (1951). *Analysis of the four-bar linkage: Its application to the synthesis of mechanisms*. Published jointly by the Technology Press of the Massachusetts Institute of Technology, and Wiley. https://wpi.primo.exlibrisgroup.com/permalink/01WPI_INST/dbokq8/alma9930277350474 6

IUCN. (2021). *Marine plastic pollution*. IUCN Issues Brief. https://www.iucn.org/resources/issues-briefs/marine-plastic-pollution#:~:text=Over%20300%20million%20tons%20of,waters%20to%20deep%2Dsea%20sediments.

Kannan, K., & Vilmalkumar, K. (2021). A review of human exposure to microplastics and insights into microplastics as obesogens. *Frontiers in Endocrinology*. https://doi.org/10.3389/fendo.2021.724989

Kim, J., Lee, Y., Park, J., Jung, S. M. (2022). Repeatable separation of microplastics integrating mineral oil extraction and a PDMS-Ni foam adsorbent in real soil. *Chemical Engineering Journal, 429.* https://doi.org/10.1016/j.cej.2021.132517

Koelmans, A. A., Mohamed, Nor. NH., Hermsen, E., Kooi, M., Mintenig, SM., & De France, J. (2019). Microplastics in freshwaters and drinking water: Critical review and assessment of data quality. *Water Research, 155*(15), 410-422. https://doi.org/10.1016/j.watres.2019.02.054

Koistinen, A., Mikloa, A., Setälä, O., & Talvitie, J. (2017). Solutions to microplastic pollution – Removal of microplastics from wastewater effluent with advanced wastewater treatment technologies. *Water Research, 123*(15), 401-407. https://doi.org/10.1016/j.watres.2017.07.005

Lange, N. (2018, May). *Development of Innovative Strategies to Protect the Aquatic Environment from Household Plastic Microfibers; Application of Electrostatic Water Filtration* [Poster Presentation] ASU INTEL ISEF 2018 Phoenix, Arizona, United States.

Lapoint, M., Farner, J. M., Hernandez, L. M., & Tufenkji, N. (2020). Understanding and improving microplastic removal during water treatment: Impact of coagulation and flocculation. *National Library of Medicine, 54*(14), 8719-8727. https://pubmed.ncbi.nlm.nih.gov/32543204/

Lebreton, L. C. M., Van der Zwet, J., Damsteeg, J. W., Slat, B., Andrady, A., & Reisser, J. (2017). River plastic emissions to the world's oceans. *Nature Communications*, *8*(1). https://doi.org/10.1038/ncomms15611

Li, C., Cui, Q., Zhang, M., Vogt, R. D., & Lu, X. (2021). A commonly available and easily assembled device for extraction of bio/non-degradable microplastics from soil by flotation in NaBr solution. *Science of the Total Environment, 759*(10). https://doi.org/10.1016/j.scitotenv.2020.143482

Lusher, A. L., Tirelli, V., O'Connor, I., & Officer, R. (2015). Microplastics in Arctic polar waters: the first reported values of particles in surface and sub-surface samples. *Scientific Reports.* https://www.nature.com/articles/srep14947

NOAA Marine Debris Program, Ocean Conservancy, SC Sea Grant. (2020). *Marine debris is everyone's problem.* https://www.whoi.edu/fileserver.do?id=107364&pt=2&p=88817

Oregon State University. (2015). Ban on microbeads offers best chance to protect oceans, aquatic species. https://today.oregonstate.edu/archives/2015/sep/ban-microbeads-offers-best-chance-protect-oceans-aquatic-species

Pallone, F. (2015, December 28). *Text - H.R.1321 - 114th Congress (2015-2016): Microbead-Free Waters Act of 2015* [Legislation]. https://www.congress.gov/bill/114th-congress/house-bill/1321/text

Perfetto, K., Richardson, A., Salvatto, S., & Sauter, E. (2020). *Strategies for Mitigating the Proliferation of Microplastics in Worcester Waterways.* Reykjavik: Worcester Polytechnic Institute. https://digital.wpi.edu/concern/student_works/bv73c361f?locale=en

Perren, W., Wojtasik, A., & Cai, Q. (2018). Removal of microbeads from wastewater using electrocoagulation. *ACS Omega*, *3*(3), 3357-3364. https://pubs.acs.org/doi/10.1021/acsomega.7b02037

Quan, M. E. (2018). Microplastics, macro problem: A novel technique to remove microplastics from water using a modified electrostatic filter. *California Science & Engineering Fair.*

Richard, J. (2012). *NON-COLLINEAR VALVE ACTUATOR* (The United States Patent and Trademark Office (USPTO) Patent).

Ruys, A. (2019). Hydrocyclones. *Bio-Based Polymers and Composites.* *https://www.sciencedirect.com/topics/materials-science/hydrocyclones*

SB-1263 Ocean Protection Council: Statewide Microplastics Strategy. (Sep. 20,). Retrieved April 30, 2022, from https://leginfo.legislature.ca.gov/faces/billTextClient.xhtml?bill_id=201720180SB1263

Schmidt, C., Krauth, T., & Wagner, S. (2017). Export of plastic debris by rivers into the sea. *Environmental Science & Technology*. https://doi.org/10.1021/acs.est.7b02368

Shen, M., Zhang, Y., Almatrafi, E., Hu, T., Zhou, C., Song, B., Zeng, Z., & Zeng, G. (2022). Efficient removal of microplastics from wastewater by an electrocoagulation process. *Chemical Engineering Journal, 428.* https://doi.org/10.1016/j.cej.2021.131161

Sun, M., Chen, W., Fan, X., Tian, C., Sun, L., & Xie, H. (2020). Cooperative recyclable magnetic microsubmarines for oil and microplastics removal from water. *Applied Materials Today, 20.* https://doi.org/10.1016/j.apmt.2020.100682

Van Emmerik, T., & Schwarz, A. (2019). Plastic debris in rivers. *WIREs Water, 7*(1). https://onlinelibrary.wiley.com/doi/full/10.1002/wat2.1398

Zhang, Y., Jiang, H., Bian, K., Wang, H., Wang, C. (2021). A critical review of control and removal strategies for microplastics from aquatic environments. *Journal of Environmental Chemical Engineering, 9(*4). https://doi.org/10.1016/j.jece.2021.105463

Appendices

Appendix A: Arduino Intake Code

```
#include <Servo.h>

#define RUNNING_INTERVAL 18000000
#define CLEANING_INTERVAL 1800000
//define Motor Controller pins
Servo servo1;
Servo servo2;
Servo servo3;
Servo ESC1;
Servo ESC2;

unsigned long loggedtime = 0;

int pos = 0;
int state = 0;


void setup() {
  // put your setup code here, to run once:
 servo1.attach(6);
 servo2.attach(9);
 servo3.attach(4);
 ESC1.attach(3);
 ESC2.attach(5);
 delay(2000);
 ESC1.write(0);
 ESC2.write(0);
 delay(3000);
```

```
}

void loop() {

  // do something different depending on the range value:
  switch (state) {
    case 0:    // your hand is on the sensor
      runIntakeone();
      break;
    case 1:    // your hand is close to the sensor
      Serial.println("dim");
      break;
    case 2:    // your hand is a few inches from the sensor
      Serial.println("medium");
      break;
    case 3:    // your hand is nowhere near the sensor
      Serial.println("bright");
      break;
  }
  delay(1);        // delay in between reads for stability
}


void runIntakeone(){
 loggedtime = millis();
 // open servo 1, open servo 2, run impeller 1 at intake speed
    servo3.write(180);  // tell servo to go to position in variable 'pos'
    servo2.write(180);
    ESC1.write(10); // run impeller 1 at 5% speed
```

```
 if (loggedtime + RUNNING_INTERVAL <millis()){
 state = 2;
 }

}

void rinseIntakeone(){
loggedtime = millis();
 // ESC1 to 0, Servo2 closed, open servo 1, ESC2 to 50%
    ESC1.write(0);
    servo2.write(0);
    servo1.write(180);
    ESC2.write(90);
 if (loggedtime + CLEANING_INTERVAL <millis()){
 state = 3;
 }

}
void runIntaketwo(){
 ESC2.write(10);
 delay(3000);
 servo2.write(180);
 servo3.write(0);
 if (loggedtime + RUNNING_INTERVAL <millis()){
 state = 4;
 }
}
void rinseIntaketwo(){
 loggedtime = millis();
 // open servo2, close servo3
    ESC2.write(0);
    delay(3000);
    servo2.write(0);
    servo3.write(180);
    delay(3000);
    ESC1.write(10);

 if (loggedtime + CLEANING_INTERVAL <millis()){
 state = 4;
 }

}
```